Summer 2016

Experimental performance evaluation and design of schemes for passive RFID network

Shadi Ebrahimi-Asl

Department: Electrical and Computer Engineering

EXPERIMENTAL PERFORMANCE EVALUATION AND DESIGN OF SCHEMES FOR PASSIVE RFID NETWORK

by

SHADI EBRAHIMI-ASL

A DISSERTATION

Presented to the Faculty of the Graduate School of the

MISSOURI UNIVERSITY OF SCIENCE AND TECHNOLOGY

In Partial Fulfillment of the Requirements for the Degree

DOCTOR OF PHILOSOPHY

In

Electrical Engineering

2016

Approved by:
Dr. Maciej Zawodniok
Dr. Mohammad Tayeb Ghasr
Dr. Reza Zoughi
Dr. David Pommerenke
Dr. Sriram Chellappan

PUBLICATION DISSERTATION OPTION

This dissertation consists of the following six articles. The papers are formatted according to Missouri University of Science and Technology specifications.

Pages 17-35, "Measuring the Structural Scattering Coefficient of a Linear RFID Antenna Using Minimum Variance Unbiased Estimator," To be submitted to IEEE Transaction of Antenna and Propagation.

Pages 36-67, "Dual Loaded RFID Tag for Higher Order Modulations," US Provisional Patent Application 62/236,490, October 2015.

Pages 68-90, "Application of Low Scattering Antennas to RFID Networks," *Best paper nominee 2016,* to be appear in proceeding of RFID Conference 2016.

Pages 91-121, "A Solution to Low Read Rate Problem in RFID Scattering Networks," which is a part of , "Implementation of Invisible Antenna with Application of RFID Systems," provisional patent application 62/248,870, October 2015.

Pages 122-135, "Preliminary study on mutual coupling effect on a passive RFID antenna array," in proceeding of IEEE International Instrumentation and Measurement Technology Conference (I2MTC), May 2013.

Pages 136-163, "Cooperative Interference Control in Neighboring Passive Antennas with Application to RFID Networks," To be submitted to IEEE Transaction of Antenna and Propagation.

ABSTRACT

Passive Radio Frequency Identification (RFID) is a short range technology for transferring information. The main advantage of passive RFID systems over active communication systems is the battery-less operation at the client sides. However, there are two major challenges that limit the widespread adaptation of passive RFID systems: short communication range and low read rate in dense deployments. This dissertation addresses these issues by studying the root causes and develops solutions for them.

In this dissertation, understanding the backscattering behavior of antennas and also the mutual coupling interactions among them are found to be the root causes of the two above-mentioned challenges for RFID networks. Thus, by studying these two main root causes solutions for them are proposed, investigated and verified, by simulations and measurements. The contributions in this dissertation include: (1) Design of a new measurement technique to estimate the structural scattering coefficient of a linear antenna. (2) Showing that the well-known *Green model* cannot completely explain the variation of the radar cross section of a T-match bowtie antenna over its Γ plane. (3) Introducing dual loading in designing RFID antenna tags to: (a) Increase the vector differential backscattering signal, (b) Produce higher order modulations. (4) Introducing a new state for RFID tags in that tags switch to a low scattering states to: (a) suppress their interference to a target antenna in the network. (b) Stabilize the RCS of the target antenna. (c) Increase read rate in RFID networks. (5) Numeric analysis of the mutual coupling impedance for two side by side scattering antennas. (6) Introducing a multi-port RFID which can switch to different load impedances to *help* a target antenna in its vicinity increase its signal over the level when the target is alone in the field.

ACKNOWLEDGEMENTS

I would like to express my sincere thanks to my advisor, Professor Maceij Zawodniok, for his supervision and support throughout my PhD journey. Without his patient guidance, this dissertation would not have been possible. I would like to express my sincere thanks to my co-advisor, Dr. Mohammad Tayeb Ghasr, who spent his time and walked with me step by step throughout the understandings and discoveries in this dissertation. I also would like to thank Professor David Pommerenke for his comments on my first paper and also for opening a new door to my next carrier life. I would like to thank Professor Reza Zoughi, from him I learned the basics of antennas and propagations to use them throughout this dissertation.

I want to thank my family: my mother and my father from them I learned to move on and never give up. I want to thank my sister, Shohreh, whose absence during my PhD studies was hard but she was in my heart, and also on Skype, in any minute. And thank you aunt Mali, I always felt your love with me miles away from home. Last but not least, I want to thank my close friend in Rolla, Mohammad, who was beside me during all moments of disappointments throughout the path of discoveries in this dissertation and gave me energy to move on.

TABLE OF CONTENTS

LIST OF ILLUSTRATIONS

Section Page

Paper III

Paper IV

LIST OF TABLES

Paper I Page

Paper II

Paper IV

Paper VI

1. INTRODUCTION

Passive Radio Frequency Identification (RFID) is a short range technology for transferring information. The main advantage of passive RFID systems over active communication systems is the battery-less operation at the client sides. Passive RFID systems have already been accepted in many applications for asset tracking and identifications as a replacement of a barcode technology. Furthermore, passive RFID tags are becoming popular in battery-less sensor area. However, there are several major challenges that limit the widespread adaptation of passive RFID systems including: short communication range and low read rate in dense deployments. This dissertation addresses these issues by studying the root causes and develops solutions for them.

A passive RFID system consists of a main base station, called RFID reader, and several clients, called RFID tags, in the field. In order to access the information from an RFID tag, the RFID reader initiates the communication. First, the reader emits a continuous wave (CW) signal to deliver energy to the tags. Tags harvest every from the RF signal to run their circuitry. Next, the reader sends out a query to tags calling out the ID of a specific tag. The RFID reader continues the query with a CW. The tags decode the query. If the ID of a tag matches with the interrogated ID in the query signal a switch in the tag is activated to switch the input impedance of the tag between two values. By doing so, the RFID tag actually changes its radar cross section (RCS) between two values. This way, the tag is able to encode its stored information based on the change in the RCS over the CW signal from the reader antenna. This method of transferring information is called: *differential*

backscattering [1], [2], [3]. Higher magnitude of the differential backscattering signal from a tag results in: (a) larger coverage (range) of the RFID reader and (b) higher probability of detection of tags. Thus, selecting two optimum loads at the RFID tag which can produce the highest differential backscattering signal is a major challenge in passive RFID area. On the other hand, when the number of tags in an RFID network increases by any query from RFID reader a chaos of backscattering signals is produced due to *antenna scattering phenomenon*. This chaos produces interference to an ongoing backscattering link between an RFID reader and an RFID tag and as a result reduces the signal to noise ratio of the communication link between them. The resultant high interference in RFID networks is the second major challenge in these networks causing low read rates in these networks. In the following two subsections the two above-mentioned major challenges are addressed in RFID networks and a literature survey for them is performed.

1.1 FIRST CHALLENGE IN RFID NETWORKS

The first challenge in passive RFID systems is an optimum selection of the two load impedances at which the maximum differential backscattering is achieved. The first comprehensive model for finding the maximum differential backscattering in backscattering links was conducted in [1] in 1963. Later on in 2007, the introduced model in [1] was used in [2] to study the maximum differential backscattering of an RFID T-match bowtie antenna. The model in [1], is still a touchstone for characterizing two scattering states for backscattering links. According to [1] (and also [3]), the scattering field E_s from an arbitrary antenna loaded by Z_L and illuminated by an arbitrary field has been modelled as

$$E_s = I_{ref}(^{E_a}/_{I_a})(A_s + \Gamma) \quad (1)$$

where I_{ref} is the induced current by the incoming field at antenna terminals when it is terminated at the load impedance (Z_L) complex conjugate of the antenna (Z_a^*), E_a is the field radiated by the antenna when the current at the antenna terminal is I_a and no external incident wave is applied to the tag antenna, A_s is a constant describing structural scattering coefficient of an antenna, and Γ is a modified current reflection coefficient such that $|\Gamma| \leq 1$ for all passive loads:

$$\Gamma = (Z_a^* - Z_L)/(Z_L + Z_a) \quad (2)$$

The scattering from an antenna in (1.1) is divided into two parts: *antenna mode scattering* and *structural mode scattering*. The antenna mode scattering accounts for the portion of the scattering from an antenna which can be manipulated by changing its load impedance. In (1.1), Γ accounts for this portion of the scattering from an antenna. Also, structural mode scattering accounts for the portion of the scattering from an antenna which is a fixed value and only depends on the antenna dimension, structure. In (1.1), A_s accounts for this portion of the scattering from an antenna.

By considering z=$(Z_L + jX_a)/R_a$ in (1.2), the modified reflection coefficient can be represented as $\Gamma = {(1-z)}/{(1+z)}$. Thus, the complex Γ ($\Gamma = \Gamma_r + j\Gamma_i$) can be plotted on the Γ plane of the antenna. At any selected Γ on this plane, a load impedance can be selected for the antenna using (1.2). The corresponding load sets the antenna in a new scattering state. The RCS (σ) at any scattering state is shown by [1]-[3]

$$\sigma = (^{\lambda^2}/_{4\pi})G^2|\Gamma + A_s|^2 \quad (3)$$

where G is antenna gain at wavelength λ. In this dissertation, equation (1.1) and (1.3) are called *Green model*. Equation (1.3) represent a circle with center $\Gamma = -A_s$ and radius $r = {(4\pi\sigma)}/{(\lambda^2 G^2)}$ on the Γ plane of an antenna. The RCS of the antenna at the center of this circle, i.e. $\Gamma_1 = -A_s$ is zero. This point is called the *invisibility point* of the antenna where the antenna is *minimum scattering* ($E_s = 0, = 0$). By moving away from this point the right side of the (1.3) increases and as a result σ increases. According to (1.3), the RCS increases monotonously until at the edge of the Γ plane of the antenna, which is the farthest point to $(-A_s)$ e.g. Γ_2, it reaches to a maximum. At this point, – at Γ_2 – the antenna is *maximum scattering*. Hence, in order to achieve the highest possible differential RCS the load of the antenna is switched between Γ_1 and Γ_2. This model is used in all current deployment of load selection for backscattering links [1]-[6]. In this dissertation, this modulation technique is called *scalar differential backscattering (SDB)*. In this type of backscattering modulation the data is encoded only in the absolute magnitude of the reflected signal. Thus, scalar differential backscattering is a type of Amplitude Shift Keying (ASK).

The RCS in (1.3) is affected by the antenna structural scattering (A_s). Hence, characterizing A_s is crucial in finding the maximum differential backscattering from an antenna [2], [3], [6]. Existing works focus on theoretical method introduced in [1] to find A_s. In this method, three Γ points not lying on the same circle in (1.3) are considered and the antenna RCS at these three scattering states are characterized. By intersecting the corresponding three scattering circles, A_s is uniquely characterized on the Γ plane of the antenna. Using this method, further research was conducted to calculate the structural scattering coefficient of different RFID antenna tags in the literature [2], [3], [5], [7]. On

the other hand, some works find the minimum scattering state of an antenna by minimizing the current distribution on an antenna structure [8]. In [9] and [10], the structural scattered *power* from an antenna was measured. Reference [11], presents an un-finished work proposing a circuit which can practically measure A_s for any antenna type. In practice, however, no work has been performed in the literature to measure A_s directly in (1.1). The main challenge is separating the structural and antenna modes scattering in (1.1) from each other. Furthermore, the magnitude of structural scattering coefficient for any passive antenna is less than 1 ($|A_s| < 1$) [3]. Thus, any noise, interference, reflections, and measurement errors result in a big change within the Γ plane of the antenna [12], [13]. Yet, measuring structural scattering coefficient A_s is desired to validate theoretical methods and to help in real world design and analysis.

The data in RFID systems can also be encoded using Phase Shift Keying. In this method, the reactance portion of the load is changed to produce a phase shift in the scattered field from the antenna [5], [14]-[17]. Thus, the stored data can be encoded in the variation of the phase of the scattered field from the RFID antenna. In this dissertation, this modulation type is called *vector differential backscattering (VDB).* In this modulation, the RFID reader must be able to detect the variation of the phase in the backscattered field from the RFID tag. The efficiency of the backscattered link in this method depends on the vector distance between two scattering states. Increasing the vector distance between the states of scattering fields result in (*i*) better resilience against noise and interference, (*ii*) higher probability of detection of a tag at the RFID reader, and (*iii*) larger communication coverage range. The maximum vector differential backscattering (VDB) is achieved if two maximum scattering states with 180 phase shift are used. This concept is depicted in Figure

1.1 which depicts the demodulated backscattered signal at the reader in the in-phase and quadrature plane. The scalar differential backscattering (SDB) is shown by a yellow arrow representing the variation in the RCS of the antenna between zero and maximum scattering. On the other hand, scattering states 1, 2 and 3 provide respectively 90°, 135° and 180° phase shift comparing to the maximum scattering of the antenna. Thus, *theoretically* by changing the load of the antenna between the maximum scattering state and scattering state 3 the maximum possible vector differential backscattering can be achieved. However, the question is: are producing two maximum scattering states with 180 phase shift realizable? According to the literature the answer is "no" since based on (1.3) only one maximum scattering state for an antenna is realizable [1]-[6]. Furthermore, producing 180° phase shift in the backscattered field by load switching at the RFID antenna is a challenge.

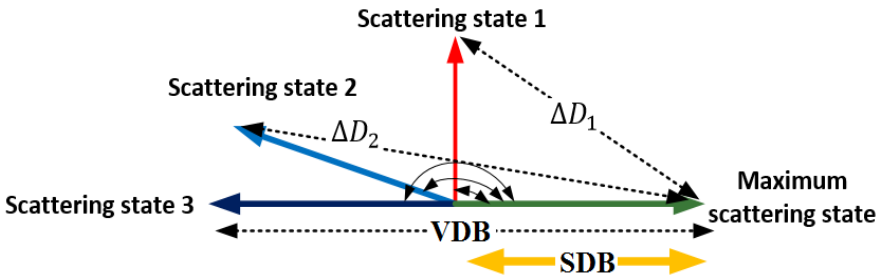

Figure 1.1. Scalar and vector differential backscattering.

In [7], a quasi-Quadrature Phase Shift Keying modulation is proposed. In the proposed method, four scattering states for an RFID antenna are used in a 90° phase span in the in-phase-quadrature plane to encode 2 bits. However, the scattering states are very close to each other and hence the separation between symbol constellations is small. Thus, boundaries of detection are defined in the 90° phase span in the in-phase-quadrature plane for detecting the scattering states of the backscattering signal at RFID reader.

Consequently, even small increase in the noise level or interference will move the one scattering state of the constellation into the adjacent detection regions of other states and as a result produces error in detection bits. Other works in the literature have studied QAM modulations with reference to a 50 Ω input impedance for RFID tag antennas [14]-[17]. In [17], a chip-less RFID tag is introduced which can produce 16-QAM using delay lines in transmission lines theory. Thus, 16 different structures of this antenna can be used for identification of 16 different objects. Thus, this antenna design is not suitable for transferring streams of data.

1.2 SECOND CHALLENGE IN RFID NETWORKS

The second main challenge in passive RFID systems arises when this technology is used in a dense deployment of RFID tags to access the stored information in tags [18]-[26]. Figure 1.2 illustrates such a scenario. When an RFID reader interrogates one RFID tag the rest of the tags in the network also receive this signal. Due to the electromagnetic scattering, current distributions are induced on all of these tags. Hence, all of them scatter back to the environment. This has two important consequences:

1) The current distribution on the target tag is altered as a result of mutual coupling and scatterings from neighbor antennas. This results in a shift in the input impedance at the target tag, low power harvesting, and a weak backscattering signal from the target tag.

2) The resultant scattered fields from the neighbor antennas cause interference in form of a destructive superposition to the source signal both at the target antenna and the RFID reader sides. This results in a decrease in the signal to noise ratio for the ongoing backscattered link.

This problem has repeatedly been reported in the literature and has been the main obstacle of the widespread adaptation of passive RFID systems in many applications [18]-[26]. According to [19], due to the multi reflections and mutual couplings among RFID tags blind spots are inevitable in an RFID network where the RFID reader cannot access to the tags and read their data. To increase the read rate in RFID networks, several methods have been studied and proposed in the literature. Some works develop collision detection and collision avoidance techniques [20], [21]. Some other works, model the RFID tags as a *virtual antenna array* based on traditional definition of mutual coupling theory [22], [23]. Spatial, frequency and polarization diversities have also been proposed in the literature [19], [24]. In [25], all RFID tags of the same type *cooperate* and will backscatter the *same pre-agreed-message* when an interrogation signal from RFID reader is received at the tags. However, synchronization of independent and randomly located RFID tags is a big challenge in this method. Furthermore, the proposed solution in [25] cannot solve the issue of blind spots in RFID networks.

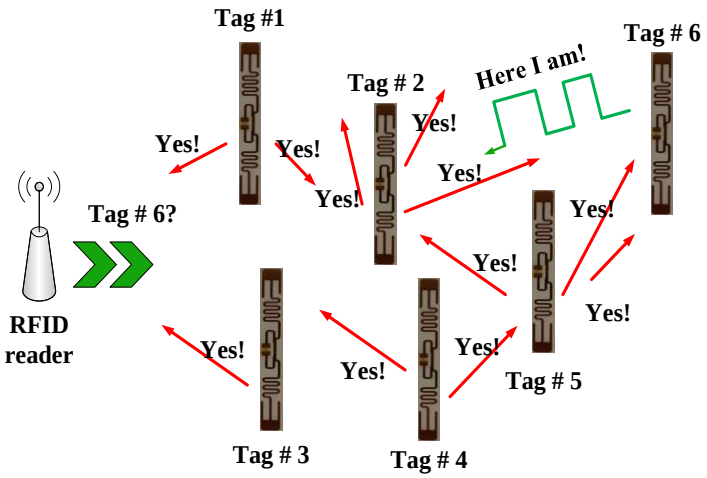

Figure 1.2. Multi reflection problem in RFID networks.

2. ORGANIZATION OF THE DISSERTATION

In this dissertation, above-mentioned two challenges are addressed by studying and understanding the underlying phenomena and proposing solutions for them. In the first two papers, the focus is on studying and analyzing the differential backscattering from one RFID antenna when it is alone in the field. In Paper 1, a new measurement methodology is deployed for *estimation* of the structural scattering coefficient (A_s) of a linear antenna. The proposed method employs a linear-minimum variance unbiased estimator and experimentally validates the effectiveness of the proposed approach for a linear half-wave dipole antenna. However, during the research it was discovered that the variation of RCS of a T-match antenna over Γ plane of the antenna does not adhere to existing Green model. Moreover, the RCS behavior of this antenna can be exploited to improve the communication performance in the RFID system. That leads us to designing a new, more efficient RFID antenna that is presented in Paper 2. In Paper 2, scalar and vector differential backscattering for two antenna types over their Γ planes (linear half-wave dipole and T-match bowtie) is studied. It is shown that the variation of the linear half-wave dipole follows Green model in (1.1). However, Green model cannot completely explain the behavior of a T-match bow tie antenna over its Γ plane. The analysis of the results lead us to performing a manipulation in the antenna structure to use dual loading in this RFID antenna type [28]. It is shown that the new antenna can maximize the vector differential RCS and produce higher order modulation. Specifically, the proposed antenna increases the modulation depth to over 176% and produce a quasi-32-QAM.

Afterward, in the next four papers the focus is on the interactions between two or more RFID tags. In Papers 3 and 4, a new scattering state for RFID tags in which they

switch to a low scattering state to suppress their interference to a target tag in the network is investigated. It is shown experimentally that by using this method read rate in RFID networks increases. In Paper 5, by using the traditional definition for mutual coupling theory RFID antennas are assumed as transmitting and receiving antennas. The driving currents for each element of an array of RFID tags based on the load impedance of the antenna element itself and the mutual coupling from its neighbor antenna tags are formulated and analyzed. Paper 6 presents the study of the mutual coupling interaction between RFID tags as scattering antennas. Since the traditional mutual coupling theory is defined for transmitting and receiving antennas the effect of the load impedance on the mutual impedances has not be considered. It is shown that the induced current in a scattering antenna with close neighbors is a function of the load impedances of the neighbors as well. Based on this, a multi-port RFID tag is proposed which, as a neighbor, can switch to different load impedances (scattering states) to help a close queried target antenna −from the RFID reader− to increase its signal over the level where the target antenna is alone in the field.

2.1 PAPER 1

In this paper, a measurement technique is used to estimate the structural scattering coefficient ($\boldsymbol{A_s}$) of a linear half-wave dipole. A minimum variance unbiased estimator is used under the assumption that the noise in the measurements are only affected by Gaussian noise. An estimator is developed for equation (1.1) which can estimate the *true value* of the structural scattering coefficient of the studied half-wave dipole antenna. The un-modulated backscattering signal of a scattering antenna in an anechoic chamber is affected

by the distribution of noise in the measurement setup and also the measuring instrument. Due to the drift and internal thermal variation of the measuring instrument, the distribution of the noise in the measurement can be non-Gaussian. In this work, measurements which are only affected by Gaussian noise are collected. *Cholesky decomposition* and whitening process are used to whiten the noise in the measurement. Next, minimum variance unbiased estimator is aplied in linear format to equation (1.1) to develop an estimation method to find A_s for the studied antenna by measurements. Estimation accuracy is a function of several factors: 1) A tradeoff between number of measurements ($\boldsymbol{N}$) and collecting Gaussian noise, 2) The dimension of covariance matrix of the collected noise, 3) Correlation between final estimated values to calculate $\boldsymbol{A_s}$. 4) Employing "*far"* elements in observation matrix. All of these issues are addressed and evaluated their effects on the accuracy of estimation.

2.2 PAPER 2

In this paper, study the variation of RCS of two antennas (linear half-wave dipole and T-match bowtie antenna) over their Γ planes both by measurements and simulations are performed. It is shown that the behavior of RCS of the linear half-wave dipole is in agreement with model (1.3) over the antenna Γ plane. However, for the studied T-match bowtie antenna model (1.3) cannot completely explain the behavior of the antenna RCS over its Γ plane. According to the simulation and measurements results the T-match bowtie antenna has two maximum scattering areas on its Γ plane. In the next step, a modification in the antenna structure of the T-match bowtie is performed to use *dual loading* in its structure. A $1mm$ gap is made at the center of the antenna [28]. At two locations on the

antenna structure load switching is employed to stimulate the antenna: 1) at the gap, 2) at the input port of the antenna. Using a combination of different loads at both stimuluses in the proposed new antenna design, it is shown show that it is possible to produce various scattering states with different magnitudes over 360° phase span. This feature of the new proposed antenna is used to: (*i*) produce two maximum scattering states with 180° phase shift and increase modulation depth to over 176%, (*ii*) produce higher order modulation. Specifically, about the latter case, the proposed antenna can produce a quasi-32-QAM in the lab environment.

2.3 PAPER 3

In this paper, the idea of using *low scattering* antennas is investigated to suppress the chaos of interference in closely spaced RFID tags. In this work, first the *accuracy* of realizing invisibility state and then *stability* in keeping the invisibility state are studied for a half-wave dipole antenna. To evaluate the accuracy of realizing invisible state of the antenna, an ideal and a realizable invisible antennas are compared. An ideal invisible antenna for a half-wave dipole is achieved by simulations at $RCS \sim -58\, dBsm$ at any angle using very fine impedances. In the lab, it is realized that invisibility state for the studied antenna at $RCS \sim -50\, dBsm$ at the main lobe of the antenna using typical load impedances. To evaluate stability, the variation of the current of a realizable invisible antenna beside a neighbor antenna is studied. It is shown that even though the realizable invisible antenna is not *accurate* still its mutual coupling interactions with the environment is small. Next, a two scattering antenna system is studied which is illuminated by a plane wave from RFID reader. One antenna is assumed to be the target and the other is a

neighbor. It is shown that if the neighbor is used at its low scattering state its interference to the target antenna is minimized and the RCS from the target antenna is stabilized.

2.4 PAPER 4

In this paper, the study in Paper 3 is extendedto a situation where a target tag is surrounded by several neighbors. Furthermore, the effect of random placement, polarization and incident angle of the neighbors on the detection of the signal from target antenna are studied. The effect of changing the substrate material of a tag on realizing its invisibility state is briefly discussed [26]. In the next step, two types of neighbor antennas are considered to study the variation of the magnitude of the received signal ($\boldsymbol{\delta}$) from the target antenna: short circuit antennas (high scattering) and low scattering antennas. It is shown that when nine high scattering antennas are used in the vicinity of the target antenna the received signal from the target antenna is immensely degraded and its magnitude is mostly close to zero. On the other hand, it is shown that when low scattering antennas are used in the vicinity of the target antenna the interference from neighbor antennas are suppressed and the magnitude of the received signal from the target is stabilized. Parameter "$\boldsymbol{\delta}$" is used to set thresholds for read rate evaluation at the reader antenna in the study when the target is surrounded by nine neighbor antennas. it is shown that when the threshold is set at "0.75 $\boldsymbol{\delta}$" the average read rate of the target antenna is 93.76% when low scattering neighbors are used whereas for the case where high scattering are used the average read rate is 14.16%.

2.5 PAPER 5

In this paper, the *traditional mutual coupling theory* is used to study and measure the variation of the mutual coupling impedance between two side by side RFID antennas ("Alien 9640 Squiggle Inlay"). A half-wave dipole is constructed. The mutual coupling impedances for two side by side dipoles is measured. The measured and simulated results of the mutual coupling impedances for both antenna types are in agreement with the well-known values of two side by side antennas [3]. Based on traditional mutual coupling theory, RFID tags in an array of tags are considered as receiving and transmitting antennas and their currents are formulated based on their own load impedances and the mutual coupling impedances from their neighbor's antennas. The obtained values from measurements and simulations are used to model the variation of current at the RFID antenna array considering the mutual coupling among the tags.

2.6 PAPER 6

In this paper, it is shown show that in addition to the load impedance of an antenna and the mutual coupling impedance from neighbors the current distribution in closely spaces RFID tags is also a function of the load impedance of neighbor antennas. The effect of loads is not considered in the traditional definition for mutual coupling theory since it is defined for transmitting and receiving antennas. Next, a numerical method is presented to evaluate the mutual coupling impedances between two scattering antennas which can well explain the mutual interactions between two side by side scattering antennas. In the next step, the idea of *cooperative* improvement of backscattering signal from a target antenna in a two scattering antenna system is proposed. In the proposed model, a neighbor antenna

switches to different load values to control its interference to a target antenna in its vicinity. In this model, the neighbor antenna will not produce interference for a target and instead it *helps* the target antenna to increase its signal over the level when the target is alone in the field. This idea is studied based on different placements of the target antenna and the neighbor antenna with respect to the incident plane wave. It is shown that depending on the placement of the neighbor antenna with respect to the incident wave and the target antenna the induced current at the target can be increased up to 3.4 dB over the case where the target antenna is alone in the field.

3. CONTRIBUTIONS OF THE DISSERTATION

The contributions in this dissertation include:

1) Design of a new measurement technique to estimate the structural scattering coefficient of a linear antenna.

2) Showing that the variation of the RCS of a T-match bowtie antenna over its Γ plane cannot completely be explained by *Green model* and the antenna has two maximum scattering areas on its Γ plane.

3) Introducing dual loading in designing RFID antenna tags to:

   i) Increase the vector differential backscattering signal.

   ii) Produce higher order modulations.

4) Introducing a new state for RFID tags in that tags switch to a low scattering states to:

   i) Suppress their interference to a target antenna in the network.

   ii) Stabilize the RCS of the target antenna.

   iii) Increase read rate in RFID networks.

5) Numeric analysis of the mutual coupling impedance for two side by side scattering antennas.

6) Introducing a multi-port RFID which can switch to different load impedances to *help* a target antenna in its vicinity increase its signal over the level when the target is alone in the field.

PAPER

I. MEASURING THE STRUCTURAL SCATTERING COEFFICIENT OF A LINEAR RFID ANTENNA USING MINIMUM VARIANCE UNBIASED ESTIMATOR

ABSTRACT

Antenna structural scattering coefficient has been studied in theory and simulations. However, there is lack of an experimental validation and measurement methodology due to challenges in measuring the small value of the coefficient. A new methodology for measurement-based estimation of the structural scattering coefficient is proposed. A minimum variance unbiased estimator is used to estimate the structural scattering coefficient ($\boldsymbol{A_s}$) of a linear rectangular half wave dipole RFID tag. A full study of the effect of noise variation and its behavior on the estimation results are presented. The estimation results are shown to be very close to the true value of the $\boldsymbol{A_s}$ found by simulations.

1. INTRODUCTION

Short-range data communication using radio frequency identification (RFID) technology is becoming more popular in many short range applications. These systems consist of one main base station, called RFID reader, and several RFID tags in the field. Data transfer from the RFID tag is possible by using *differential backscattering* in that the input impedance of the tag is switched between two values to modulate the stored data on top of the source signal from RFID reader. One of the challenges in this scenario is selecting two optimal load impedances for the RFID antenna to maximize the differential backscattering signal.

A touchstone model for selecting loads in backscattering links was first introduced in [1] and later on in [2]. In this model, the scattering field E_s from an arbitrary antenna loaded by Z_L and illuminated by an arbitrary field has been modelled as

$$E_s = I_{ref}\frac{E_a}{I_a}(A_s + \Gamma) \quad (1)$$

where I_{ref} is the current induced by the incoming field at antenna terminals, when it is terminated at complex conjugate of the antenna (Z_a^*); E_a is the field radiated by the antenna when the current at the antenna terminal is I_a and no external incident wave is applied to the tag antenna; A_s is structural scattering coefficient of the antenna. In (1), Γ is a modified current reflection coefficient such that $|\Gamma| \leq 1$ for all passive loads: $\Gamma = \frac{Z_a^* - Z_L}{Z_L + Z_a}$, where Z_L is the load of the antenna. Considering $z=(Z_L + jX_a)/R_a$, the modified reflection coefficient can be represented as $\Gamma = \frac{1-z}{1+z}$ and can be plotted on Γ plane of the antenna. In (1), A_s and Γ respectively account for the *structural mode* and *antenna mode* scattering from an antenna. In this model, the radar cross section of the antenna is characterized by

$$\sigma = \frac{\lambda^2}{4\pi} G^2 |\Gamma + A_s|^2 \quad (2)$$

where G is antenna gain at wavelength λ. Equation (2) represent a circle with center $\Gamma = -A_s$ and radius $r = (\frac{4\pi\sigma}{\lambda^2 G^2})$ on Γ plane of an antenna.

Characterizing A_s is crucial in finding the maximum differential backscattering from an antenna [1]-[7]. The introduced method in [1], still is used in the literature to find A_s for any scattering antennas. In this method, three Γs not lying on a same circle are considered and the antenna RCS at these three scattering states are characterized. By intersecting the corresponding three circles A_s is uniquely characterized on the Γ plane of the antenna [4], [5], [6]. Using this method, further research was conducted to calculate the structural scattering coefficient of different RFID antenna tags in the literature [2], [3]-[6]. Some works, find the minimum scattering state of an antenna by minimizing the current distribution on an antenna structure [8]. Measuring the structural scattered power from an antenna also discussed in [9] and [10]. Reference [11], presents an un-finished work proposing a circuit which can practically measure A_s for any antenna type. But, no work has been performed in the literature to measure A_s in (1). The reason for this is that extracting the structural and antenna modes scattering from each other in (1) is very challenging. The main reason for this is that, the magnitude of structural scattering coefficient for any passive antenna is less than 1 ($|A_s| < 1$) [12]. Thus, any error in the measurements due to the noise, interference, reflections result in a big error in measuring this parameter [4]. Yet, measuring structural scattering coefficient is desired to validate theoretical methods and to help in real world design and analysis [2].

Estimation theory is used where a direct measurement of a parameter of interest (θ) is not possible due to a random component in the empirical data [13], [8]. The key factor

in estimation is that all N measurements are affected by random components, which can be modeled by a PDF. The parameter estimation problem is then to determine from a set of N observations, represented by the N-dimensional vector $\boldsymbol{x}$, the values of parameters denoted by the vector $\boldsymbol{\theta}$. In this paper, *Linear Minimum Variance Unbiased Estimator* is used to *estimate* A_s in (1). The main assumption in using this estimator is the the observation matrix, $\boldsymbol{x}$, should have a white Gaussian noise PDF. The unmodulated signal from a linear half-wave dipole in an anechoic chamber is measured by measuring 1-port VNA measurement. It is shown that the added noise in the measuring instrument is generally non-Gaussian and colored over time. This is the limiting factor in this method. Thus, the measurements is repeated until a Gaussian noise is observed in the measurement. Afterward, *Cholesky decomposition* is used to whiten the noise in the measurement and find the covariance matrix of the noise afterward. Finally, the proposed *Linear Minimum Variance Unbiased Estimator* for (1) is used to estimate the structural scattering coefficient (A_s) of the studied linear half-wave dipole. The factors affecting the accuracy in our estimation are: 1) a tradeoff between number of measurements and collecting Gaussian noise, 2) The dimension of covariance matrix of the collected noise, 3) correlation between estimated values in $\boldsymbol{\theta}$ matrix. 4) Employing far elements in observation matrix. These items are discussed in details in Section 2.3 and 2.4.

This work, first has been presented in [2] to estimate A_s of a T-match bowtie antenna based on the assumption of white Gaussian noise in the measurement setup. In this work, the assumption on *white noise* is relaxed. Furthermore, in [15] it have been shown that the model in (1) cannot completely explain the scattered field from a T-match bowtie antenna over its Γ plane. Thus, since the scattered field from a T-match bowtie antenna is

not linear anymore the proposed method cannot be used for measuring the structural scattering coefficient form the antenna either. In this paper, a linear half-wave dipole is considered whose scattered filed can be characterized by (1) as it has been investigated and shown in [15]. The rest of this paper is organized as follows. In Section 2, the proposed model for estimating structural scattering coefficient is proposed. In Section 3, noise analysis is presented. In Section 4, measurement results and discussions are presented. Conclusions are presented in Section 5.

2. THE PROPOSED MVUE FOR ESTIMATING A_s

In this Section, we propose our method for estimation of the structural scattering coefficient of a linear antenna. In case a measured parameter is corrupted by noise and/or interference, the *estimation theory* can be used to *estimate* the "*true value"* of a parameter of interest. An estimator is then used to take the measured data ($\boldsymbol{x}$) as input and produces an estimate of the parameter of interest with a corresponding accuracy ($\hat{\theta}$). The estimation error $\varepsilon(r)$ equals the estimate minus the actual parameter value: $\varepsilon(r) = \hat{\theta} - \theta$. Among all estimators for an unknown deterministic parameter, a *minimum variance unbiased estimator* yields an estimation with the least variability as shown by the Cramer-Rao Lower Bound (CRLB).

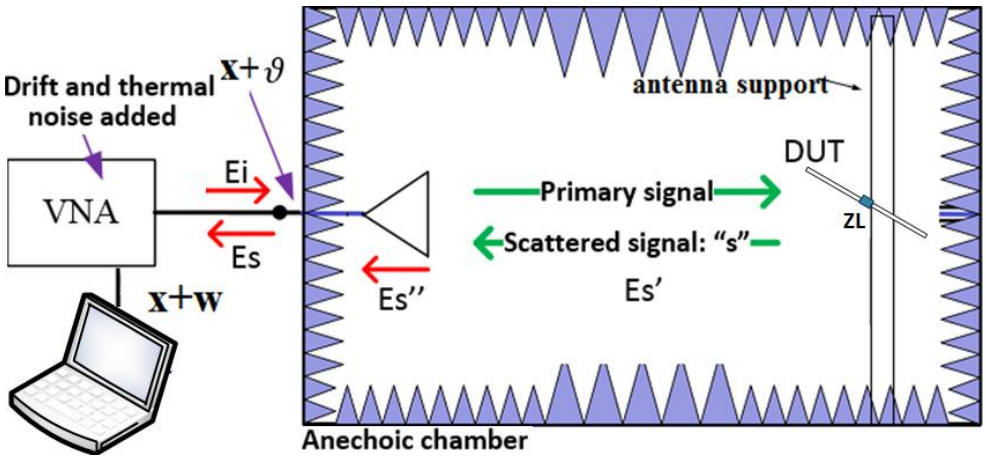

Figure 2.1. The proposed measurement set up.

A measurement set up is prepared as shown in Figure 2.1 in an anechoic chamber with dimension of $2 \times 2.5 \times 3\ m$ and using VNA Agilent E5061B. The RFID reader and RFID antenna are used in horizontal polarization such that the residual backscattering from

the antenna support is minimized. The antenna is placed at approximately 2 m away from antenna reader. The incident electric field at the port of reader is characterized as E_i. The backscattered signal from the antenna uncer test is characterized by E_s'. The total received scattering back at the reader port is $E_s = E_s{}' + E_s{}'' + \vartheta$ where $E_s^{"}$ represents the scattering from the reader antenna. The noise in the measurement setup before the port of the RFID reader is shown by ϑ and is assumed to be Gaussian $\vartheta \sim \mathcal{N}(0, \mathcal{C})$. At reader port, the ratio of the received field to the incident field is measured ($x = S_{11} = \frac{E_s}{E_i}$). Using (1), we have $x = \frac{I_{ref}\frac{E_a}{I_a}}{E_i}.(A_s + \Gamma) + \frac{E_s^{"}}{E_i} + \frac{\vartheta}{E_i}$. We use $\Gamma_a = E_s^{"}/E_i$ which represents the reflection coefficient of the reader antenna. In the measuring instrument, the drift and internal noise of the instrument is also added to x. The total noise in x is shown by w. We *assume* that $w \sim \mathcal{N}(0, \boldsymbol{C})$. Considering $\alpha = \left(I_{ref}\frac{E_a}{I_a}\right)/E_i$, $x = \Gamma_a + \alpha\,(A_s + \Gamma)$ +w. To simplify, we use $\beta = \alpha.A_s : x = \Gamma_a + \beta + \alpha.\Gamma + \mathrm{w}$.

By performing N measurements, $\boldsymbol{x} = \left[x[0], x[1], \dots, x[N-1]\right]^T$ and $\boldsymbol{w} = \left[w[0], w[1], \dots, w[N-1]\right]^T$ are obtained which make a set of equations as:

$$\boldsymbol{x} = \boldsymbol{H}.\boldsymbol{\theta} + \Gamma_a + \boldsymbol{w} \tag{3}$$

where $\boldsymbol{\theta} = [\alpha\ \beta]^T$ and

$$\boldsymbol{H} = \begin{bmatrix} \Gamma(0) & 1 \\ \Gamma(1) & 1 \\ \vdots & \vdots \\ \Gamma(N-1) & 1 \end{bmatrix} \tag{4}$$

In (3), all parameters are deterministic except $\boldsymbol{w}$ which is a random variable with Gaussian noise. Also, $\boldsymbol{\theta}$ is deterministic but unknown. If the PDF of $\boldsymbol{w}$ is white and Gaussian then we can use linear-minimum variance unbiased estimator to estimate $\boldsymbol{\theta}$. Since

$\boldsymbol{w}$ is colored $\boldsymbol{w}\sim\mathcal{N}(0,\boldsymbol{C})$ a whitening approach can be used to whiten the noise. Since $\boldsymbol{C}$ is assumed to be positive definite $\boldsymbol{C^{-1}}$ is also positive definite and so $\boldsymbol{C^{-1}} = \boldsymbol{D}^T.\boldsymbol{D}$ where **D** is an $N \times N$ invertible matrix. we multiply (2) by $\boldsymbol{D}$

$$\boldsymbol{D}.(\boldsymbol{x} - \Gamma_a) = \boldsymbol{D}.(\boldsymbol{H}.\boldsymbol{\theta} + \boldsymbol{w}) \quad (5)$$

Using $\boldsymbol{x'} = \boldsymbol{D}.(\boldsymbol{x} - \Gamma_a)$, $\boldsymbol{w'} = \boldsymbol{Dw}$ and $\boldsymbol{H'} = \boldsymbol{DH}$

$$\boldsymbol{x'} = \boldsymbol{H'\theta} + \boldsymbol{w'} \quad (6)$$

The noise is whitened since $\boldsymbol{w'} = \boldsymbol{D}.\boldsymbol{w}\sim\mathcal{N}(0,I)$ and the MVU estimator of $\boldsymbol{\theta}$ is [8]

$$\hat{\theta} = \left(\boldsymbol{H'}^T\boldsymbol{H'}\right)^{-1}\boldsymbol{H'}^T\boldsymbol{x'} \quad (7)$$

$\boldsymbol{x'}$is an $N \times 1$ vector of observations and $\boldsymbol{H}$ is a known $N \times 2$ observation matrix of rank *2*, $\boldsymbol{\theta}$ is a 2×1 vector of parameters to be estimated, and $\boldsymbol{w'}$ is an $N \times 1$ in white noise vector with $PDF\ \mathcal{N}(0,\sigma^2\boldsymbol{I})$. After estimating α and β, A_s can simply be obtained by dividing the values of α and β [13]: $\hat{A}_s = \beta/\alpha$.

The covariance matrix for $\boldsymbol{\theta}$ is calculated as

$$C_{\hat{\theta}} = (\boldsymbol{H}^T\boldsymbol{C}^{-1}\boldsymbol{H})^{-1} \quad (8)$$

For the general linear model the MVU estimator is efficient in that it attains the CRLB, i.e $CRLB = C_{\hat{\theta}}$. The c_{11} and c_{22} in matrix $C_{\hat{\theta}}$ are the standard deviation (σ_1^2 and σ_2^2) and c_{12}, c_{21} are the correlation coefficient between estimated values (α and β). Since a covariance matrix is symmetric we have $c_{12} = c_{21}$. In general, a low value for correlation coefficient is desirable in that the estimation of the parameters will have low correlation.

The accuracy in estimating $\hat{A}_s$ depends on several factors: 1) the main assumption in (3) is that $\boldsymbol{w}$ is Gaussian noise. If this assumption does not hold or the noise is *semi-Gaussian* there will be error introduced in estimation process. 2) Sufficient statistics must be performed for an accurate estimation. In ideal case $N \to \infty$ results in a perfect

estimation. However, a big challenge is that the drift and temperature variation in the measuring instrument changes frequently over time. Therefore, the measurement time must be selected in such a way that the variation of noise in the measurement instrument is still Gaussian while enough data has been recorded. 3) The estimation results in much better result if several $\Gamma(i)$ $(i = 0, \dots, N)$ are used in (3) which are far from each other on Γ plane of the antenna. If all selected $\Gamma(i)$ are close to each other or if only one Γ is used the estimation accuracy decreases. In this paper, $Z_{L1}, .. Z_{L5}$ tabulated in Table 2.1 is used for estimating A_s. In this selection, $\Gamma_1, \Gamma_2, \Gamma_3$ are far from each other while $\Gamma_2, \Gamma_4, \Gamma_5$ are very close to each other.

Table 2.1. Selected loads and their RCS.

	Load Impedance (f=1GHz)	Simulated RCS in CST
Z_{L1}	20Ω + 0.5pF	214.79 cm^2
Z_{L2}	10 Ω + 1pF	409.46 cm^2
Z_{L3}	10 Ω + 5pF	156.99 cm^2
Z_{L4}	20 Ω + 1pF	353.93 cm^2
Z_{L5}	30 Ω + 1pF	309.09 cm^2

3. NOISE ANALYSIS

In this section, three topics are presented. First, we discuss how we collect measurements with Gaussian noise distribution. Second, we discuss the whitening process. Third, we show how we calculate the covariance of the collected noise. Loads in Table 2.1 are soldered to antennas and were put individually in the anechoic chamber for measurement. Measurements were performed for each load for $N = 10'000$ ($N \to \infty$) which takes approximately $10\ minutes$ for each load. The noise in the whole measurement setup is calculated by $\boldsymbol{w'} = \boldsymbol{x} - \bar{\boldsymbol{x}}$. Figure 3.1 (a) shows the histogram of the real and imaginary values of the noise for all measurements. It is observed that the noise variation has no specific distribution.

There are several different phenomena contributing in the non-Gaussian noise in a VNA measurement including thermal noise, shot noise, transient time noise, flicker noise, etc [3]. In this work, after each measurement for a load the noise in the measurement is checked. If the noise is non-Gaussian the measurement is repeated for that load until a Gaussian noise profile is obtained. A uniform Gaussian noise variation throughout the experiment is the key and prerequisite factor for an accurate estimation. Figure 3.1 (b) shows the histogram of the noise for a case with $N = 1'000$ for each load. In this case, the PDF of the noise is approximately Gaussian for both real and imaginary parts.

Next, the color of the noise has to be determined and if necessary whitened. To investigate if the noise is white the autocorrelation of $\boldsymbol{w}$ is calculated as $R_{\boldsymbol{w}}(n,k) = E[(\boldsymbol{w} - n).(\boldsymbol{w} - k)]$. The normalized autocorrelation of the measured $\boldsymbol{w}$ is depicted in Figure 3.2 (a) by a blue trace. The autocorrelation of $\boldsymbol{w}$ at sample number 0 is the highest showing the correlation of the data sample with itself. By moving the autocorrelation frame

on the recorded data it is understood that the data is not white. The power spectral density of the $R_w(n,k)$ is defined as $S_{ww}(f) = \mathcal{F}\{R_{xx}(\tau)\} = \int_{-\infty}^{\infty} R_{xx}(\tau)e^{-j2\pi f\tau}d\tau$ and is depicted in Figure 3.2 (b) by a blue trace. In general, the measured $\boldsymbol{w}$ behaves similar to gray noise rather than white. In the next step, *Cholesky decomposition* is performed on $\boldsymbol{w}$ to whiten the noise. The red traces in Figure 3.2 (a) and (b) represent the autocorrelation and the power spectral density of $\boldsymbol{w}$ respectively. As expected, the autocorrelation of the whitened noise is very close to an impulse. Also the power spectral density is very close to a uniform distribution over frequency spectrum.

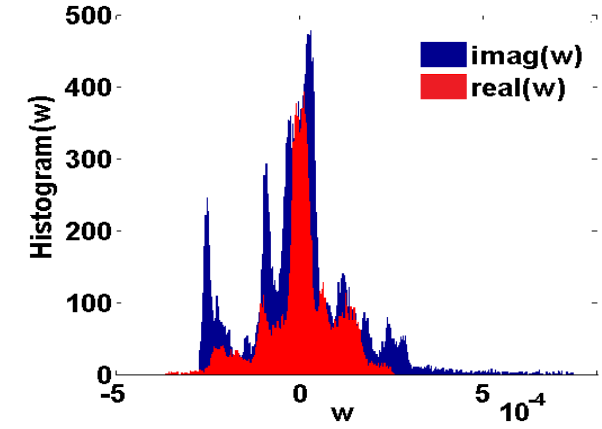

(a) N=10’000 for each load

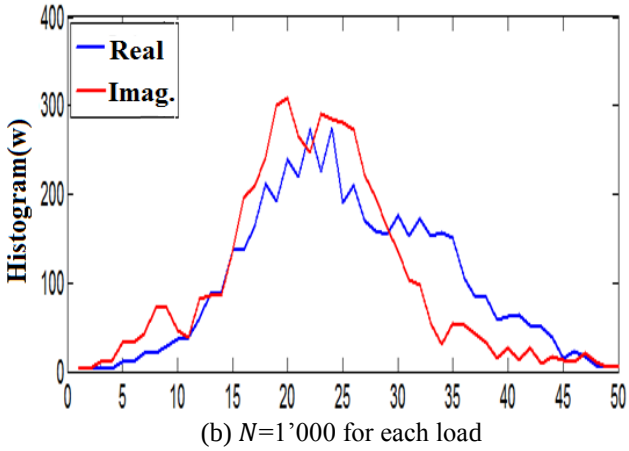

(b) N=1’000 for each load

Figure 3.1. Histogram of real and imaginary of $\boldsymbol{w}$.

Finally, the covariance matrix of the noise is calculated. The noise matrix $\boldsymbol{w}$ is calculated using $\boldsymbol{w} = \boldsymbol{x} - \bar{\boldsymbol{x}}$ in (2) where $\bar{\boldsymbol{x}}$ represents the mean value of observation matrix $\boldsymbol{x}$. The covariance matrix of noise (C) is then calculated at size $L \times L$. A window of noise elements is created as ω =[0 0 ... $w(0)\, w(1) \ldots . w(k)]_{L\times 1}$ and covariance matrix is calculated using

$$C = \frac{1}{N}\sum_{k=0}^{N+L-1} \omega.\omega' \qquad (9)$$

The accuracy of the covariance matrix increases with ration of N/L. In practical implementations, an averaging is used such that $L \leq 0.1N$.

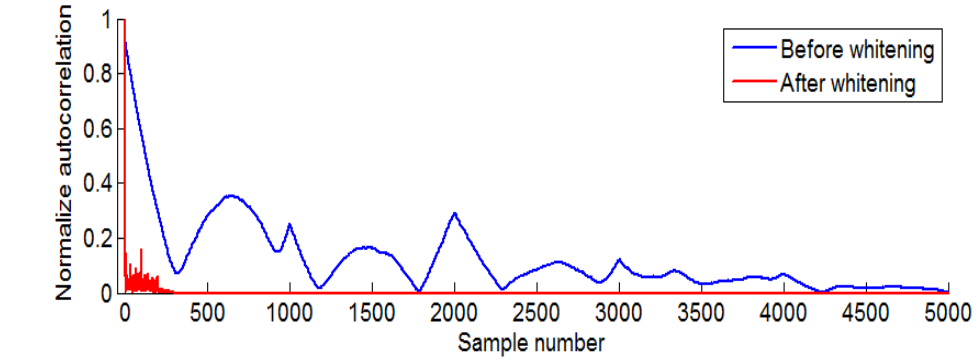

(a) Autocorrelation

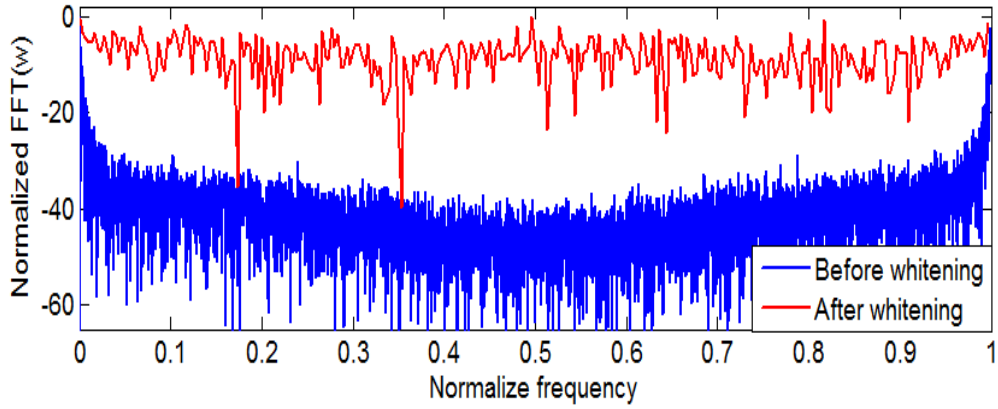

(b) Spectral density

Figure 3.2. Autocorrelation and power spectral density of noise.

4. MEASUREMENT RESULTS AND DISCUSSION

A linear half wave dipole at $f = 1GHz$ is considered for measurement. The antenna support is $16cm \times 1cm$ Rogers RO4350 with $\varepsilon_r = 3.66$. The antenna and the support thicknesses are $0.05\,mm$ and $0.5\,mm$ respectively. The structural scattering coefficient (A_s) of the studied antenna has been investigated in [14] by simulations. With resolution of "0.005" over the Γ plane of the antenna, $(-A_s)$ is found at $\Gamma = -0.965 - j\,0.28$ with $RCS = -75dBsm$ at the main lobe of the antenna [14]. Two sets of measurements are considered: *Estimation 1*: estimating A_s by using three *far reflection coefficients* $\Gamma_1, \Gamma_2, \Gamma_3$ over Γ plane and *Estimation 2*: estimating A_s by using *close reflection coefficients*: $\Gamma_2, \Gamma_4, \Gamma_5$. All Γs are shown in Figure 4.1. As described before, the estimation accuracy depends on selecting "far" Γs in H matrix. Single measurement dataset includes $N = 1000$ samples. Using the created channel between Matlab and VNA it takes approximately 70 seconds to perform 1000 measurements for each individual load. The results were evaluated and those sets which have non-Gaussian PDF are ignored. Whitening process is performed and covariance of noise C is calculated. Finally (6) is used to estimate $\theta = [\alpha\ \beta]^T$. Afterward, by using transformation structural scattering coefficient is found by $\hat{A}_s = \beta/\alpha$.

Figure 4.1 shows the result of estimation for Estimation 1 and Estimation 2 for 11 sets of measurements. The true value of $(+A_s)$ is shown as a blue triangle in the figure. As expected the results of estimation 1, shown in red circle, which uses *far* Γ values, are close to the true value of A_s. On the other hand, the results of estimation 2 which uses *close* Γ values, shown in green circles, have large variation indicating large error in estimating the value of A_s.

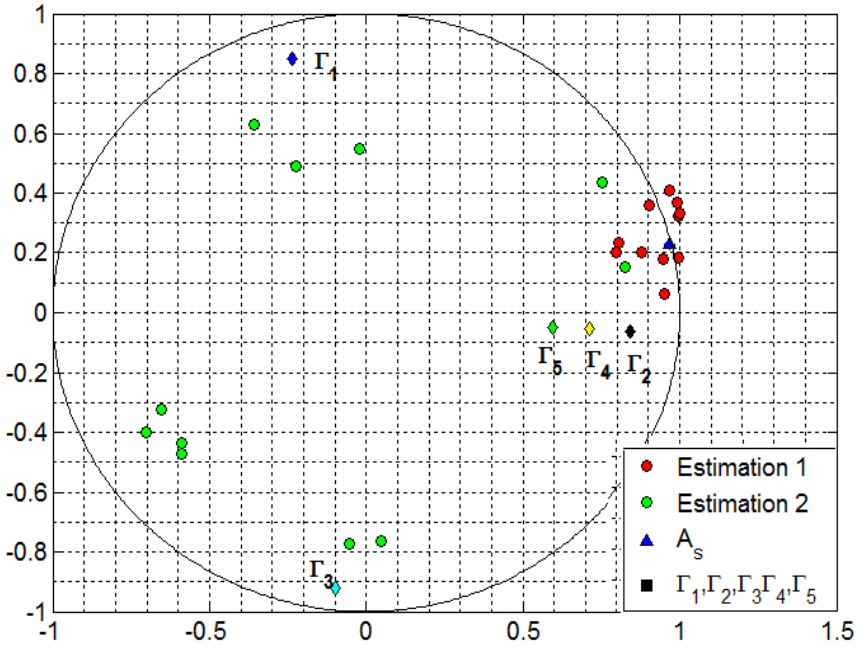

Figure 4.1. Estimation results over Γ plane of the antenna.

Since the estimated A_s is a transformation of the estimated values $\theta = [\alpha\ \beta]^T$ the accuracy of estimating A_s depends on how uncorrelated $\theta = [\alpha\ \beta]^T$ have been estimated. To evaluate this $C_{\hat{\theta}}$ in (7) is examined. The value of c_{12} for 11 sets of measurements are calculated and then normalized to the highest value of them. A histogram of c_{12} parameter of $C_{\hat{\theta}}$ for the results is depicted in Figure 4.2. It is understood that the correlation between the estimated values in θ for Estimation 1 is very low comparing to Estimation 2. As mentioned previously, the CRLB for minimum variance unbiased estimator in linear format is the same as the covariance matrix in (7). Thus, if for an estimation we have $|error| = |A_s - \hat{A}_s| \sim 0$ then the covariance matrix of that estimation is $C_{\hat{\theta}} = CRLB$. The error terms for estimation trials are tabulated in Table 4.1. The lowest possible estimation error is yield at "0.0544"which can be claimed to be the closest estimation attaining CRLB.

Table 4.1. Estimated values for A_s.

A_s	$\|error\|$	% error
0.9943 + 0.3236i	0.0525	5.22
0.9029 + 0.3610i	0.1021	10.15
1.0008 + 0.3336i	0.0645	6.41
0.9481 + 0.1783i	0.1031	10.26
0.8773 + 0.2031i	0.1166	11.60
0.8044 + 0.2330i	0.1673	16.65
0.9912 + 0.3681i	0.0919	9.14
0.9655 + 0.4094i	0.1294	12.87
0.7982 + 0.2027i	0.1838	18.29
0.9495 + 0.0650i	0.2156	21.45
0.9960 + 0.1840i	0.1009	10.03

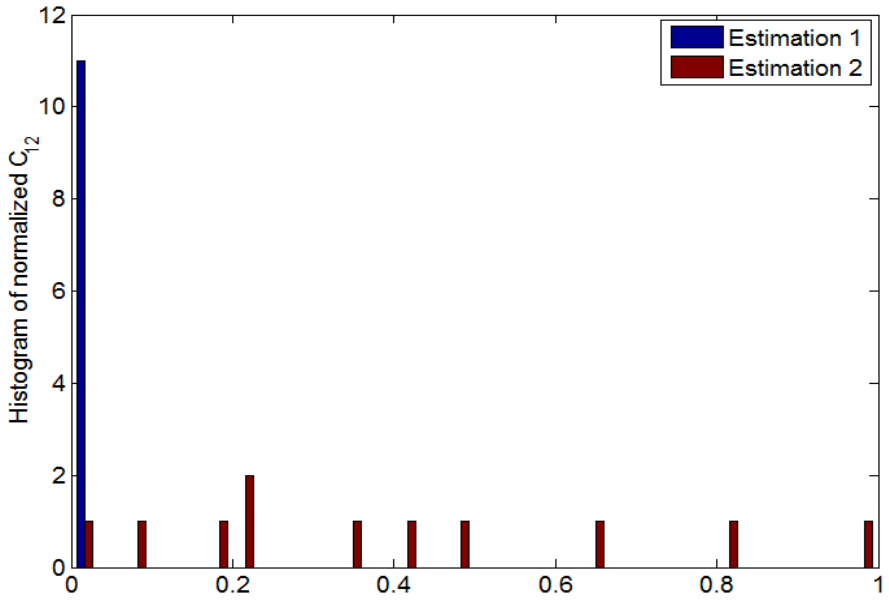

Figure 4.2. Normalized c_{12} for all measurements.

The length of the gathered data in (7) must be at least 10 times of the dimension of the desired covariance matrix. It means that for 3 set of measurements of length 1000 the optimum dimension for covariance matrix will be 300×300. Figure 4.3 shows a comparison among estimations when different L is used in the estimation scenario. At low values of L, i.e. $L = 30,120$, it is understood that the estimation results are very scattered and far from the true value of A_s. At $L = 300$ we notice that the estimation results are generally much more concentrated toward the true value of A_s. At $L = 900$ the estimation results start to be more scattered compared to the true value of A_s. And at $L = 2700$ which is very close to the length of measured data (3000) the estimation results are way off from the true value of A_s.

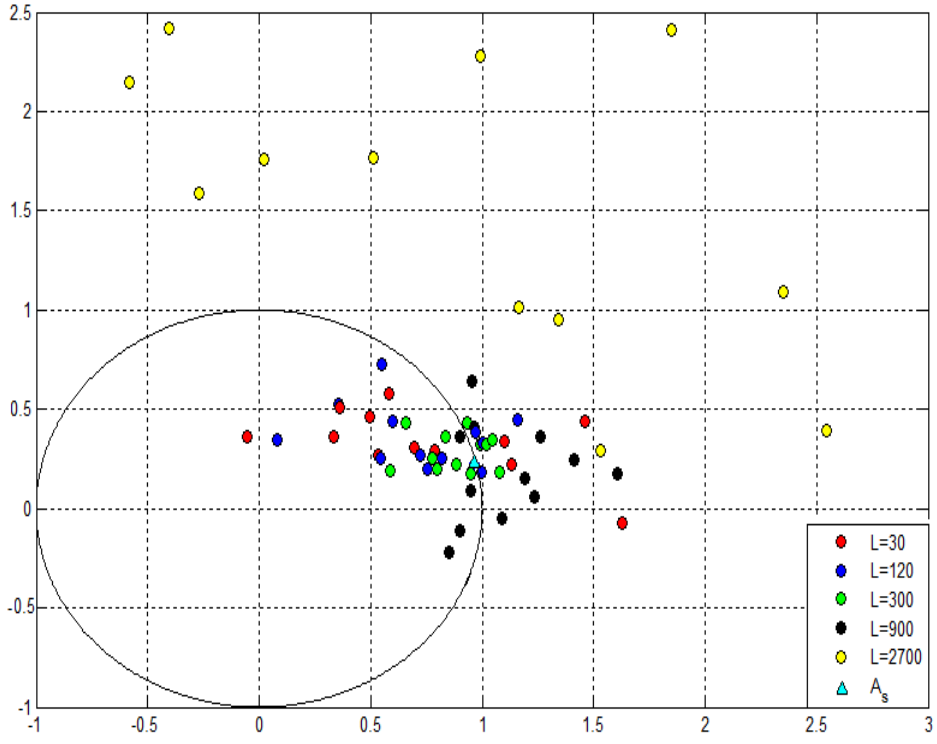

Figure 4.3. The effect of L in the estimation of A_s over Γ plane of the antenna.

5. CONCLUSION

In this paper, a measurement based method for estimating the structural scattering coefficient of a linear half-wave dipole is proposed using linear model of *minimum variance unbiased estimator*. In order to achieve a high accuracy estimation, one needs to: 1) select *far* elements (Γ^i) in observation matrix $\boldsymbol{H}$; 2) ensure a uniform Gaussian noise PDF in the measurement; 3) low correlation between α and β in $\boldsymbol{\theta}$ (small c_{12}); 4) whiten the colored noise; 5) select sufficient number of measurements to calculate covariance matrix (i.e. at least 10x the size of the covariance matrix). The proposed method is asymptotically efficient since it uses a non-linear transformation [13]. In order to preserve efficiency in estimating A_s in (2) *Baysian* or *maximum likelihood* methods can be used as for future works. In that case, knowing the $PDFs$ of both α and A_s is necessary.

REFERENCES

[1] R. B. Green, The general theory of antenna scattering, unpublished Ph.D. dissertation, The Ohio State University, Columbus, december 1963.

[2] Chih-Chuan Yen, Gutierrez, A.E., Veeramani, D., van der Weide, D., "Radar Cross Section Analysis of Backscattering RFID Tags," Antennas and Wireless Propagation Letters, vol. 6 , pp. 279 – 281, 2007.

[3] Ebrahimi-Asl S., Behgam, M. Zawodniok, M.T Ghasr, "Experimental validation of minimum variance unbiased estimator of structural scattering Coefficient for an RFID antenna using linear model," Proceedings of I2MTC, May 2014, pp. 1005 – 1009.

[4] Bletsas, A., Dimitriou, A.G. ; Sahalos, J.N., " Improving Backscatter Radio Tag Efficiency," IEEE Transactions on Microwave Theory and Techniques , June 2010 Volume: 58 , Issue: 6 , Page(s): 1502 – 1509.

[5] Dimitriou, A.G., Bletsas, A., Sahalos, J.N. "Practical considerations of ASK modulated passive tags," Antennas and Propagation (EUCAP), 2012 6th European Conference on , March 2012, Page(s):3476 – 3480.

[6] A. Bletsas , A.G. Dimitriou, J.N. Sahalos, "Backscattering improvement of UHF RFID tag efficiency," Antenna Technology iWAT, pp. 1 – 4, 2010.

[7] Chen, H., Bhadkamkar, A., van der Weide, D. W., "Piggyback modulation for UHF RFID sensors," Microwave Symposium Digest (MTT), May 2010.

[8] T. Sawaya, M. Taromaru, T.Ohira, B. Komiyama, "Experimental Proof of Electrically Invisible State of Inductively Loaded Dipole and Proposal of Electrically Invisible Meander-Lines," IEEE Transac. Antenn. Propag., vol. 54, no. 11, pp. 3374 – 3382, Nov. 2006.

[9] Kastner, R. , Avraham, T., Sternfeld, L., Socher, E., "Structural scattering and the virtual aperture of a half-wavelength dipole antenna," APSURSI, 2012 IEEE, pp. 1 – 2, July 2012.

[10] N. Nakamoto, T. Takahashi, T. Nomura, M. Otsuka, "A method to measure the antenna mode and structural mode for antenna RCS reduction using circulator and phase shifter," ISAP, pp. 21 – 22, Kaohsiung, Dec. 2014 .

[11] A. G. Dimitriou , J. Kimionis, A. Bletsas, J. N. Sahalos , "A fading-resistant method for RFID-antenna structural mode measurement," International RFID-TA, pp. 443 – 448, Nice, Nov. 2012.

[12] C. A. Blanis, Antenna Theory: Analysis and Design, 3rd ed. Hoboken, NJ:Wiely, 2005.

[13] Steven, M. Kay, Fundamentals of Statistical Signal Processing: Estimation Theory, Prentice Hall PTR, 1993, New Jersey.

[14] Shadi Ebrahimi-Asl, M.T Ghasr, M. Zawodniok, "Application of Low Scattering Antennas to RFID Networks," to be appear in proceeding of RFID Conference 2016.

[15] Shadi Ebrahimi-Asl, M.T Ghasr, M. Zawodniok, " Method and Device for Improving Performance of RFID Systems," US Provisional Patent Application 62/236,490, October 2015.

II. DUAL LOADED RFID TAG FOR HIGHER ORDER MODULATIONS

ABSTRACT

Scalar and vector differential backscattering for RFID tags are discussed. Green model has long been used as a touchstone for selecting the scattering states in scalar differential backscattering from RFID tags. In this paper, first the radar cross section of a half-wave dipole and a T-match bowtie antenna over their Γ planes are studied. Simulation and measurement results show that the RCS of the linear half-wave dipole can well be explained by Green model. However, we show that a T-match bowtie antenna has two maximum scattering areas on its Γ plane. This behavior of the RCS for T-match bowtie antenna is not explained by Green model. Next, we propose a new antenna design by using dual loading in the antenna structure of the studied T-match bowtie antenna. The proposed antenna can provide different scattering states with different magnitudes in 360° phase span in in-phase and quadrature plane. This property of our proposed antenna can be used to: (1) increase the modulation depth to 170%, (2) provide a quasi-32-QAM.

1. INTRODUCTION

Passive Radio frequency identification (RFID) systems have been very popular recently in numerous short range data communication applications (e.g. sensor networks, data acquisition, object tracking, retail industry, etc.). The basic operation of a passive RFID system is as follows. An RFID reader sends out an interrogation signal to a target RFID tag. By impinging the signal on the antenna structure of the target an induced current is formed on its antenna structure. This current can help the tag to run its internal circuitry and check if its ID has been interrogated. When a specific tag ID is queried, the tag sends backs its stored data by *differential backscattering* technique [1]-[6]. To this end, the tag switches its load impedance between two values to encode either "0" or "1" bit from its stored data. By switching the load impedance, the antenna is placed in different *scattering states* while changing the antenna radar cross section (RCS). This change of RCS at the reader can be characterized as a stream of data. Since differential backscattering is performed by a change in the amplitude of backscattered signal it is regarded as an Amplitude Shift Keying modulation type. In this paper, we call this modulation as *scalar differential backscattering* (SDB).

Selecting two optimum impedances in SDB links is very critical in achieving the maximum differential RCS. The bigger the differential RCS is: (a) the more immune the backscattering link is in response to the environment noise and interference, (b) the farther the reader can detect it. A touchstone model to select two scattering states is the scattering model introduced by Green in [4] which later on was studied again in [5]. In this model, the RCS from an antenna with impedance Z_a ($Z_a = R_a + jX_a$), loaded with Z_L and illuminated by an arbitrary field is shown by

$$\sigma = \frac{\lambda^2}{4\pi} G^2 |\Gamma + A_s|^2 \quad (1)$$

where G is antenna gain at wavelength λ, A_s is a constant describing structural scattering coefficient of the antenna, and Γ is a modified current reflection coefficient:

$$\Gamma = (Z_a^* - Z_L)/(Z_L + Z_a) \quad (2)$$

such that $|\Gamma| \leq 1$ for all passive loads. The complex modified reflection coefficient ($\Gamma = \Gamma_r + j\Gamma_i$) can be plotted on Γ plane of the antenna by considering $z=(Z_L + jX_a)/R_a$ and $\Gamma = \frac{1-z}{1+z}$. In this case, the Γ plane represents a current Smith chart with reference to z. in this paper, we call equation (1) as *Green model*. Equation (1) represent a circle with center $\Gamma = -A_s$ and radius $r = (\frac{4\pi\sigma}{\lambda^2 G^2})$ on Γ plane of an antenna. The RCS of the antenna at the center of this circle is zero. This point on the Γ plane is called the invisibility point of the antenna. By using the corresponding load at this point, the antenna becomes a *minimum scattering antenna* [6]. In order to find ($-A_s$) on the Γ plane three Γs not lying on the same circle are considered and the antenna RCS at these loads are measured. The intersection of these three circles on Γ plane uniquely shows the point $(-A_s)$ [2], [4], [5].

Figure 1.1 shows the 3 scattering circles and $(-A_s)$ point for a half-wave dipole at $f = 1GHz$ which we study in this paper. If a Γ close to $(-A_s)$ is selected as the load for the antenna, e.g. Γ_1, the right side of (3.1) takes a lower value and the antenna RCS of the antenna becomes low. On the other hand, if a Γ which is the farthest to $(-A_s)$ is selected, e.g. Γ_3, the right side of (3.1) takes the highest value and the antenna RCS becomes maximum. The antenna at this scattering state is called a *maximum scattering antenna*. In current deployments of differential backscattering links the two scattering states of an

RFID antenna are selected as $\Gamma_{state1} = -A_s$ and $\Gamma_{state2} = \Gamma_3$. This provides the maximum possible differential RCS from the antenna.

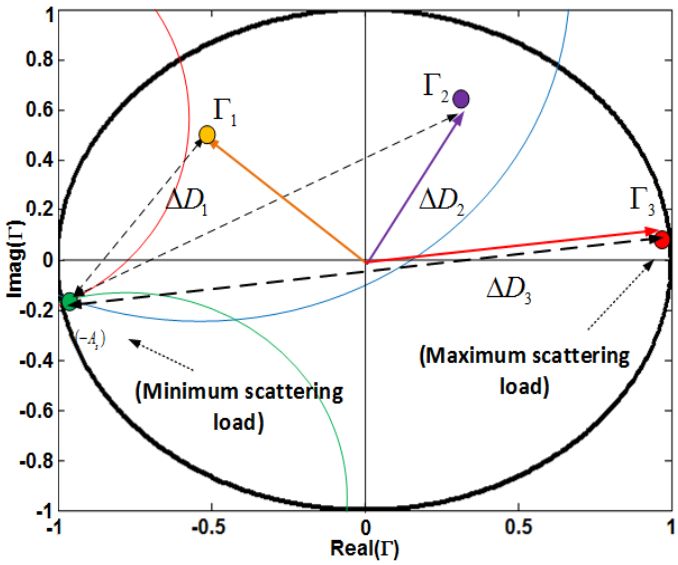

Figure 1.1. Representation of (-A_s) for the studied half wave dipole at $f = 1GHz$.

Phase Shift Keying modulation for backscattering links was first discussed in [3]. In this modulation, the reactance portion of the load is changed to produce a change in the phase of backscattered field from the RFID antenna. Thus, in this modulation method for backscattering links the data is encoded in the variation of the phase in the backscattered field. In this method, a scattering state is recognized by its RCS and also the phase of the backscattered field form the antenna. The change in the reactance may not result in a big change in the RCS of the antenna. Thus, the reader antenna must be able to detect the variation of the phase in the backscattered field (a coherent detector). In this paper, we call this modulation type *vector differential backscattering* (VDB). The maximum vector differential RCS in VDB is achieved if two maximum scattering states with 180° phase shift are used. However, there are two issues about this. First of all, according to (3.1) an

antenna has only one maximum scattering state. Second, the variation of the induced phase on the antenna based on different loads on its Γ plane must be studied to figure out if two "high scattering states" with 180° phase shift can be obtained. We discuss about this more in Section 2 and 3.

In [7], a quasi-Quadrature Amplitude Shift Keying (QAM) is discussed. The four studied scattering states are spread in 90° phase span in the in-phase and quadrature (I-Q) plane. In order to detect the signal at the reader, detection boundaries are defined in the first quadrature of I-Q plane. However, since the proposed scattering states are closely spaced in 90° phase span, by any interference or noise in the environment scattering states are drifted into the detection boundaries of other states resulting in a fault detection. Some other works in the literature have studied QAM modulations for backscattering links. However, they all use a 50 Ω impedance to characterize the input impedance of the antenna in (2) [8]-[11]. In [12] a chip-less RFID tag is introduced which can produce 16-QAM using delay lines in transmission lines theory. However, this RFID tag, can be used for identification of 16 different objects and cannot be used for transferring streams of data.

Dual loading, and multiple loadings, has been used in the literature for reducing measurement errors in material characterizations [12], [13]. In this paper, we use dual loading to introduce a new RFID tag antenna design which can produce scattering states with various amplitudes within 360° phase span [15]. By load switching at two stimuluses on the antenna structure, the proposed antenna design can provide a quasi-32-QAM. In the first step, we study the RCS of a linear half wave dipole and the T-match bowtie antenna from [5] over their Γ planes. We show by measurements and simulations that the variation of RCS for the linear half-wave dipole is as described by (1). But, RCS for the studied T-

match bowtie antenna is not completely defined by (1). In addition to the main maximum scattering area on the Γ planes defined by (1) the T-match bowtie antenna also has a secondary maximum scattering area which is located right next to its minimum scattering area of the antenna on its Γ planes. We also, show that although for both antennas two scattering states with 180° phase shift can be accomplished over their Γ planes the resultant vector differential RCS is smaller than that of SDB. Next, we introduce our proposed antenna in Section 3. We make a $1mm$ gap at the center of the studied T-match bowtie antenna. This is the first stimulus on the antenna and is called *operation mode* of the antenna. The second stimulus of the antenna is set at the original input port of the antenna and is called *operation state* of the antenna. We show by measurements that by load switching at both of the stimuluses of the antenna, it is possible to produce several scattering states with different magnitude and phase characteristics. This property of the proposed antenna can be used to introduce a higher order modulation (up to quasi-32-QAM) for the backscattering link of the antenna.

2. LINEAR AND RESONANT RFID ANTENNAS

In this Section, we study the variation of RCS and the phase of the induced current on a linear half-wave dipole and the T-match bowtie antenna from [5] over their Γ planes by simulations and measurements. The phase of the induced current is directly proportional to the phase of the scattered electric field from the antennas. In measurements, the magnitude and phase of the scattered fields are measured using modulated scattering technique. The behavior of the studied linear half-wave dipole is in agreement with Green model. However, we show by simulations and measurements that the studied T-match bowtie antenna has two maximum scattering areas on its Γ plane. This behavior cannot be modeled by Green model in (1).

2.1 LINEAR HALF-WAVE DIPOLE

A linear half-wave dipole at $f = 1GHz$ is considered on Rogers RO4350 substrate for simulations and measurements. The substrate and antenna thickness are $0.5\,mm$ and $0.05\,mm$ respectively. The antenna input impedance at the design frequency is $Z_a = 114.53 + j171.38$ using CST Studio simulations. The minimum scattering point for this antenna is $\langle \Gamma_r = -0.965, \Gamma_i = -0.28 \rangle$ with $RCS\sim -58\,dBsm$ [6]. On each point on Γ plane the impedance is calculated using (2). The step size is considered as $\Delta\Gamma = 0.1$. The RCS and the induced phase over the Γ plane are then simulated. Figure 2.1 (a) and (b) show the simulated RCS and the induced phase at the input port of the antenna over the Γ plane. By using the resolution of "0.1", the minimum scattering point of the antenna on this grid is found at $\langle \Gamma_r = -0.95, \Gamma_i = -0.3 \rangle$ with $RCS\sim -45dBsm$. By moving away from this minimum scattering point $(-A_s)$ the RCS increases. At the right side of the Γ plane RCS

reaches to a maximum around $RCS\sim -10dBsm$. This behavior is as described by Green model in (1) and also previously investigated in Figure 1.1 in Section 2.

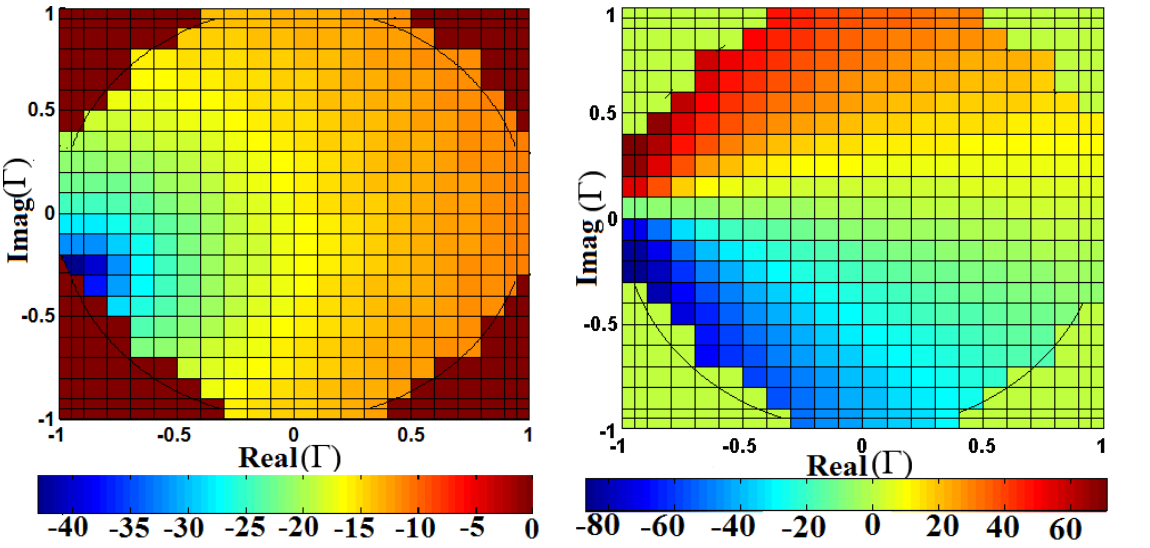

(a) RCS ($dBsm$) (b) Phase of the current (degree)

Figure 2.1. Variation of RCS and induced phase for half-wave dipole.

The variation of the phase of induced current at the input port of the antenna in the bottom side ($\Gamma_i < 0$) and top side ($\Gamma_i > 0$) of Γ plane is respectively negative and positive as understood form Figure 2.1 (b). Furthermore, the variation of induced phase on the line $\Gamma_r = 0.98$ which is in the most right side of Γ plane, i.e. maximum scattering area, is almost $\Delta\Phi\sim 25°$. On the other hand, the variation of the induced current phase on line $\Gamma_r = -0.98$ which is on the most left side of the Γ plane, i.e. the minimum scattering area, reaches to $\Delta\Phi\sim 160°$. Although a wide variation of phase can be achieved on $\Gamma_r = -0.98$ the variation of RCS is very negligible on this line.

2.2 RESONANT T-MATCH BOWTIE ANTENNA

The T-match bowtie antenna design from [5] is considered for our study at the same design frequency of $f = 915MHz$. The antenna input impedance at the design frequency is found as $Z_a = 3.86 + j149.56$ using CST Studio simulations. The impedance at each point on Γ plane is calculated using (3.2). The RCS and induced phase at the antenna input is simulated over Γ plane. We noticed that the variation of both RCS and induced phase in the left side of the Γ plane of the antenna is considerably higher comparing to the right side of the Γ plane. Figure 2.2 (a) and (b) show the simulated RCS and induced phase at the input port of the antenna in the left side of the Γ plane of the antenna. From Figure 2.2 (a), it is understood that at $\langle \Gamma_r = -0.97, \Gamma_i = -0.25 \rangle$ RCS reaches to a minimum around $\sim -35\ dBsm$. However, immediately at the right side of this area there is a maximum scattering area with $RCS \sim -15\ dBsm$. The variation of the phase in this area on Γ plane is very steep as shown in Figure 2.2 (b). As an example at $\langle \Gamma_r = -0.99, \Gamma_i = -0.15 \rangle$ the induced phase is $\varphi \sim -100°$. While the induced phase at $\langle \Gamma_r = -0.99, \Gamma_i = +0.15 \rangle$ is $\varphi \sim +60°$. The RCS at both of these scattering states are approximately $RCS \sim -22\ dBsm$. Although the distance of these two scattering states on Γ plane is very small ($\Delta\Gamma = 0.3$) they can provide $\sim \pm 160°$ phase shift at the backscattering from the antenna.

A better representation of the Figure 2.2 (a) is shown in Figure 2.3 (a). It shows the simulated RCS for several constant Γ_r lines as a function of Γ_i on the antenna Γ plane. On the most left side of Γ plane ($\Gamma_r = -0.97$) the RCS is minimum at $\langle \Gamma_r = -0.97, \Gamma_i = -0.24 \rangle$. Next, on the line $\Gamma_r = -0.92$, RCS starts with a maximum ($\sim -15dBsm$) at $\langle \Gamma_r = -0.92, \Gamma_i = -0.4 \rangle$, then plunges to $\sim -24dBsm$ at $\langle \Gamma_r = -0.92, \Gamma_i = -0.24 \rangle$ and

then increases to $\sim -19\,dBsm$ at $\langle \Gamma_r = -0.92, \Gamma_i = 0.4 \rangle$. This behavior repeats for constant lines $\Gamma_r = -0.9, -0.86, -0.7$. At $\Gamma_r = 0.5$, RCS reaches to a constant value at $\sim -18dBsm$ for all imaginary values on Γ plane. Finally, at the most right side of the Γ plane again the RCS is constant on line $\Gamma_r = 0.98$.

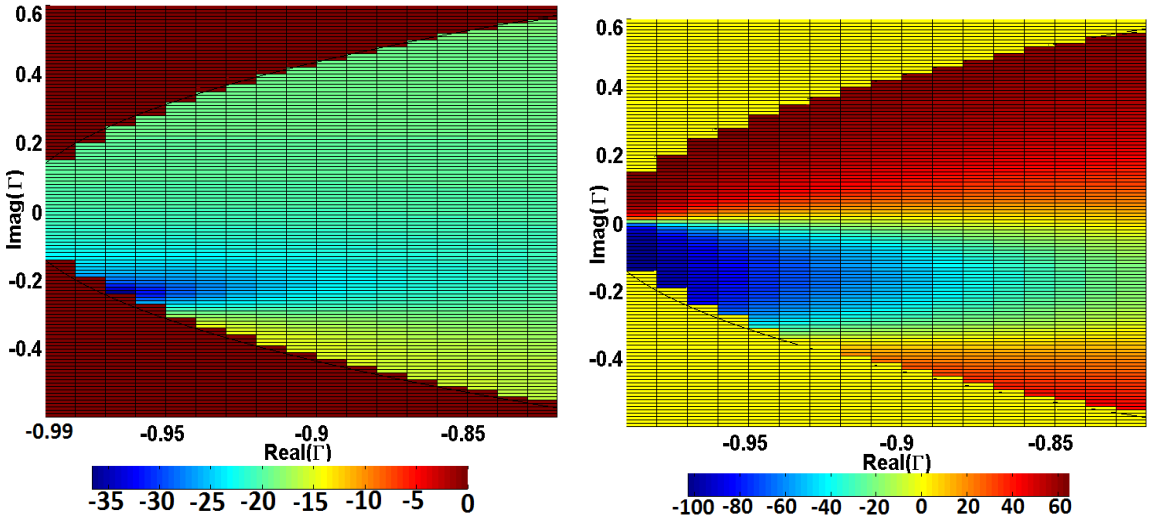

(a) RCS (b) Induced phase

Figure 2.2. Variation of RCS and induced phase in minimum scattering area.

According to the results, the T-matched bowtie antenna has two primary and secondary maximum scattering areas. The primary scattering area is predicted by Green model in (3.1) at the right side of the antenna's Γ plane. The RCS at this area is found around $\sim -19dBsm$. On the other hand, the secondary maximum scattering area has not been predicted by Green model. Interestingly, the RCS at this area is approximately $\sim -15dBsm$ which is higher than the RCS in the primary maximum scattering area.

The induced phase at the input port of the antenna for several constant Γ_r lines over Γ_i are depicted in Figure 2.3 (b). At the most left side of the Γ plane on the line $\Gamma_r = -0.97$ the induced phase changes from $\varphi_1 \sim -90°$ at $\langle \Gamma_r = -0.97, \Gamma_i = -0.25 \rangle$ to $\varphi_2 \sim -65°$ at

$\langle \Gamma_r = -0.97, \Gamma_i = 0.25 \rangle$. By moving toward the right side of Γ plane the induced phase tend to take a constant value over the entire imaginary values on Γ plane. At the most right side of Γ plane the induced phase on line $\Gamma_r = 0.98$ is a constant value at $\varphi \sim 58°$.

It should be mentioned that using the modified current reflection coefficient in (2), results in very negligible variation of both real (resistance) and imaginary (reactance) values of the impedance on the right side of Γ plane for T-match bowtie antenna. This results in the constant RCS and induced phase on the right side of Γ plane in Figure 2.3. However, on the left side of Γ plane using (2) results in steep variation of impedance which causes steep variation both in phase and RCS in this area. On the other hand, for the studied linear half-wave dipole the variation of the impedance is distributed over the entire Γ plane. Thus, the variation of RCS and phase are also spread over entire its Γ plane.

2.3 MEASUREMENTS

In this section, we present the measurement results for the backscattering of the two studied antennas at different scattering states.

2.4 MEASUREMENT SETUP

To measure the scattering properties of the two aforementioned antennas, several load impedances were selected as shown in Tables 3.1 and 3.2. These load impedances were selected to place the antenna scattering on a desired area of the Γ plane as shown in Figure 2.4 (a). In Figure 2.4 (a) each load impedance is represented by a color and a marker type. Yellow and blue markers represent the corresponding loads for half-wave dipole and

T-match bowtie antennas respectively. The marker shapes represent the load number for each antenna based on Table 2.1 and 2.2.

A pin diode is used at the input port of the antennas to modulate their backscattered fields. The modulation of the backscattered field of the antenna is necessary to extract it from the clutter of background noise in the environment. The diode is biased by connecting the antenna through thin wires to rectangular signal generator Agilent 81150A. The signal generator creates a pulse train at $f = 10Hz$ and $\pm 0.7v$. To isolate the induced ac current on the antennas from the thin bias wires, inductors (L=100μH) are soldered between the pin diode and wires as shown in Figure 2.4 (b). Wires are made orthogonal to the polarization of the antenna and reader to minimize their interference.

Table 2.1. Selected loads for half wave dipole antenna.

Z_{L1}= 20Ω +0.7pF	Z_{L4}= 50Ω +2pF	Z_{L7}= 17.8Ω +110nH
Z_{L2}= 4.5Ω +1pF	Z_{L5}= 118Ω +0.5pF	Z_{L8}= 10Ω +22nH
Z_{L3}= 50Ω +0.6pF	Z_{L6}= 118Ω +12nH	Z_{L9}= 118Ω +0.2pF

Table 2.2. Selected loads for T-match bowtie antenna

Z_{L1}=0.2 Ω+ 1pF	Z_{L5}=10 Ω +5pF	Z_{L9}=2.26 Ω +1.3pF
Z_{L2}=10 Ω+ 0.94pF	Z_{L6}=0.5 Ω +1.8pF	Z_{L10}=0.5 Ω +1.26pF
Z_{L3}=0.9pF	Z_{L7}=5.1 Ω +1.5pF	Z_{L11}=15 Ω +1.15pF
Z_{L4}=50 Ω +0.9pF	Z_{L8}=2.26 Ω +1.4pF	Z_{L12}=0.5 Ω +1.15pF

A horn antenna is used as the reader antenna and is connected to the VNA Agilent E5061B. We measure S_{11} at the input port of the horn antenna. Figure 2.5 depicts S_{11} for one measurement case. As understood from the figure 2.5 by biasing the diode the scattered field form the antenna under test is modulated between two states. The modulation depth for the backscattered signal is defined as [1], [14]

$$MD = \frac{|V_{high} - V_{low}|}{|V_{high}|} \tag{3}$$

and it shows by how much the modulated variable of the carrier signal varies around its unmodulated level. The measured S_{11} is proportional to the vitiation of backscattered field from the antenna. Since the scattered field also is proportional to the induced current on the antennas (I) we have $S_{11} \propto I$ [6]. Furthermore, since the RCS of an object is

$$\sigma = \lim_{r \to \infty} 4\pi r^2 \frac{|E_s|^2}{|E_i|^2} \tag{4}$$

where E_s is the scattered field from the antenna and E_i is the incident wave form reader, the RCS from the antenna and its current are related by $\sqrt{\sigma} \propto I$. To demodulate the backscattered field we use: $p_d = \frac{1}{N_p} \sum_{n=1}^{N} S_{11}(n).\Lambda(n)$ where $\Lambda(n)$ is a sign function which is triggered to $+1/-1$ when the diode changes its state. We have $p_d = |p_d| \sphericalangle p_d = \delta e^{j\varphi}$. Since p_d is the integral of the measured S_{11} we also have $p_d \propto I$ and $p_d \propto \sqrt{\sigma}$.

One important factor in comparing the phases of different scattering states for an antenna is that they all must be compared by the same references: (1) All backscattering signals (p_d) are measured with reference to the open circuit state (reverse bias of diode) at the antennas. (2) The antennas must be placed exactly at the same place on the antenna support shown in Figure 2.4 (b) for all measurements. (3) All received signals must be integrated with the same $\Lambda(n)$ to keep the information of the phase of the signal. To this

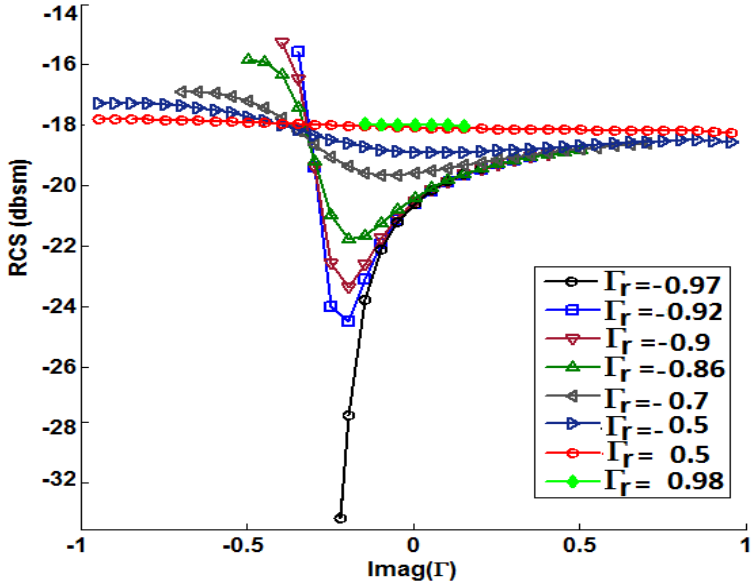

(a) Variation of RCS on different Γ_r line.

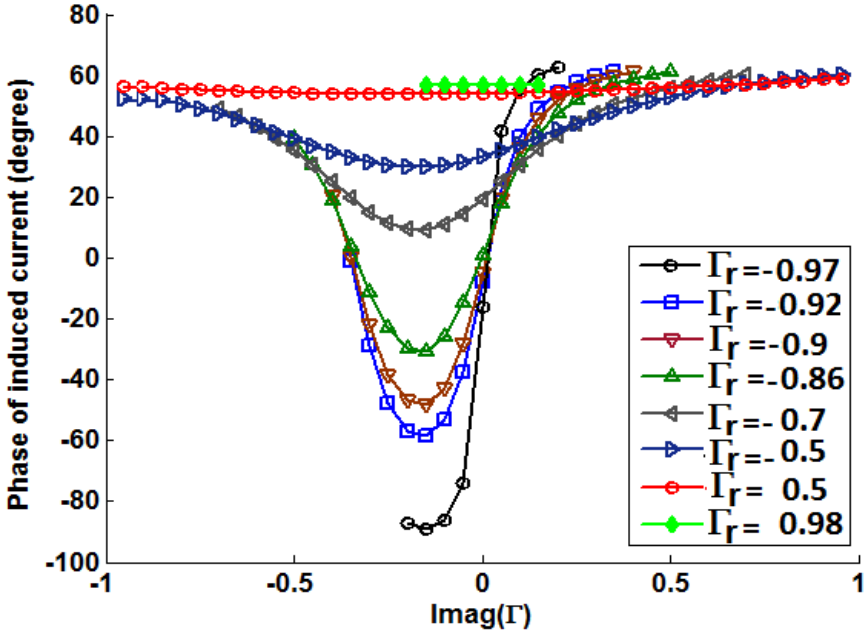

(b) Induced phase (Φ) on different Γ_r line.

Figure 2.3. Variation of RCS of T-match bowtie antenna.

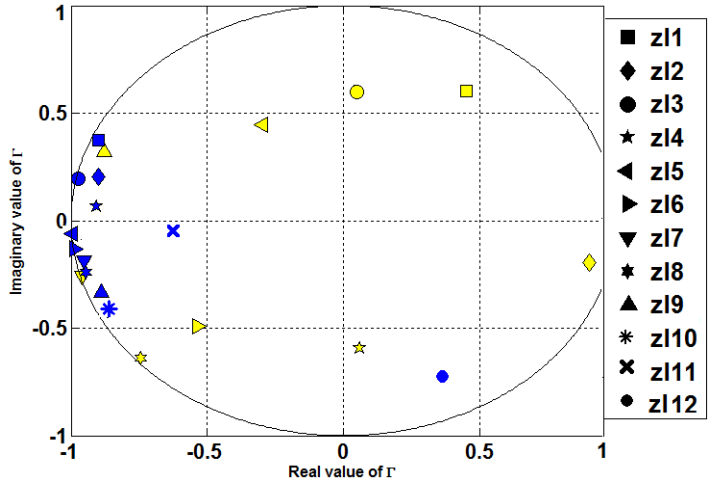

(a)

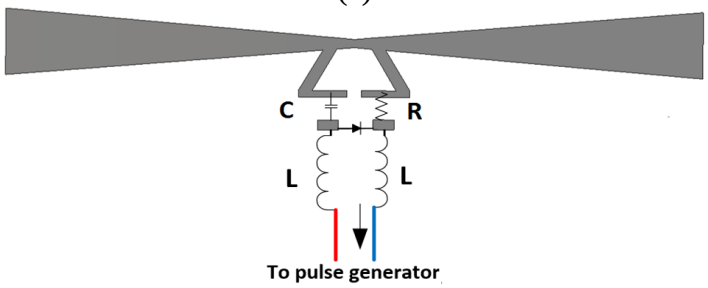

(b)

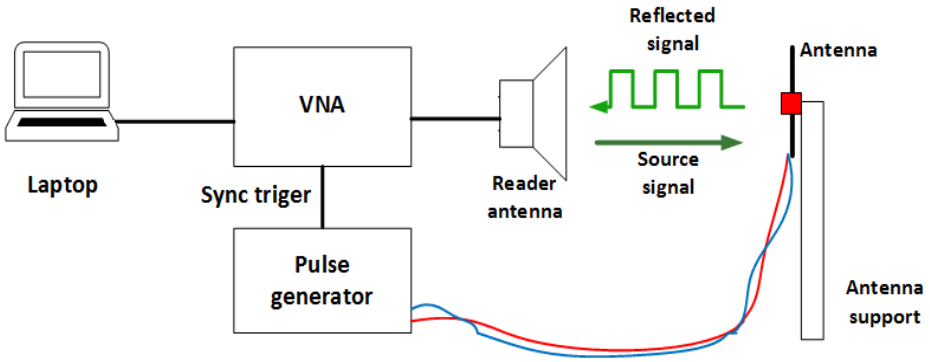

(c)

Figure 2.4. (a) Load impedances from each antenna's Γ plane are selected and are shown on a common Γ plane. The impedance of the diode in its forward bias (1Ω+0.7nH) is also added to the total load at the input port of the antennas. (b) Prepared T-match antenna for measurements (c) Measurement set up.

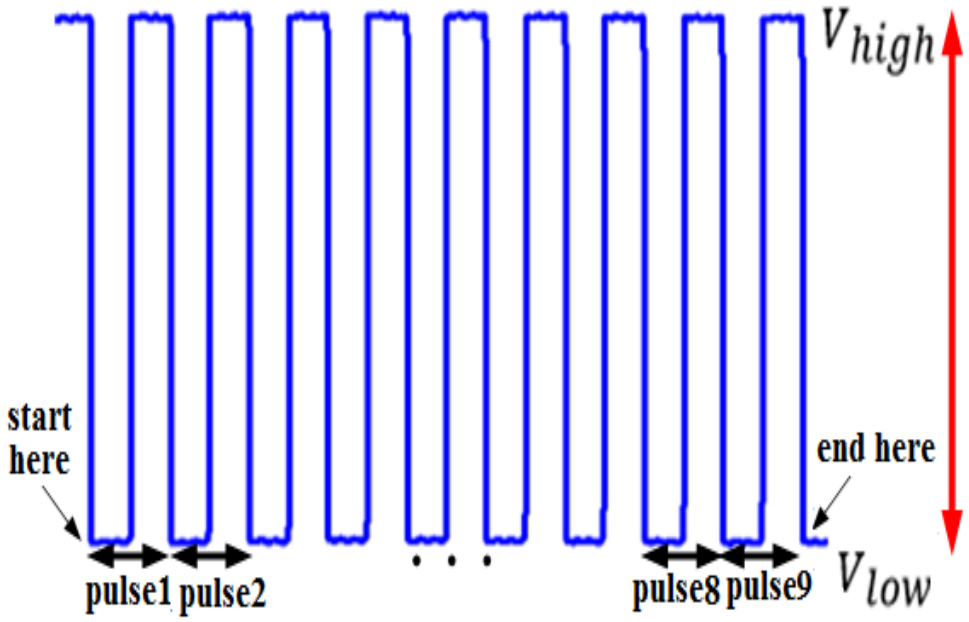

Figure 2.5. The measured S_{11}.

end, in each measurement the starting point of a complete pulse in the received backscattered signal is found as shown in Figure 2.4. Afterward, the same $\Lambda(n)$ function is used to integrate 9 following pulses from the backscattered signal. For this setup, we use $N = 500$ and $N_p = 9$.

2.5 MEASUREMENT RESULTS

The impedances tabulated in Table 2.2 and 2.3 are soldered to the antennas. Antennas are put individually on the measurement setup as shown in Figure 2.4 (c). The measurement for each scattering state is repeated for 3 times. Figure 2.6 (a) and (b) show the real and imaginary values of the demodulated signal (p_d) for different scattering states of respectively half-wave dipole antenna and T-match bowtie antenna.

We notice error in measurement for each scattering states. This error can be attributed to the error in placing the antennas at the exact previous location on the antenna support. Also, any movements in the antenna support itself can be considered as the reason for this error. In general, however, we notice almost the same behavior (magnitude and phase of demodulated signal) for the measurements in all scattering states. For half-wave dipole antenna, it is understood from Figure 2.6 (a) that by using Z_{L7} and Z_{L2} the antenna RCS reaches to a minimum and a maximum respectively. These results were expected from Figure 2.1 (a) and 3.5 (a) since these loads are selected very close to the minimum and maximum scattering states of the antenna.

According to Figure 2.6 (a), the induced phase at scattering states Z_{L1}, Z_{L3}, Z_{L5}, Z_{L9} lead the induced phase at Z_{L2} . This observation is in agreement with Figure 2.1 (b) where loads Z_{L1}, Z_{L3}, Z_{L5}, Z_{L9} lead the induced phase at Z_{L2} by $\Delta\Phi\sim40°$, $\Delta\Phi\sim50°$, $\Delta\Phi\sim60°$, $\Delta\Phi\sim85°$ respectively. At the same time, we observe a gradual decrease in the magnitude of p_d while we move away from Z_{L2} and passing through scattering states Z_{L1}, Z_{L3}, Z_{L5}, Z_{L9}. We also notice the same behavior of RCS of the antenna from Figure 2.1 (a). On the other hand, for loads Z_{L4}, Z_{L6}, Z_{L8} which are located in the bottom side of Γ plane the induced phase at the antenna lag the phase in Z_{L2} state as noticed from measurement results in Figure 2.6 (a). This lag in phase is $\Delta\Phi\sim-15°, \Delta\Phi\sim-60°, \Delta\Phi\sim-70°$ respectively for loads Z_{L4}, Z_{L6}, Z_{L8}. Furthermore, we also observe a gradual decrease in magnitude of p_d as we move away form Z_{L2} and passing through these loads Z_{L4}, Z_{L6}, Z_{L8}. We understand the same behavior in the simulated RCS of the antenna in Figure 2.1 (a).

For T-match bowtie antenna, the backscattering characteristics of Z_{L1} to Z_{L4} which are on the upper ($\Gamma_i > 0$) left side of Γ plane have approximately the same RCS and induced

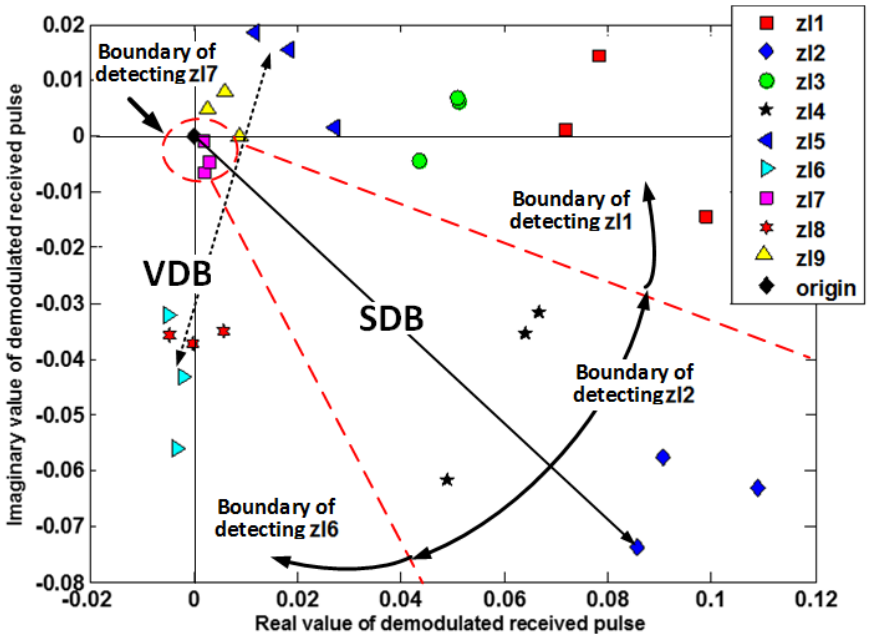

(a) Demodulated signal from half-wave dipole antenna

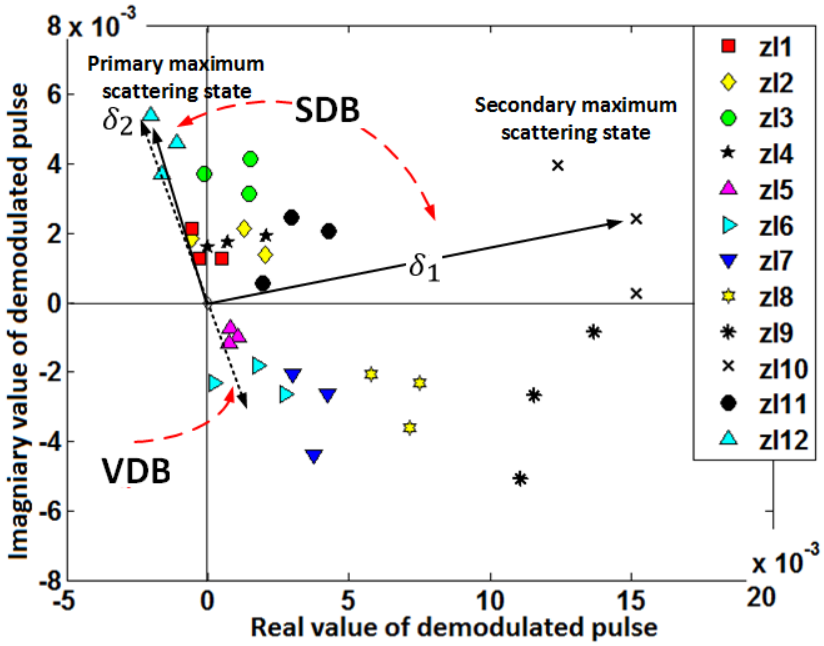

(b) Demodulated signal fromT-match bow tie antenna.

Figure 2.6. The measured differential backscattering from antennas.

phase. This was also understood in the simulations results in Section 3.3.1. By moving to $\Gamma_i < 0$ on the left side of Γ plane a big change in the induced phase is noticed as understood from the backscattering of Z_{L5}. This wide variation in the induced phase is predicted in simulation as described in Figures 3.3 (b) and 3.4 (b). By moving toward the secondary maximum scattering area (Z_{L6} to Z_{L10}) an increase in the RCS of the antenna is noticed as suggested from simulations results in Figures 2.2 (a) and 2.3 (a).We observe this in the magnitude of demodulated p_d in Figure 2.6 (b) in that $|p_d|$ increases while moving from Z_{L6} to Z_{L10}. At the same time, the induced phases of demodulated p_d grow more positive when moving from Z_{L6} to Z_{L10}. This behavior is observed in Figure 2.4 (b) where the demodulated signals from Z_{L6} to Z_{L10} are leading in phase comparing the phase of Z_{L5} ($\Phi_{ZL5} < \Phi_{ZL6} < \Phi_{ZL7} < \Phi_{ZL8} < \Phi_{ZL9} < \Phi_{ZL10}$). For Z_{L12} which is close to the primary maximum scattering area of the antenna the variation of the phase is close to that of Z_{L1} to Z_{L4} as expected from simulations results. The steep variation of RCS of T-match bowtie antenna in a small area has both advantages and disadvantages. Using this characteristic of the antenna by switching between a small values of impedance large variation of RCS is achieved which is an advantage. On the other hand, a disadvantage of this antenna characteristic can be attributed to the shift of impedance due to temperature and sensitivity of the components resulting in an un-wanted change in the impedance and as a result the corresponding RCS of the antenna.

For scalar differential backscattering defined by Green model, scattering states $\{Z_{L7},\ Z_{L2}\}$ for half-wave dipole can be used which respectively produce the minimum and maximum scatterings from the antenna. For T-match bowtie antenna, scalar differential backscattering defined by Green model can be produced by using Z_{L12} and the minimum

scattering state of the antenna. In this paper, by using the typical impedance values in the lab, this minimum scattering state could not be realized. The secondary maximum scattering states of the antenna can be achieved at Z_{L10} or Z_{L11}. As understood from Figure 2.6 (b) the magnitude of the signal at primary scattering state (δ_2) is lower than the magnitude of the signal at secondary maximum scattering state (δ_1). To conclude: (1) T-match bowtie antenna has two maximum scattering areas on its Γ plane: primary and secondary. The secondary maximum scattering area is not described by Green model. (3.2) The RCS of T-match antenna at its secondary maximum scattering state is higher than antenna RCS in primary maximum scattering state.

According to the measurement results, for both antennas two scattering states with phase difference close to $\varphi \sim 180°$ can be achieved. These scattering states are $\{Z_{L5},\ Z_{L6}\}$ for half-wave dipole and $\{Z_{L6},\ Z_{L12}\}$ for T-match bowtie antenna. However, the resultant vector differential backscattering are not higher than that that of scalar differential backscattering obtained by Green model. Thus, using VDB cannot increase the modulation depth over SDB.

Scattering states with different phases can be used for increasing the bit rate in backscattering links. As an example, by using Green model for half-wave dipole antenna each of the two scattering states $\{Z_{L2}, Z_{L7}\}$ characterizes one bit: ”0” or “1”. However, if four scattering states are considered as $\{Z_{L1}, Z_{L6}, Z_{L2}, Z_{L7}\}$ then they can account for 2 bits to encode {00, 01, 10, 11} in a stream of data. To this end, boundaries of detection must be characterized for each scattering states so that the reader can decode any of the four scattering states. These boundaries are characterized in Figure 2.6 (a) for these four scattering states.

3. THE PROPOSED ANTENNA DESIGN

In this section, we explain our proposed dual loading design for the T-match bowtie antenna. A 1 mm gap is created in the center of the antenna where a load impedance can be soldered to establish an "operation mode" as shown in Figure 3.1. Another load is connected to the input port of the antenna as shown in Figure 3.1. This sets the "operation state" (OS). In this paper, only inductive stimulus and an open circuit (O.C) case for OM is studied. All studied OMs are listed in Table 3.1. All studied OSs in this paper are tabulated in Table 3.2. In this section, we show that by using different combinations of OM and OS, the antenna is set at different scattering states. The resultant scattering states can provide a variety of magnitudes over 360° phases span in I-Q plane. Consequently, this can be used to: (1) increase the modulation depth, (2) increase the bit rate in the backscattering link.

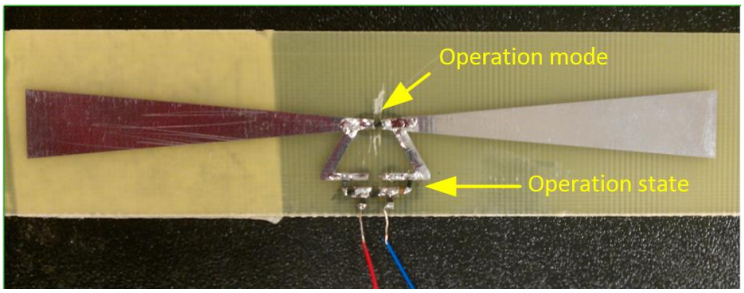

Figure 3.1. The proposed design for dual loading in the studied T-match antenna.

Table 3.1. Studied operation modes (OMs).

Operation mode						
$\mathbf{2.2nH}$	$3.3nH$	$5.1nH$	$10nH$	$12nH$	$22nH$	Open circuit (O.C)

Table 3.2. Selected loads for using in operation states (OS) of the antenna.

$Z_{L1} = 20\ \Omega, 0.5pF$	$Z_{L6} = 1.47\ \Omega, 0.6pF$	$Z_{L11} = 34.8\ \Omega, 0.2pF$
$Z_{L2} = 30\ \Omega, 44nH$	$Z_{L7} = 50\ \Omega, 0.05pF$	$Z_{L12} = 357\ \Omega, 0.6pF$
$Z_{L3} = 10\ \Omega, 5pF$	$Z_{L8} = 0.1\ \Omega, 770nH$	$Z_{L13} = 71.5\ \Omega, 1.2pF$
$Z_{L4} = 15\ \Omega, 4pF$	$Z_{L9} = 180\ \Omega, 0.1pF$	$Z_{L14} = 34.8\ \Omega, 10nH$
$Z_{L5} = 20\ \Omega, 1pF$	$Z_{L10} = 50\ \Omega, 100nH$	$Z_{L15} = 34.8\ \Omega, 0.3pF$

3.1 USING ONE OPERATION MODE

In this section, the backscattering from the antenna is studied for all the operation modes listed in Table 3.1. All 15 operation states of the antenna as tabulated in Table 3.4 were considered in each operation mode. Measurement for each scattering state is repeated for two times.

Figure 3.2 shows the real and imaginary values of the demodulated signal (p_d) in each operation mode for two differential backscattering scenarios: scalar differential backscattering (SDB) and vector differential backscattering (VDB). For SDB, two minimum and maximum scattering states of the antenna by Green model are characterized. For VDB, two high scattering states of the antenna which can provide the biggest phase difference are characterized. At different operation modes, different loads provide the highest VDB and SDB. These scattering states are all tabulated in Table 3.3. In some cases, using VDB has no superiority over SDB in increasing the differential backscattered signal (e.g. $OM = 10nH, 12nH, OC$). However, for other OMs the improvement in differential backscattered signal in VDB over SDB is substantial ($OM = 2.2nH, 5.1nH, 22nH$). The

modulation depth for VDB and SDB for all cases in Figure 3.2 were calculated and are tabulated in Table 3.3. For SDB, the modulation depth is limited to 100% ($93\% < MD < 99.68\%$). However, for VDB the modulation depth takes higher values than 100%. According to the results, the achieved modulation depth for VDB is $124.56\% < MD < 176.16\%$. The reason for this is that in VDB the two scattering states are not in the same quadrature of I-Q plane and the vector distance between two scattering states increases.

Table 3.3. Modulation index for using single operation mode.

OM	**SDB**	**States**		$\boldsymbol{max}\,\lvert\delta\rvert$	**VDB**	$\lvert\Delta\delta\rvert$	**States**	
	MD (%)	**max**	**min**	$\times \mathbf{10^{-3}}$	**MD (%)**	$\times \mathbf{10^{-3}}$	$\boldsymbol{s_1}$	$\boldsymbol{s_2}$
22nH	99.23	Z_{L14}	Z_{L12}	30.0	124.56	35.1	Z_{L2}	Z_{L6}
12nH	95.84	Z_{L14}	Z_{L10}	25.4	158.21	33.7	Z_{L2}	Z_{L11}
10nH	95.68	Z_{L5}	Z_{L9}	24.3	162.62	31.2	Z_{L4}	Z_{L14}
5.1nH	93.95	Z_{L5}	Z_{L10}	17.9	173.69	23.7	Z_{L1}	Z_{L14}
3.3nH	99.68	Z_{L14}	Z_{L10}	5.9	141.96	8.3	Z_{L4}	Z_{L14}
2.2nH	96.40	Z_{L2}	Z_{L10}	4.3	176.16	6.2	Z_{L4}	Z_{L14}
O.C	99.55	Z_{L14}	Z_{L9}	13.5	138.38	14.5	Z_{L2}	Z_{L3}

Another interesting observation in the results is that by increasing the inductance value in the operation mode from 2.2nH to 22nH the magnitude of the maximum scattering states ($max\{|p_d|\}$) for this antenna design increases. As an example, the simulated RCS of the antenna in OM=2.2nH/OS=Z_{L2} and OM=22nH/OS=Z_{L2} are $54Cm^2$ and $294Cm^2$

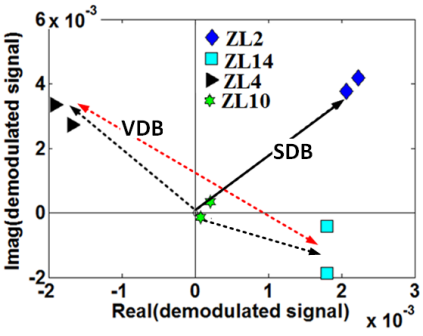

(a) OM=2.2nH

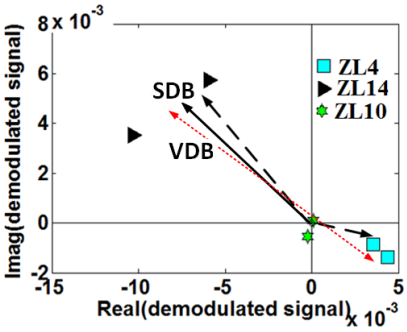

(b) OM=3.3nH

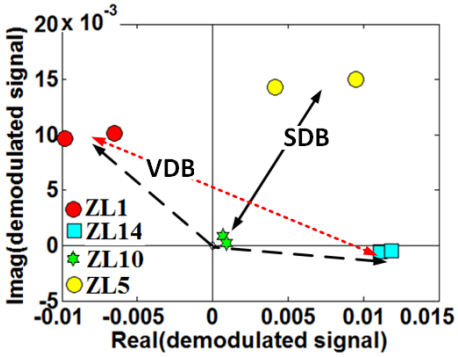

(c) OM=5.1nH

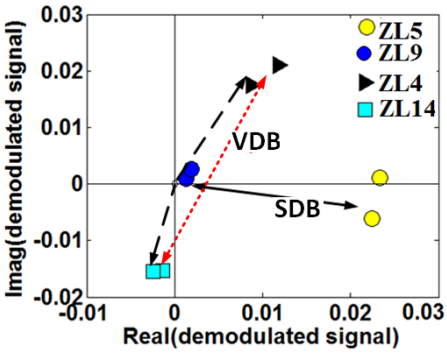

(d) OM=10nH

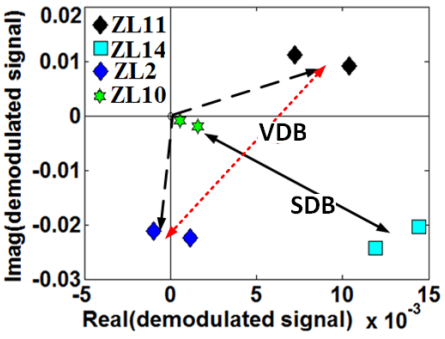

(e) OM=12nH

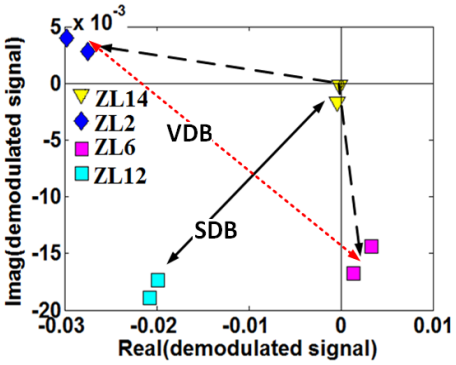

(f) OM=22nH

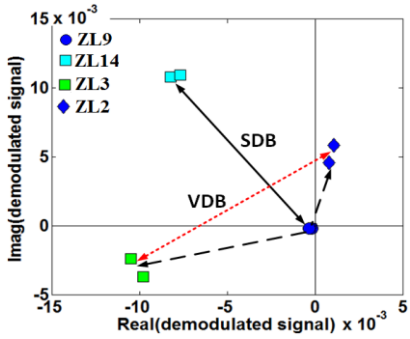

(g) OM=O.C

Figure 3.2. Scalar and vector differential backscattering at different OMs.

respectively. The magnitude of the demodulated backscattered signal from the antenna in these two scattering states are $4.3 \times 10^{-3}$and 30×10^{-3} respectively.

3.2 USING SEVERAL OPERATION MODES

In this section, the VDB from the antenna is studied when two or several of the operation modes in Table 3.1 are used. The demodulated backscattering signal of all operation modes can be compared with each other when the same $\Lambda(n)$ is used for demodulating the received signals for all operation modes. Consequently, a variety of scattering states can be achieved. Furthermore, high scattering states with phase difference $\Delta\varphi \sim 180°$ can be used to improve the differential RCS and also the modulation depth. If two exactly symmetric scattering states are found it is possible to increase the modulation depth to 200%. Figure 3.3 shows two high scattering states of the antenna in two different operation modes: $\{OM = 22nH/OS = Z_{L2}\}$ and $\{OM = 10nH/OS = Z_{L4}\}$.

As shown in Figure 3.3, these two scattering states have approximately $\sim\Delta\varphi = 160°$ phase shift comparing to each other. Boundaries of detection for each scattering state in Figure 3.3 are shown by a dashed line. If the demodulated signal falls above this line "state 1" is detected. On the other hand, if the demodulated signal falls below the boundary line "state 2" is detected. Since the two scattering states are not exactly symmetric the achieved modulation depth increases to 166.17%. However, the magnitude of the vector differential backscattering signal increases to $|\Delta\delta| = 49.8 \times 10^{-3}$. According to the results in Table 3.3, the magnitude of the vector differential backscattered signal when only one operation mode is used is bounded in $6.2 \times 10^{-3} < |\Delta\delta| < 35.1 \times 10^{-3}$. By using higher signal in backscattering links the signal is more immune to the noise and

interference in the environment. Furthermore, the coverage range in backscattering links can be increased without increasing the power at the reader antenna.

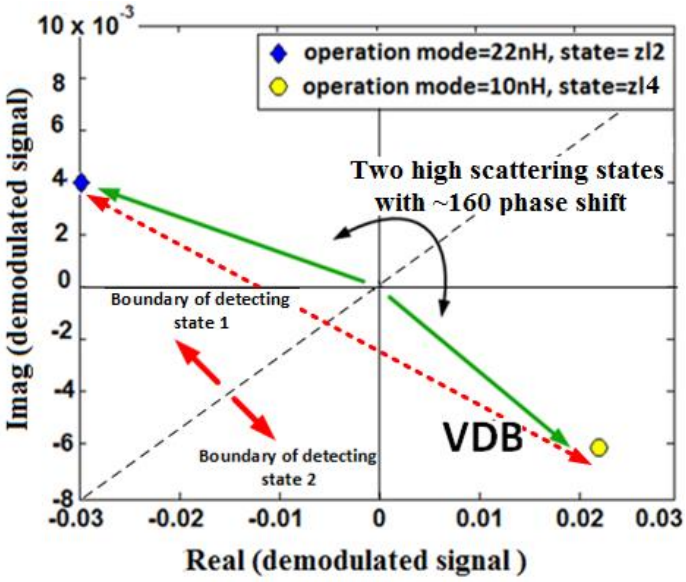

Figure 3.3. Two high scattering states with approximately $\sim\Delta\varphi = 160°$.

VDB can also be used to increase the bit rate of the backscattered links in the proposed antenna. The proposed antenna can provide different scattering states with various magnitude ($\delta = |p_d|$) and phase ($\varphi = \sphericalangle p_d$). By changing the antenna's operation mode and operation state it is possible to move the scattering state of the antenna on in phase-quadrature (I-Q) plane. Figure 3.4 shows 32 scattering states of the antenna. Each scattering state is measured for 2 times and is denoted by a marker color and a type. The color of the scattering state shows its OM. The type of the scattering state shows its OS. The boundaries of detection for each scattering state is characterized by red dashed lines. All of these scattering states are tabulated in Table 3.4. The scattering states can be categorized based on the magnitude of the demodulated signal (δ). Four boundaries for the

magnitudes are considered: (1) $\delta > 0.02$, (2) $0.01 < \delta < 0.02$, (3) $0.005 < \delta < 0.01$, (4) $\delta < 0.005$. Figure 3.4 (a) shows the scattering states with $0.01 > \delta$ and Figure 3.11 (b) shows the scattering states with $0.01 < \delta$.

Scattering states $\{s_1, s_8, s_9, s_{10}, s_{11}, s_{13}, s_{15}\}$ are high scattering states which are located at $\delta > 0.02$. These 7 scattering states are located in approximately $\Delta\varphi \sim 260°$ phases span. Scattering states $\{s_{21}, s_{32}, s_{14}, s_{16}, s_{19}, s_{12}, s_{20}, s_2, s_4, s_{30}\}$ are located in $0.01 < \delta < 0.02$. These 10 scattering states are located in a $\Delta\varphi \sim 360°$ phase span. Scattering states $\{s_7, s_3, s_5, s_{17}, s_{18}, s_{22}\}$ are located in $0.005 < \delta < 0.01$. These 6 scattering states are located in a $\Delta\varphi \sim 360°$ phase span. Scattering states $\{s_{31}, s_{29}, s_6, s_{24}, s_{26}, s_{24}, s_{23}, s_{27}\}$ are located in $0.0025 < \delta < 0.005$. These 8 scattering states are located in a $\Delta\varphi \sim 360°$ phase span. And lastly, scattering state s_{28} are at the $\delta \sim 0.0025$ and $-45° < \varphi < 0°$ phase span.

Table 3.4. Scattering states for the proposed quasi-QAM-32.

OM	Z_{L1}	Z_{L2}	Z_{L3}	Z_{L4}	Z_{L5}	Z_{L6}	Z_{L7}	Z_{L8}	Z_{L10}	Z_{L11}	Z_{L13}	Z_{L14}
marker	+	●	■	▲	▶	◀	✽	★	x	*	▼	♦
22nH	-	s_1	s_2	s_3	s_4	-	s_5	s_6	s_7	-	-	s_8
12nH	-	s_9	s_{10}	s_{11}	s_{12}	s_{13}	-	-	-	s_{14}	-	-
10nH	-	-	-	s_{15}	-	s_{16}	s_{17}	s_{18}	-	-	s_{19}	s_{20}
5.1nH	-	-	-	s_{21}	-	s_{22}	-	-	-	-	-	-
3.3nH	-	-	-	-	-	-	s_{23}	-	-	-	-	s_{24}
2.2nH	-	s_{25}	s_{26}	s_{27}	-	-	-	-	-	-	-	s_{28}
O.C	s_{29}	-	s_{30}	-	-	-	-	-	-	-	s_{31}	s_{32}

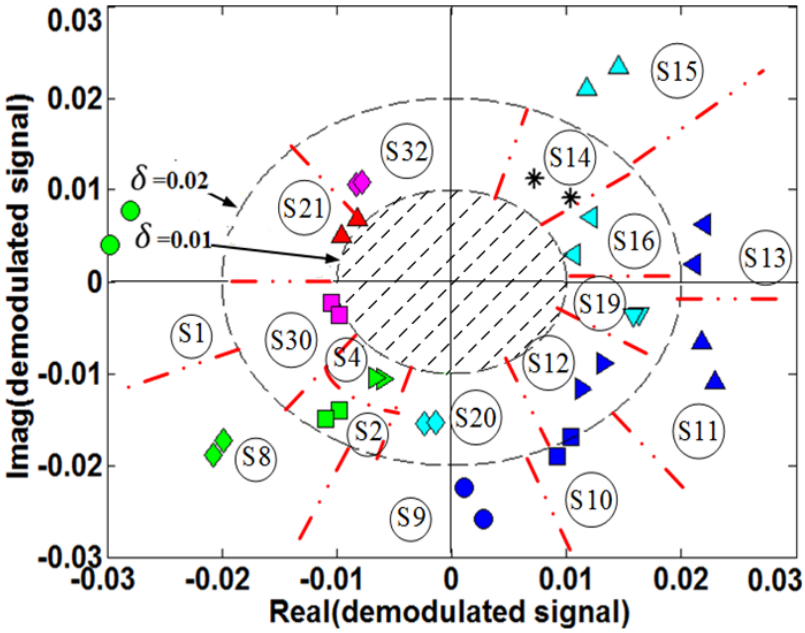

(a) Scattering states in quasi QAM-32 with δ >0.01

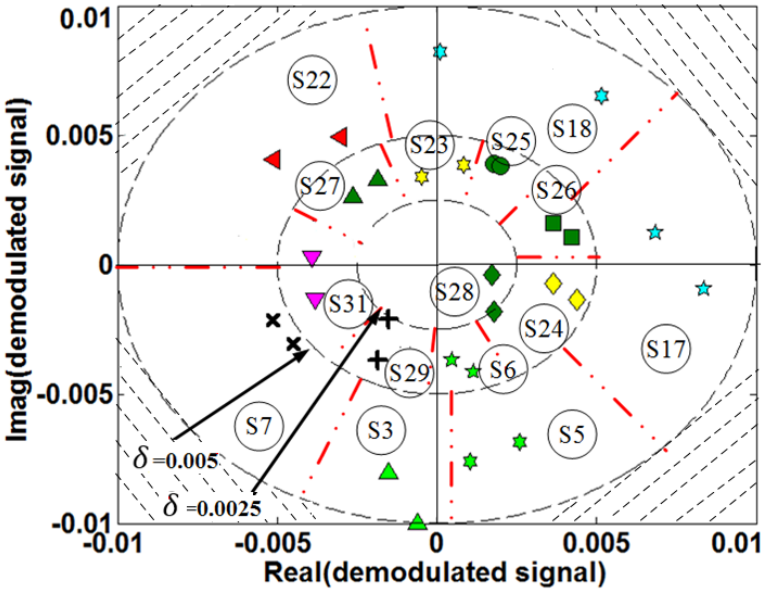

(b) Scattering states in quasi QAM-32 with δ <0.01

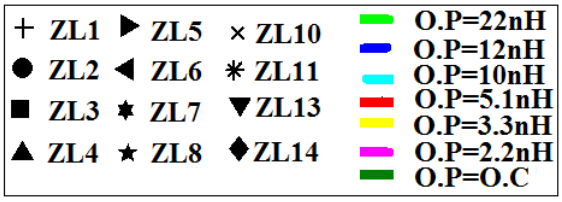

Figure 3.4. QAM 32 modulation backscattering.

The characterized scattering states, however, are not orthogonal. Thus, they can provide a quasi-32-QAM. This quasi-32-QAM can encode 5 bits in a backscattered link. However, if the noise and interference from the environment is high the scattering states are drifted from their boundaries to other boundaries and error in detection in RFID reader can be generated. Thus, in this case lower bit rate (e.g. quasi-16-QAM) must be used to avoid errors.

4. CONCLUSION

In this paper, first we presented a study on RCS and variation of phase of current for a linear half wave dipole and a resonant T-match bowtie antenna over their Γ planes. The simulation and measurement results show that the behavior of a linear antenna can be well predicted by the well-known Green model (1). However, we showed both by measurements and simulations that against the widespread assumption in the literature the RCS of a T-match bowtie antenna cannot be predicted by Green model. We showed that a T-match bowtie antenna has two maximum scattering areas on its Γ plane. Next, we introduced a new design for RFID antennas by using dual loading. We showed by measurements that the proposed deign can produce various scattering states with different magnitudes and phases. This property of the proposed antenna can be used to: (1) improve the backscattering signal strength and modulation depth, (2) increase the bit rate in backscattering links.

REFERENCES

[1] P.V Nikitin, K.V.S. Rao, "Theory and measurement of backscattering from RFID tags," IEEE Ant. Propag. Mag., vol 48 , no.6, pp. 212 – 218, Dec. 2006.

[2] A. Bletsas , A.G. Dimitriou, J.N. Sahalos, "Improving Backscatter Radio Tag Efficiency," IEEE Transactions on Microwave Theory and Techniques , June 2010 Volume: 58 , Issue: 6 , pp. 1502 – 1509.

[3] P. V. Nikitin, K. V. S. Rao, and R. Martinez, "Differential RCS of RFID tag," Electronics Letters, vol. 43, no. 8, pp. 431-432, 2007.

[4] R. B. Green, "The general theory of antenna scattering," Report No. 1223-17, ElectronScience Laboratory, Columbus, OH, Nov, 1963.

[5] Chih-Chuan Yen, A.E. Gutierrez, D. Veeramani, D. van der Weide, "Radar Cross Section Analysis of Backscattering RFID Tags," Antennas and Wireless Propagation Letters, vol. 6 , pp. 279 – 281, 2007.

[6] Shadi Ebrahimi-Asl, M.T Ghasr, M. Zawodniok, "Application of Low Scattering Antennas to RFID Networks," to be appear in proceeding of RFID Conference 2016.

[7] Huan-Yang Chen, Bhadkamkar, A.S., Tzu-Han Chou, Van Der Weide, "Vector Backscattered Signals Improve Piggyback Modulation for Sensing With Passive UHF RFID Tags," Microwave Theory and Techniques, IEEE Transactions, vol. 59, no. 12, pp. 3538-3545, November 2011 .

[8] S.J. Thomas, E. Wheeler, J. Teizer, M.S. Reynolds, "Quadrature Amplitude Modulated Backscatter in Passive and Semipassive UHF RFID Systems ," IEEE Transactions on Microwave Theory and Techniques, vol. 60, no. 4, pp. 1175 – 1182, February 2012.

[9] J. Besnoff, M. Abbasi, D. S. Ricketts, "High Data-Rate Communication in Near-Field RFID and Wireless Power Using Higher Order Modulation," IEEE Transactions on Microwave Theory and Techniques, vol. 64, no. 2, pp. 401 – 413, February 2016.

[10] S. J. Thomas, M. S. Reynolds, "A 96 Mbit/sec, 15.5 pJ/bit 16-QAM modulator for UHF backscatter communication," RFID (RFID), 2012 IEEE International Conference on, pp. 185: 190, April 2012, Orlando FL.

[11] C. Mandel, M. Schüßler, M. Nickel, B. Kubina, R. Jakoby, M. Pöpperl, M. Vossiek, "Higher order pulse modulators for time domain chipless RFID tags with increased information density," European Microwave Conference, Sept. 2015, Paris.

[12] Donnell, K.M., Abou-Khousa, M.A., Belayneh, M., Zoughi, R., "Dual-Loaded Modulated Dipole Scatterer as an Embedded Sensor," Instrumentation and Measurement, IEEE Transactions on, 2011, Volume: 60, pp. 1884 – 1892.

[13] M.A. Abou-Khousa, R. Zoughi, "Multiple Loaded Scatterer Method for E-Field Mapping Applications" , Antennas and Propagation, IEEE Transactions, on Volume: 58 , Issue: 3 , 2010 , pp. 900 – 907.

[14] C. A. Blanis, Antenna Theory: Analysis and Design, 3rd ed. Hoboken, NJ:Wiely, 2005.

[15] Shadi Ebrahimi-Asl, M.T Ghasr, M. Zawodniok, " Method and Device for Improving Performance of RFID Systems," US Provisional Patent Application 62/236,490, October 2015.

III. APPLICATION OF LOW SCATTERING ANTENNAS TO RFID NETWORKS

ABSTRACT

An established backscattering link between an RFID tag and reader suffers from high interference from other RFID tags in the network. This interference results in low read rates in RFID networks. In this paper, we investigate a new state for an RFID tag in which the tag switches to an *invisible* (i.e. low scattering) state when a communication link between an RFID reader and another target RFID tag is ongoing. We show both by simulations and measurements that by using this method the interference to the backscattering link is minimized and thus the read rate increases.

1. INTRODUCTION

Radio frequency identification (RFID) is a short-range wireless technology for transferring data. An RFID system consists of a main base station called RFID reader and several RFID tags in the field. The basic operation of an RFID system is as follows: the main base station sends out a signal to the field calling out an RFID tag ID. The source signal induces an energy at the antenna of the interrogated tag. This energy is partially absorbed and partially scattered back to the reader. By switching between two load impedances connected to the antenna at the interrogated tag it is possible to modulates the backscattered signal on top of the continuous source signal. Finally, the reader decodes the message from the tag.

One of the main challenges in an RFID network is that the read rate in these networks decreases as a result of increasing the number of tags in the field. This scenario is shown in Figure 1.1 with two RFID tags in the field. During an interrogation from RFID tag 1 the other tag in the field also receives this signal. Due to electromagnetic scattering, RFID tag 2 will also partially scatter energy to the environment. This scattered signal can result in destructive interference at RFID tag 1 causing non-efficient power harvesting and weak backscattering signal. Furthermore, it can interfere at the RFID reader causing low read rates.

Interference from closely spaced RFID tags results in degrading the read rate in large number of tags. This have been one of the main complaints from RFID consumers and the main obstacle in widespread usage of this technology in some applications. Some researchers have tried to approach to this problem by developing collision avoidance and detection techniques [1][2]. However, while these methods can help controlling the order

in which tags are read, they cannot affect the scattering from neighbor tags in an ongoing interrogation. Some works model this interference using mutual coupling theory for scattering antennas [3][4]. Still these models have not been successful in proposing solutions in suppressing interference in RFID networks. In [5], the effect of the load impedance of the target antenna on the level of destructive interference from neighboring tags is studied. On the other hand, the interference from a neighbor RFID tag can actually be used to increase the backscatter signal from the target tag [6]. However, the results of study in [6] show that the neighbor tag should switch to different load impedances to keep its constructive effect at different placements and distances to the target with respect to the incident wave from the reader. A study on the effect of tag polarization on the level of interference at a target RFID tag is also investigated in [7]. This study represents the fact that circularly polarized tags play superior to linearly polarized ones in controlling interference.

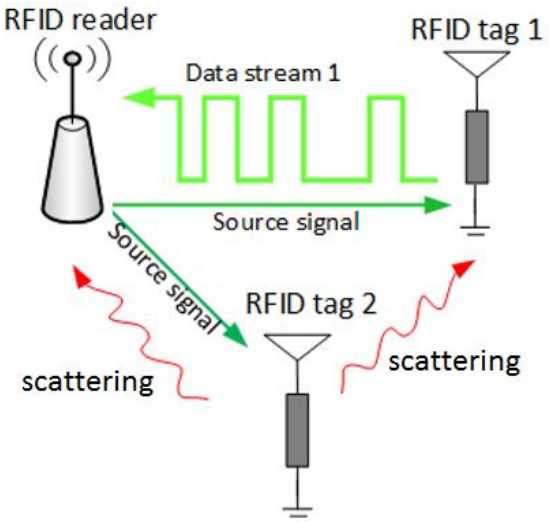

Figure 1.1. The scattering from tag 2 causes interference for the backscattering link between the RFID reader and tag 1.

Invisible antennas have long been studied in the literature [8], [9], [10]. An invisible antenna is basically a scatterer which is loaded with proper impedances such that its scattering is minimized. The first comprehensive model for finding the invisibility load of an arbitrary antenna was first discussed in [8]. This model still is used in the literature for RFID antennas. In this model, the radar cross section (RCS) from a scatterer with impedance Za loaded with ZL and illuminated by an arbitrary field is described by

$$\sigma = \frac{\lambda^2}{4\pi} G^2 |\Gamma + A_s|^2 \quad (1)$$

where G is antenna gain at wavelength λ, A_s is a constant describing structural scattering coefficient of the antenna, and Γ is a modified current reflection coefficient: $\Gamma = (Z_a^* - Z_L)/(Z_L + Z_a)$ such that $|\Gamma| \leq 1$ for all passive loads. In (4.1), Γ and A_s stand respectively for antenna mode scattering and structural mode scattering. In this model by selecting $\Gamma = -A_s$ the RCS from the antenna is zero ($\sigma = 0$) and the antenna is minimum scattering. On the other hand, [9] uses a different method to find the invisibility load of an antenna. In this work the low scattering state of an antenna is found by minimizing the integral of the induced current distribution of the antenna. By minimizing the integral of the current the backscattering from the antenna is also minimized. Although [8] and [9] use different methods their results and analysis are in agreement with each other.

The idea of using low scattering antennas in RFID networks first was discussed in [11]. In [11] it has been shown that by changing the capacitive load impedance of a tag it is possible to reduce its RCS to a low scattering state ($RCS \sim 15cm^2$ or approximately $-28dbsm$). This method is used to reduce interference in a fixed array structure of RFID tags and increase read rate accordingly.

In [6], we have shown that depending on the selected load at a neighbor tag the interference to a target can be either constructive or destructive. In this paper, we extend our study in [6] to a case where the neighbor tag has minimal effect ($RCS < 0.1cm^2$ or $-50dbsm$) on a target tag. In contrast to [11], in this work we provide in depth study of the invisible state and its effect on the performance of the RFID system. In the first step, we evaluate the degree of invisibility that can be practically achieved for an antenna. We call this feature the accuracy of the invisibility point of an antenna. Next, we perform a study to see if the mutual coupling effect form the target tag can affect the invisible antenna and force it away from its invisibility point. We call this feature the stability of the invisibility point of an antenna. We show that the effect of a nearby tag (target antenna) on the invisible antenna is negligible and the invisible antenna remains in low scattering region. Next, we use the low scattering antenna as a neighbor for a target tag in an ongoing backscattering link between the target and a reader. We show by measurements and simulations that by using a low scattering antenna the interference from neighbor is kept in a low value. In this situation the current at the target antenna is stabilized. Furthermore, we show that the invisibility state for the used antenna type (half-wave dipole) is maintained over a large range of frequencies. Thus, by selecting one invisible state for the antenna this method can be used at wide range of frequencies and application. The rest of this paper is organized as follows. In Section 2, we discuss the accuracy and stability of the invisibility of the studied antenna. Section 3, we present and discuss measurement and simulations results. Conclusions are presented in Section 4.

2. INVISIBLE ANTENNA

In this section, we discuss how accurate (or ideal) an invisible antenna can be achieved. Also, we discuss if placing a realizable invisible antenna beside a target antenna can drive the invisible antenna away from its low scattering region.

2.1 ACCURACY IN ACHIEVING INVISIBILITY STATE

The induced current distribution on a linear cylindrical antenna which is placed on z axis and illuminated by an electric field E_{inc} having the same polarization z can be found using Hallen equation

$$\frac{\mu}{4\pi}\int_{-l/2}^{l/2} I(z')G(z-z')dz' = -j\omega\mu\epsilon\,(\partial_z^2 + k^2)^{-1}\,E_{inc}(z) \qquad (2)$$

where $I(z')$ is the current distribution on the antenna with length l and radius a and $G(\mathrm{z}-z') = \frac{1}{2\pi}\int_0^{2\pi}\frac{e^{-jkR}}{R}d\emptyset,\ R = \sqrt{(z-z')^2 + 2a^2 - 2a^2 Cos\emptyset}$. The integral equation must be solved subject to the constraint that the current $I(z)$ vanishes at the antenna ends $I(l\ /\ 2) = I(-l\ /\ 2) = 0$.

The induced current on the antenna surface will consequently produces an electric field. It has been shown that the far field electric field of the antenna on z axis has E_θ component and $E_r = 0, E_\emptyset = 0$ [12]. The far field pattern of the antenna can be found

$$E_\theta = \int_{-l/2}^{l/2} dE_\theta = j\eta\frac{ke^{-jkr}}{4\pi r}Sin\theta\left[\int_{-l/2}^{l/2} I(x',y',z')e^{jkz'Cos\theta}\,dz'\right] \qquad (3)$$

Equation (3) models the scattering from an antenna. This scattering is proportional to the integral of the distribution of the current on its structure. Thus, in order to put a

scatterer in its invisibility state the integral of current on its structure must be minimized ($\int_{-l/2}^{l/2} I = 0$). This can be done by selecting appropriate load impedances for the antenna.

The distribution of the induced current on the scatterer depends on the selected load impedance and the antenna impedance itself. The antenna impedance for most RFID tags is partially resistive and inductive. Thus, by selecting a capacitive load (conjugate match) we can expect a higher current distribution on the antenna. Figure 2.1 (a) and (b) show the magnitude and phase distribution on a thin cylindrical dipole at three load impedances: resistive $Z_{L1} = 50\Omega$, capacitive $Z_{L2} = 1pF$ and inductive $Z_{L3} = 60nH$. In this paper, CST Studio is used for all simulations. We understand that for capacitive and resistive loads the magnitude of the current takes a big value. Furthermore, the distribution of phase is a constant value on the length of the antenna. However, at inductive load first the magnitude of the induced current is small. And second, the distribution of phase undergoes ~180 degrees shift at the center of the antenna. Thus, the integral of the current on this antenna is minimal. However, for the capacitive and resistive loads since the sign of the current is fixed the integral of the current on the antenna surface take a big value.

To study invisibility, in this paper a printed half-wave dipole at f= $1GHz$ on Roger RO4350 support is considered. The invisibly state of the antenna is investigated using the method introduced in [8]. As mentioned earlier, using this method it is also expected that the integral of the current to be minimized. The ideal invisibility state is achieved at "R~ 0.0002 Ω" and "L= 100.3254 nH" for the selected antenna using. We select $R = 0\,\Omega$ and $L = 100\,nH$ as practical values for measurement and simulations. Thus, the only difference between the ideal and realizable invisible antennas is the used impedance at the antenna input.

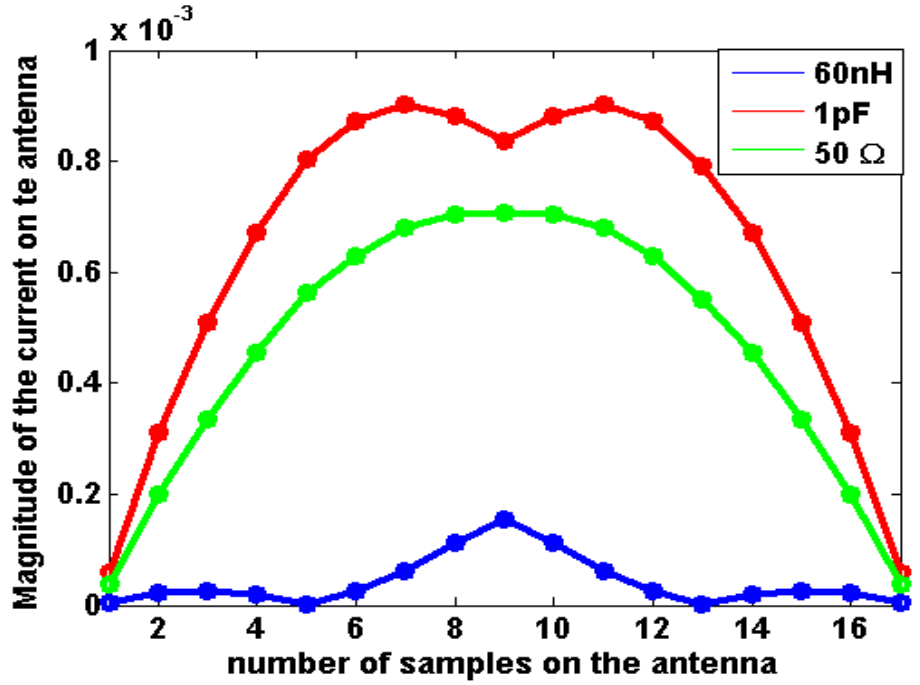

(a) Distribution of magnitude

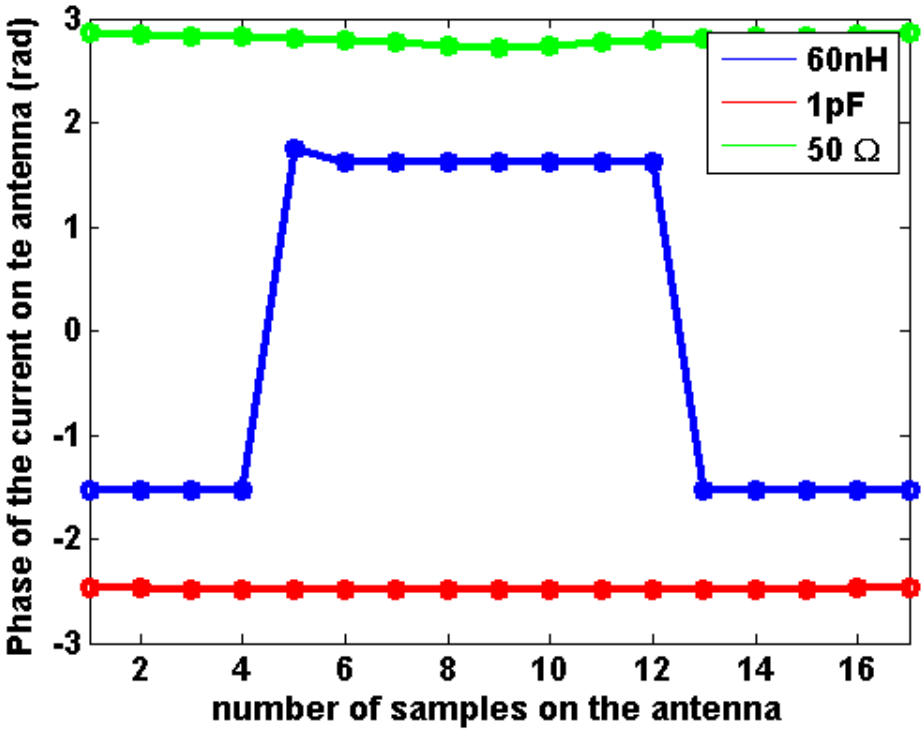

(b) Distribution of phase

Figure 2.1. Magnitude and phase distribution on a half-wave cylindrical dipole at f=1GHz (radius=0.5mm) using three different load impedances.

A comparison of the RCS from the ideal and realizable invisible antenna is shown in Figure 2.2 (a). It is understood that for the realizable invisible antenna the RCS at the main lob is slightly above -50 dBsm. However, for the ideal invisible antenna the RCS at any angles is less than -58dBsm. A comparison of the magnitude and phase of current distribution also is shown in Figure 2.2 (b) and (c) respectively. In general, Figure 2.2 (b) and (c) represent the distribution of current at a low scattering antenna which results in a minimized integral of the current on the antenna structure. For the ideal invisible antenna the distribution of the phase of the current is negative in a wider area at the center of the antenna. This makes the integral of the current of the ideal invisible antenna to be closer to zero. It is interesting to note the additional nulls at the main lobe of the antenna at ideal invisible state. These nulls happen due to the unique current distribution of the antenna at this state. As understood from Figure 2.2 (c) in this state half of the antenna has positive and half of the antenna has negative phase distribution. By employing this distribution of current on the antenna in (3) additional nulls at the main lobes of the antenna pattern will appear. We evaluate the stability of sustaining low scattering state in the next section.

2.2 STABILITY IN SUSTAINING INVISIBILITY STATE

In this section, we perform a brief study on how stable the current distribution of an invisible antenna is in response to placing another antenna in its vicinity. From mutual coupling theory we know that adjacent antennas affect and degrade the current distribution at their neighbors [12]. More specifically, in [6] we have shown that for closely spaced RFID tags this disturbance in the current distribution is very immense and can totally change the current distribution on the tags. Knowing this, a valid question about reducing

interference using invisible antennas is that if placing an invisible antenna in the vicinity of a target antenna could drive it away from its invisibility point. In this Section, we investigate the stability of maintaining invisibility state at an invisible antenna when it is placed in the vicinity of a neighbor. In another words, we examine how strong the variation of the integral of current at the invisible antenna is in this situation.

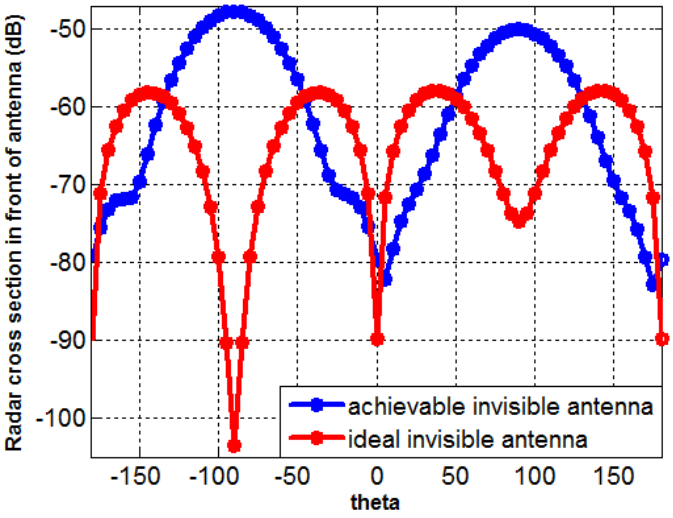

(a) RCS

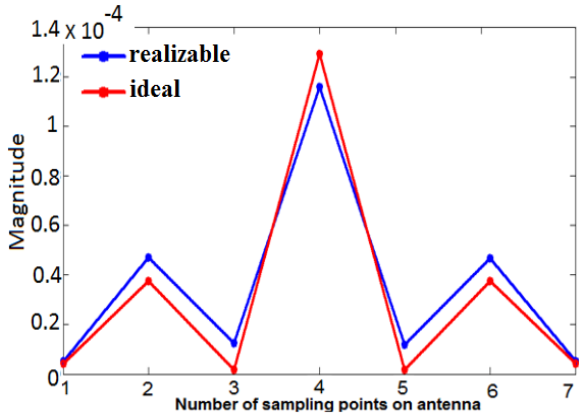

(b) Magnitude of current distribution

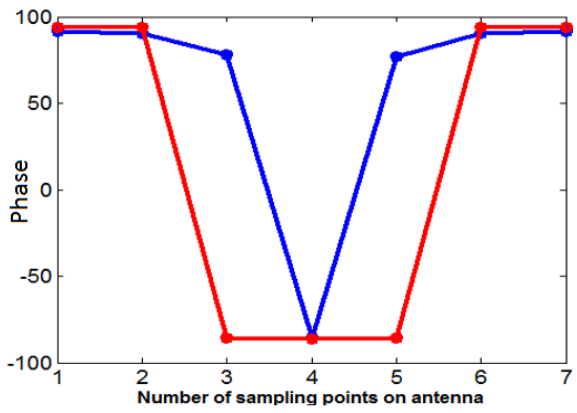

(c) Phase of current distribution

Figure 2.2. Ideal and realizable invisible antennas.

To study the stability of maintaining invisibility state, a low scattering state of the studied antenna in the previous section is considered at $R = 17\ \Omega$ and L= 107 nH (main lobe RCS at -37dbsm or ~$2cm^2$). From [6] we know that in a two tag system depending on the placements of the tags with respect to the incident wave from the RFID reader different current distribution is formed on the antennas. Thus, in this work we also consider three cases in that the target antenna is placed beside, behind and in front of the invisible antenna with respect to the incident wave. We call these cases respectively side, back and front neighbor scenarios. The distance between antennas is set at d=2.5cm. Using $\Gamma = (Z_a^* - Z_L)/(Z_L + Z_a)$ a parameter sweep over the impedance of the load of neighbor antenna (Z_L) is performed with "0.1" resolution steps for Γ. This sweep is performed to find the load impedance at the neighbor antenna which can drive the low scattering antenna the most from its invisibility point. In another words, using this impedance at the neighbor antenna the integral of the current at the low scattering antenna will be maximum. At the used resolution step the impedance at the neighbor antenna is considered at $Z_L = 5.69\Omega +$ 0.964pF for front and side scenarios and at $Z_L = 12.726\Omega + 0.5329pF$ for back scenario. Figure 3.2 (a) and (b) show respectively the variation of the magnitude of the integral of the current at the low scattering and neighbor antenna based on the normalized distance between the antennas for three cases. It is understood that although the magnitude of the current at the low scattering antenna changes for all three cases this change is bounded to $\Delta i < 3 \times 10^{-5}$. Also, for all cases when the distance between antennas increased the magnitude of the current at the low scattering antenna is converged to a fixed value where the neighbor antenna has no effect on the variation of the current distribution anymore. As for the variation of the integral of the current at the neighbor antenna we understand at

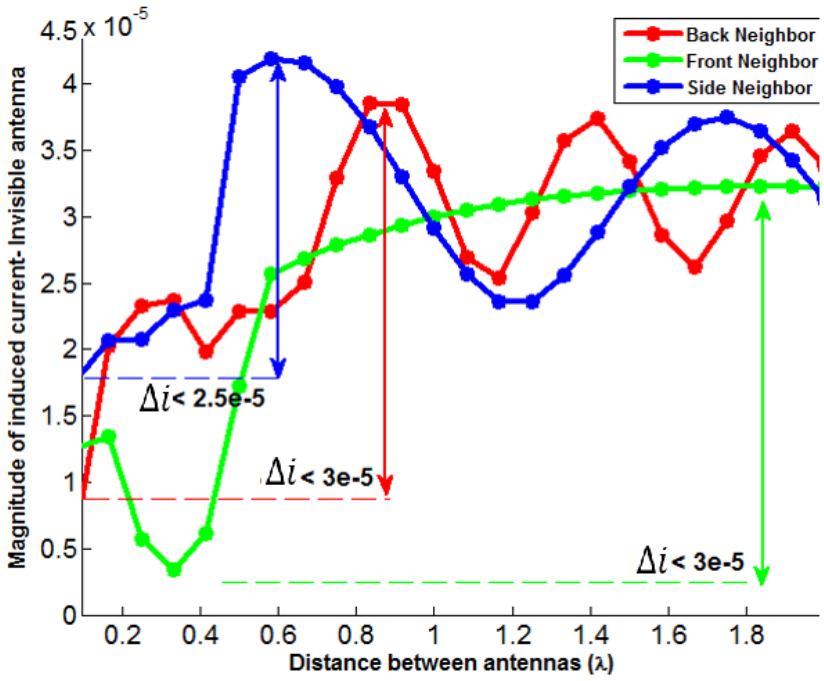

(a) Magnitude of current at the invisible antenna

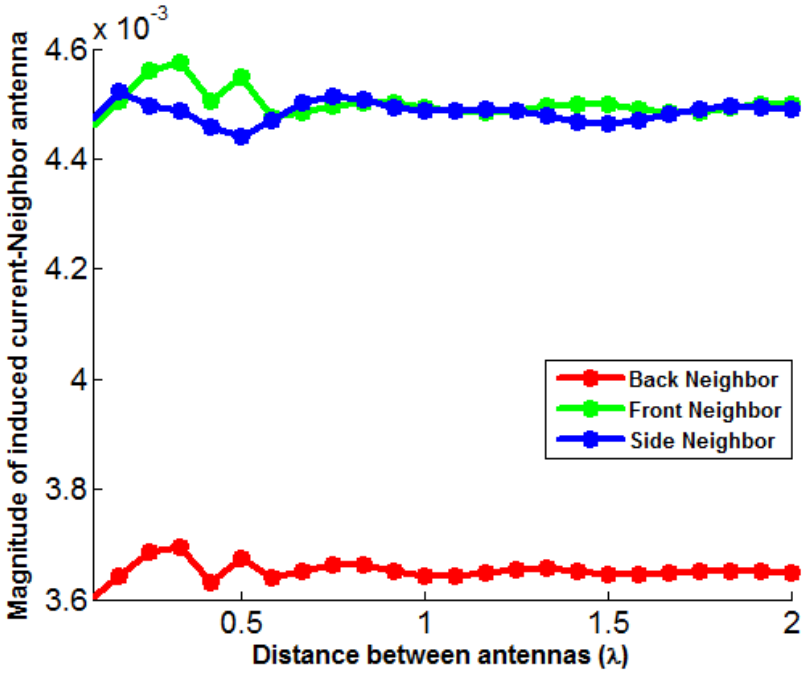

(b) Magnitude of current at the neighbor antenna

Figure 2.3. Variation of the currents of an invisible antenna and a target.

$d < 0.5\lambda$ the integral of the current experience some insignificant variation but at $d > 0.5\lambda$ the integral of current is converged to a fixed value. In this situation the low scattering antenna has no effect on the neighbor antenna. Furthermore, in this study it is noticed that although the magnitude of the distribution of current at the low scattering antenna changes in different cases the general format of the current distribution of the low scattering antenna does not change and is as described in Figure 2.2 (b) and (c). It is concluded that although a non-ideal invisible antenna is used and the neighbor has the strongest effect on it still the non-ideal invisible antenna stays in the minimum scattering region.

3. MEASUREMENT RESULTS

In this section, we investigate the variation of the backscattered signal from a target antenna when a neighbor antenna is placed beside it. A printed half-wave dipole at $f = 1GHz$ on a Roger RO4350 substrate loaded with a pin diode is considered as a target antenna as shown in Figure 3.1 (a). Two-conductor pads $1\ mm \times 1\ mm$ are added to the antenna structure for soldering impedances to the antenna structure. The antenna and the structural support thickness are $0.05\ mm$ and $0.5\ mm$ respectively. A minimum and a maximum scattering antenna are prepared to be used as neighbors beside the target antenna. The minimum scattering antenna is prepared by considering $R = 0$ and $L = 100nH$. The maximum scattering antenna is also considered for comparison by selecting $R = 4.5\ \Omega$ and $C = 1pF$. The measurement setup is prepared as shown in Figure 3.1 (b). The target antenna is connected to rectangular pulse generator Agilent 81150A to bias the pin diode and modulate the backscattered wave. To isolate the ac current L=100μH is soldered between the pin diode and the bias wires. Wires are made orthogonal to the polarization of the reader antenna and antennas to minimize interference. The pulse generator is set at f=10Hz and $\pm 0.7v$.

A horn antenna is used as the RFID reader and is connected to the Agilent E5061B VNA. The variation of the measured S_{11} at VNA is proportional to the variation of scattered field from target antenna. According to (4.3) the scattered field has a direct relation with the integral of current n the target antenna ($E_s \propto I$). And $S_{11} = \frac{E_s}{E_i}$ where E_i is the incident wave from the reader. Thus, the measured S_{11} represents the variation of the current at the target antenna. On the other hand, the RCS from the target tag can be shown by

$$\sigma = \lim_{r\to\infty} 4\pi r^2 \frac{|E_s|^2}{|E_i|^2} \quad (4)$$

We can conclude that the relation between RCS of the antenna and its current distribution is $\sigma \propto I^2$.

The VNA is set at $f = 1GHz$, sweep time=1 s, with EXT trigger. Minimum and maximum scattering antennas are placed in turns as a neighbor beside the target antenna to investigate the variation of the current at the target antenna. Three cases are considered in that the neighbor antenna (minimum and maximum scattering antennas) is put beside, behind and in front of the target antenna. The distance between antennas (d) is increased and the variation of scattered signal from the target antenna is measured. The signal from target is demodulated using $p_d = \frac{1}{N_p}\sum_{n=1}^{N} s_{11}(n).\Lambda(n)$ where $s_{11}(n)$ is the received pulse at the VNA, $\Lambda(n)$ is a sign function which is triggered to $+1/-1$ when the signal in ON/OFF. In this setup $N = 500$ and $N_p = 10$.

Figures 3.2 (a), (b), and (c) show the simulation and measurement results for the variation of the normalized current at the target antenna based on the distance d when the minimum and maximum scattering antennas are placed in turns as a neighbor respectively in the back, front and beside the target antenna. The measured and simulated induced current at the target antenna when it is alone in the field are shown by green and yellow symbols. As discussed in [6], we understand that the induced current at the target tag is immensely degraded when a maximum scattering antenna is used in the vicinity in all three cases. Depending on the position of the maximum scattering antenna with respect to the incident wave this degradation can be either destructive or constructive. In contrast, the degradation in the induced current at the target when the minimum scattering antenna is used beside the target is very small in all three cases. In other words, the minimum

scattering antenna acts as if it is invisible and if the target antenna is alone in the field. The slight change between measurement and simulation results for minimum scattering antenna can be attributed to the parasitic resistance and inductance due to soldering impedances to the antenna pads.

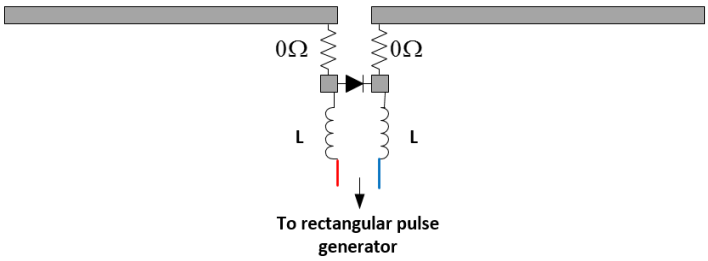

(a) Prepared half-wave dipole for measurements

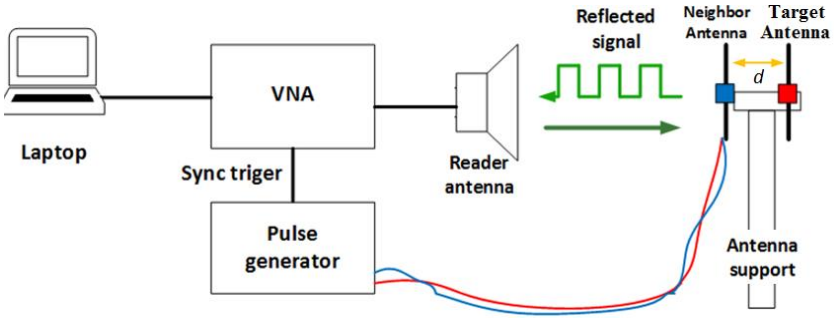

(b) Measurement setup

Figure 3.1. (a) Target antenna (b) Experiment setup.

In the next step, a new experiment setup is prepared as shown in Figure 3.3. The minimum scattering antenna is placed beside the target antenna in a random position within one block and two blocks as shown in Figure 3.3. Each block is 10cm$\times$ 10cm. For comparison, a case where a short circuit antenna is placed beside the target antenna is also examined. Figure 3.4 (a) and (b) show the demodulated signal from the target tag when a neighbor antenna (short and minimum scattering antenna) is placed beside it respectively

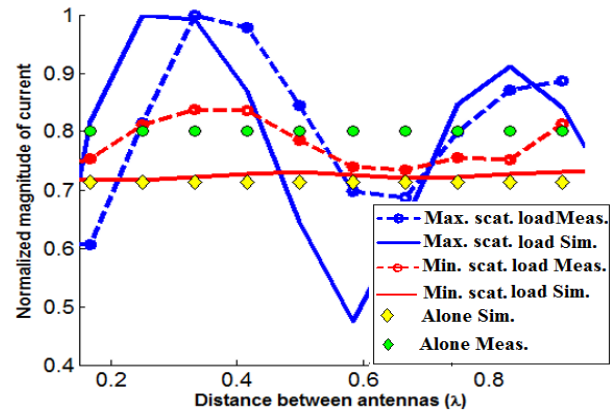

(a) Neighbor behind the target.

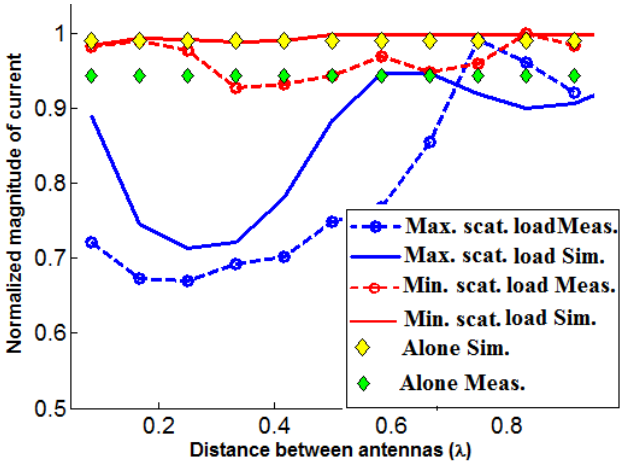

(b) Neighbor in front of the target.

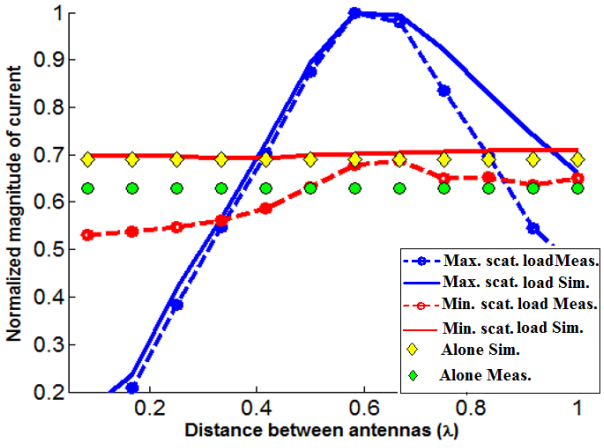

(c) Neighbor beside the target.

Figure 3.2. Measurement and simulation results for the variation of the normalized induced current at the target antenna when a neighbor antenna (max. and min. scattering antennas) are placed beside it.

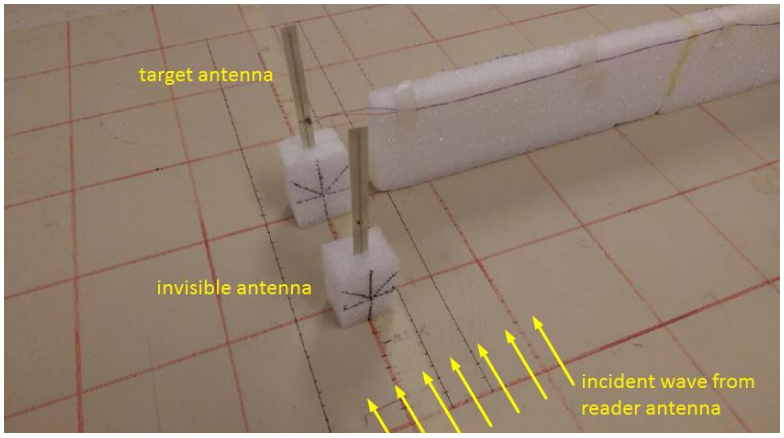

Figure 3.3. Minimum scattering and short antennas are placed in turns in a random position beside the target antenna.

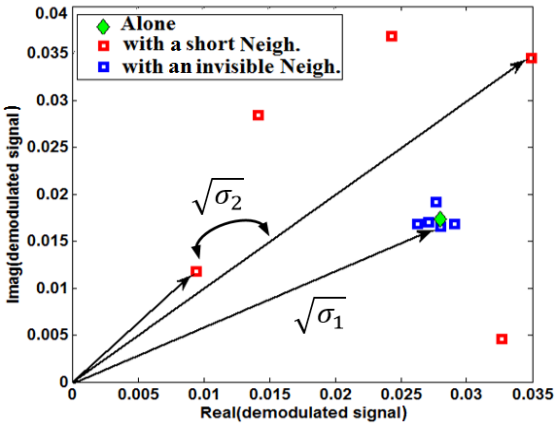

(a) One block

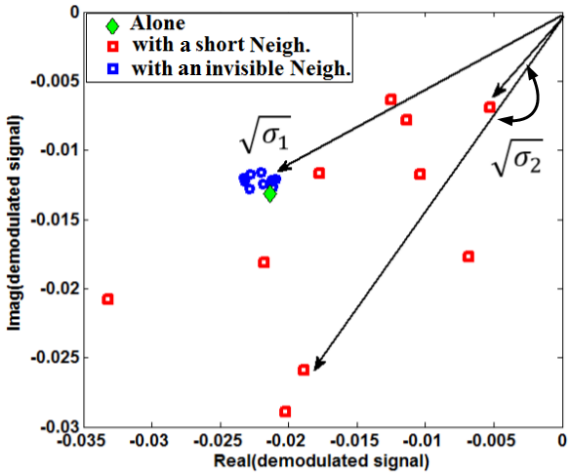

(b) Two blocks

Figure 3.4. Variation of the demodulated signal from the target. σ_1 and σ_2 are respectively the RCS of the target when it has one invisible and one short neighbor.

one and two block away. As discussed earlier, the variation of the RCS of the antenna is proportional to square of current distribution of the antenna ($\sigma \propto I^2$). From figure 4.8 (a) and (b) we understand that the variation of RCS of the antenna is almost constant when an invisible antenna is placed beside it. However, when a short antenna is placed beside the target RCS has substantial variation which can be either higher or lower than that of alone state of the antenna. Overall, we understand that by using a low scattering antenna beside a target antenna the variation of the current and RCS of the target are minimized.

4. INVISIBILITY OVER FREQUENCY DOMAIN

A valid question about using an invisible state for RFID tags is how stable the invisibility state of the antenna over a band of frequencies is. We consider the UHF frequency band of RFID tags ($860MHz$ to $960MHz$) and we perform this study for the antenna in Figure 3.1 (a). The pin diode is replaced with a short circuit impedance.

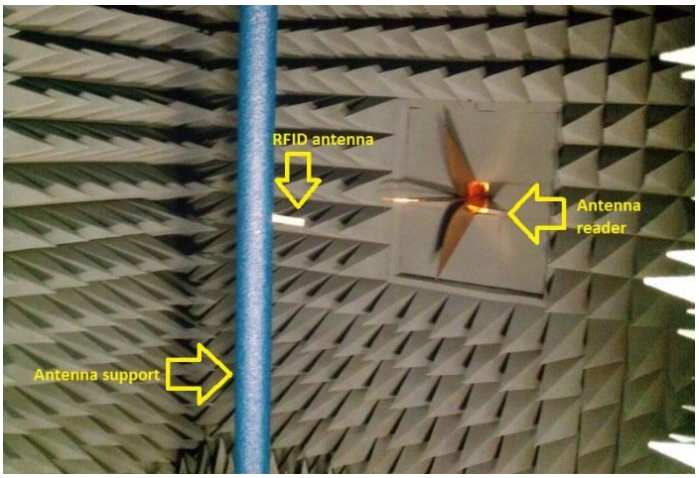

Figure 4.1. Measuring RCS of invisible antenna.

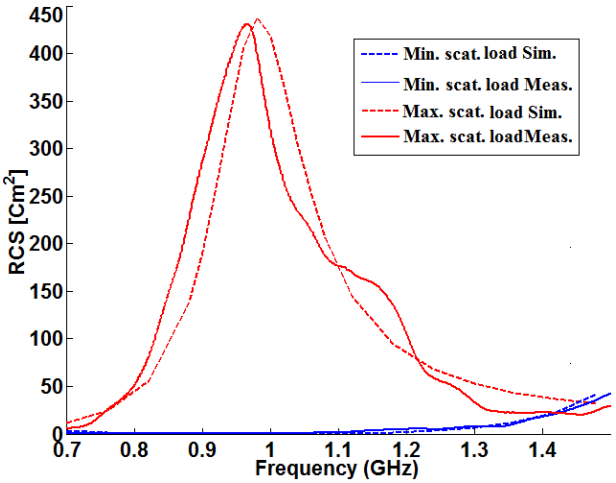

Figure 4.2. Simulated and measured RCS from min/max scattering antennas.

The RCS of the minimum and maximum scattering antennas is measured inside an anechoic chamber as shown in Figure 4.1 using the same setup in [13]. The antenna is placed is front of a reader antenna orthogonal to the foam support. The reader antenna is used in horizontal polarization matching the polarization of the antenna. The antenna reader is connected to the VNA where S_{11} is measured. The RCS from the antenna can be found by $\sigma = |S_{11}|^2 \frac{(4\pi)^3 r^4}{G^2 \lambda^2}$ where r and G are respectively the distance to the reader and the gain of the antenna under test [13]. Figure 4.2 shows the measured and simulated RCS. It is understood that the minimum scattering property of this antenna is maintained over a wide frequency range ($0.7GHz < f < 1.2GHz$. However, as understood from the results by moving to higher frequencies over $1.2GHz$ the RCS increases and thus the antenna will no longer be an inviable antenna.

5. CONCLUSIONS

In this paper, we proposed a low scattering state for RFID tags. This new state for RFID tags can be used to minimize the interference from a closely spaced tag to a target antenna. We showed that the effect of the target tag on the low scattering antenna is negligible and the low scattering antenna remains at low scattering region in any placements beside the target antenna. This property of a low scattering antenna can be used in RFID networks to suppress interference in these networks to improve read rates. In future works, we evaluate using invisible antenna in a dense network of RFID tags.

REFERENCES

[1] Lijuan Zhang, Wei Xiang, Xiaohu Tang, "An Adaptive Anti-Collision Protocol for Large-Scale RFID Tag Identification," IEEE Wireless Comm. Lett., vol. 3, no. 6, pp 601 – 604, Sep. 2014.

[2] A. Bletsas, S. Siachalou, J.N. Sahalos, "Anti-Collision Backscatter Sensor Networks," IEEE Trans. on Wireless Comm., vol. 8, no. 10, pp. 5018 – 5029, Oct. 2009.

[3] S. Ebrahimi-Asl, M.T Ghasr, M. Zawodniok, K.E. Robinson, "Preliminary study of mutual coupling effect on a passive RFID antenna array," in IEEE Intl. I2MTC Conf. 2013, pp. 138 – 141.

[4] Feng Lu, XiaoSheng Chen, Terry T. Ye, "Performance analysis of stacked RFID tags," in IEEE Int. RFID Conf., April 2009, pp. 330 - 337.

[5] Y. Tanaka, Y. Umeda, O. Takyu, M. Nakayama, K. Kodama, "Change of read range for UHF passive RFID tags in close proximity," in IEEE Int. RFID Conf., April 2009, pp. 338 – 345.

[6] S. Ebrahimi-Asl, M.T Ghasr and M. Zawodniok, "Improving Backscattering Using a Forward Scatterer," in IEEE Int. RFID Conf., April 2014.

[7] Qi Zhang, M.J. Crisp, R.V Penty, I.H. White, "Reduction of Proximity Effects on UHF Passive RFID Systems by Using Tags With Polarization Diversity," IEEE Transac. Antenn. Propag., vol. 63, no. 5, pp. 2264 - 2271, Feb. 2015.

[8] R. B. Green, "The general theory of antenna scattering," Report No. 1223-17, ElectronScience Laboratory, Columbus, OH, Nov, 1963.

[9] T. Sawaya, M. Taromaru, T.Ohira, B. Komiyama, "Experimental Proof of Electrically Invisible State of Inductively Loaded Dipole and Proposal of Electrically Invisible Meander-Lines," IEEE Transac. Antenn. Propag., vol. 54, no. 11, pp. 3374 – 3382, Nov. 2006.

[10] W.K.Kahn, H. Kurss, "Minimum-scattering antennas ," IEEE Transac. Antenn. Propag., vol. 13, no. 5, pp. 671 - 675 , Sep 1965.

[11] Daniel Mark Dobkin, "RFID Systems Including Tags Having Low RF Scattering Mode," U.S. Patent 2007/0115098 A1, May. 24, 2007.

[12] C.A. Balanis, Antenna Theory. New Jersey: John Wiley & Sons, 2005.

IV. A SOLUTION TO LOW READ RATE PROBLEM IN RFID SCATTERING NETWORKS

ABSTRACT

High interference and low read rate have repeatedly been the main drawback of RFID technology. We propose a solution to this problem by employing low scattering antennas. We investigate a new state of scattering for RFID tags in that tags will switch to low scattering states to suppress interference to an ongoing backscattering link between an RFID reader and a target tag. We evaluate the efficiency of our proposed solution by random deployment of tags in a network of 10 antennas. We show the read rate is 93.76% when the threshold of detecting signal at the reader is set as high as $0.75\boldsymbol{\delta}$ where $\boldsymbol{\delta}$ is the magnitude of the backscattered signal from the target antenna when it is alone in the field.

1. INTRODUCTION

Radio frequency identification (RFID) has been used in recent years in many applications for tracking and identifying items in large quantities. In many applications RFID has already been accepted as a replacement for barcode technology. One of the reasons for the popularity of RFID systems in comparison with barcode technology is that data can be accessed and manipulated wirelessly. However, using RFID technology in large quantities has one main challenge: low read rate.

A representation of using an RFID system in large quantities is depicted in Figure 5.1. An RFID system consists of a main RFID reader and several RFID tags in the field. When the reader decides to interrogate one tag it sends out a signal and calls out the ID of the tag. By impinging the signal on the tag a current is induced on its antenna structure. If the tag finds out that its ID is called out it changes its scattering state between two states to modulate its stored data onto the backscattered wave. Changing the scattering states of the tag is performed by switching a load impedance at the input port of the tag between two values. This method of transferring data is called *differential backscattering* [1]. However, as soon as the number of tags in the field increases the interference in the network increases and consequently read rate drops. A representation of this scenario is shown in Figure 1.1 showing the fact that data communication by differential backscattering links is not always successfully accomplished. We explain this issue more in the next paragraph.

Multi reflections and high interference are the main reason for low read rate in RFID networks. When the RFID reader interrogates one RFID tag the rest of the tags in the filed also receive this signal. Due to electromagnetic scattering phenomenon all of these tags will also scatter back to the environment. These scatterings will produce interference

at the interrogated tag. This interference will result in poor power harvesting and as a result poor backscattering signal from the interrogated tag. On the other hand, the scattering from all tags also will produce interference at the reader antenna which results in low signal to noise ratio. This will result in low read rate at the RFID reader.

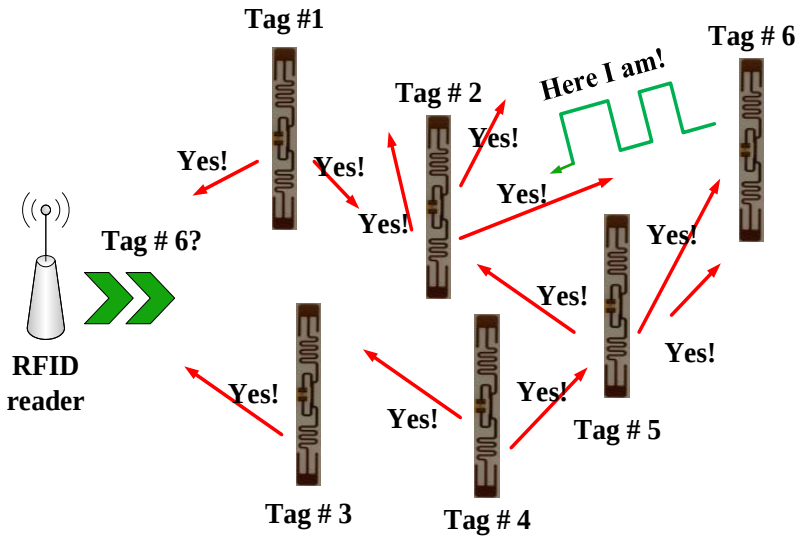

Figure 1.1. Multi reflection problem in RFID networks.

Several resources have addressed this issue in RFID networks and proposed solutions to overcome low read rate problem in RFID networks [2]-[7]. Some resources propose collision avoidance and detection techniques to help improving the low read rate problem [2], [3]. Some resources propose using spatial, frequency or polarization diversity to help increasing the low read rate problem in RFID networks [4], [5]. Other works try to approach this problem by developing mutual coupling equations for the *virtual antenna array* formed by all the tags in the network [6], [7]. However, all of these works are methods and algorithms at the RFID reader side. Whereas the low read rate problem in RFID networks is generated because of high scatterings and the resultant interference at

the tags side. Thus, these methods are indeed unable to propose solutions for suppressing the interference.

Invisible antennas have long been studied in the literature [8]-[14]. An invisible antenna is simply a scatterer -antenna- which is loaded with proper impedance so that its backscattering is minimized [8]. In [15], we proposed the concept of using low scattering antennas in RFID systems. In our proposed solution for a two tag system, one tag (the neighbor antenna) switches to a low scattering state to suppress its interference to the other tag (the target antenna). We studied the effect of *accuracy* of invisibility state on the level of interference to the target antenna and the *stability* of sustaining invisibility state when the invisible antenna is placed in the close vicinity of the target antenna. The result of our study showed that a non-ideal invisible antenna still remains in low scattering region when it is placed in the close proximity of a target antenna. Also, we showed that the variation of the current of the target antenna in the presence of a non-ideal invisible antenna is very small.

In this work, we extend our study to a network of neighbor antennas in the vicinity of one target antenna. We evaluate the effect of increasing the number of neighbor antennas in random positions and alignments on the detection of the signal of the target antenna at the reader antenna. We consider two types of neighbor antennas in our study: short circuit neighbors (highly scattering with $RCS{\sim}135Cm^2$) and low scattering antennas ($RCS{\sim}0.1Cm^2$). We show that when high scattering antennas are placed as neighbors in the vicinity of the target antenna the radar cross section (RCS) from the target is immensely degraded and mostly takes a value close to zero. Next, we show that by using low scattering antennas as neighbors of the target antenna the interference to the target is suppressed. In

this situation, the RCS from the target antenna is stabilized and takes a value close to the RCS of the antenna when it is alone in the field (alone state). Finally, we perform a read rate study in our measurements. We show that when the threshold of detecting signal of the target antenna is set to 0.75δ where δ is the magnitude of the signal from the target antenna at its alone state, the read rate is 93.76% in a random deployment of 9 low scattering neighbor antennas. Conversely, by using high scattering neighbor antennas at the same configurations the read rate of 14.16% is achieved. Finally, we present a study about the absorption cross section of invisible antennas and its effect on the bulk reading in RFID applications.

2. BACKSCATTERING LINKS

In this section, we perform a quick overview to the basics of the operation of backscattering links in RFID systems. Backscattering links in RFID systems work based on scattering phenomenon. In order to interrogate an RFID tag, an RFID reader sends out a command calling out the ID of the tag. We show this signal by $E_i(r) = E_0 e^{-jkr}$where E_0 is a complex vector. The incident electric field at the target will produce a current distribution on the antenna. This current distribution will consequently result a scattered field from the antenna. The far-field scattered field from the antenna placed on z axis can be shown by [16]

$$E_s^{\theta} = \int_{-l/2}^{l/2} dE_{\theta} = j\eta \frac{ke^{-jkr}}{4\pi r} Sin\theta \left[\int_{-l/2}^{l/2} I(x', y', z') e^{jkz' Cos\theta}\, dz' \right] \quad (1)$$

Equation (5.1) shows the far-field radiation from the RFID antenna. For far-field scattered filed $E_s^r = 0, E_s^{\emptyset} = 0$ [16]. The scattered field in (5) can be written as $E_s^{\theta} = \frac{e^{-jkr}}{kr} F(\hat{r})$ where $F(\hat{r})$ is the far field pattern function. According to (1), we understand that the scattering from an antenna is directly related to the integral of the current distribution on its structure [8], [15].

The energy at the target antenna is partially absorbed and partially scattered by the target antenna. The relation between absorption and scattering cross section at an antenna is explained by *Forward scattering theorem* or *optical theorem* for receiving and scattering antennas [17]

$$\sigma_t = \sigma_s + \sigma_a = \frac{4\pi}{k^2} Im\{\frac{\hat{p}_0 . F(\hat{k}_i)}{E_0}\} \quad (2)$$

where $\hat{p}_0$ shows the unit incident filed vector for the linearly polarized filed. In (2), σ_s and σ_a are respectively scattering and absorption cross sections. The scattered and absorbed

energy from the antenna can be denoted by $P_s = \sigma_s P_{in}$ and $P_a = \sigma_a P_{in}$. Scattering cross section is also known by radar cross section (RCS) and is characterized by

$$\sigma_s = \lim_{r\to\infty} 4\pi r^2 \frac{|E_s|^2}{|E_i|^2} \tag{3}$$

in that E_s is characterized by (1) and E_i is the incident wave form reader. Two factors characterize the scattering cross section of a scatterer: load impedance and antenna structure [16]-[18]. The RCS from a scatterer with impedance Z_a loaded with Z_L and illuminated by an arbitrary field is modeled by [18], [19]

$$\sigma_s = \frac{\lambda^2}{4\pi} G^2 |\Gamma + A_s|^2 \tag{4}$$

where G is antenna gain at wavelength λ, A_s is a constant describing structural scattering coefficient of the antenna, and Γ is a modified current reflection coefficient:

$$\Gamma = (Z_a^* - Z_L)/(Z_L + Z_a) \tag{5}$$

such that $|\Gamma| \leq 1$ for all passive loads. Considering $\Gamma = \Gamma_r + j\Gamma_i$), the modified reflection coefficient can be characterized on the Γ plane of the antenna. The Γ plane of the antenna is actually a current Smith chart by considering z=$(Z_L + jX_a)/R_a$ and $\Gamma = \frac{1-z}{1+z}$.

In (4), Γ and A_s represent the load mode scattering and antenna mode scattering. The load mode scattering is a portion of the scattering form the antenna which can be manipulated by changing its load impedance. The antenna mode scattering, on the other hand, is the portion of the scattering from the antenna which is fixed and depends only on its structure. By selecting $\Gamma = -A_s$ in (4) the RCS from the antenna is zero and the antenna will turn to a minimum scattering antennas [18], [19]. Accordingly, at this scattering state we have $E_s = 0$ in (1) and (3). Thus, at low scattering state the integral of the current on the antenna ($\int I$) is minimum [8], [15]. On the other hand, the Γ which has the farthest

distance to (-A_s) on the Γ plane of the antenna will maximize the right side of (4). At this Γ, σ_s is maximum and the antenna turns to a maximum scattering antenna. Normally, an RFID tag in its standby mode is set to its matched state to absorb the maximum energy [1], [16]. The absorbed energy must be above threshold P_a^{th} for a successful operation of the tag. To this end, the absorption cross section of the antenna must be above a threshold (σ_a^{th}).

3. STABILITY IN KEEPING THE INVISIBILITY STATE

In this section we present a brief study for evaluating the factors which can drive an invisible antenna away from its invisibility state. Throughout this paper a half-wave dipole antenna at $f = 1GHz$ on Roger RO4350 support is considered for our study. The antenna and the structural support thickness are $0.05\,mm$ and $0.5\,mm$ respectively. The accuracy of the invisibility of the studied antenna is evaluated in [15]. The ideal invisibility state for the antenna under test is achieved using a load of "R~ 0.0002 Ω" and "L= 100.3254 nH". In this paper, we consider $R = 0\,\Omega$ and $L = 100\,nH$ as realizable values for measurement and simulations.

3.1 MATERIAL

An RFID tag is normally designed to tag different objects which have different material characteristics. In this section, we evaluate the stability in keeping invisibility state of an antenna when it is placed on different materials. The realizable invisible antenna from previous section is considered. The antenna is placed on a $30Cm \times 30Cm \times 0.5\,Cm$ substrate of different material types. The RCS of the antenna at its main lobes ($\theta = 90$) is studied. The result of this study is tabulated in Table 3.1. It is understood that by changing the substrate material, the RCS from invisible antenna increases. In another words, when the invisible antenna is placed on different material it is no longer in its low scattering region.

In [20], the relation between the invisibility point of the antenna on its Γ plane and the permittivity of the substrate material that the antenna is placed on is studied. It has been shown in [20] that the invisibility point of the antenna on its Γ plane is predictable based

on the permittivity of the substrate. Using this property, it is possible to maintain the minimum scattering feature of the antenna by load switching. In this method when tags are placed on different materials the tag is switched to an appropriate load to keep the low scattering state of the antenna.

3.2 THE EFFECT OF NEIGHBORS

It is well understood that the mutual coupling in closely spaced antennas immensely affects the distribution of the currents [15], [16]. Since the invisibility state at an antenna is achieved by minimizing the integral of its current distribution, a valid question is if the mutual coupling effect from neighbor antennas can drive an invisible antenna away from its invisibility point. In this section, we consider a maximum scattering neighbor antenna and place it beside the realizable invisible antenna from previous section to study the variation of the current on both antennas. A maximum scattering state of the studied antenna is achieved by using $R = 4.5\ \Omega$ and $C = 1pF$ [18]. This antenna is called antenna 1. The realizable invisible antenna is called antenna 2. Three case studies are examined. In the first case, antenna 1 is placed beside antenna 2. In case 2, antenna 1 is placed in front of antenna 2. And in case 3, antenna 1 is placed behind antenna 2. The variations of magnitude of the induced currents on both antennas are studied when the antennas are illuminated by a plane wave having the same polarization as the antennas (linear).

Figure 3.1 shows the variation of the currents at the center of the antennas based on the normalized distance between them. It is understood that the current at the invisible antenna (antenna 2) experiences some variation. This variation in case study 3 is the maximum. In this case study, the invisible antenna is illuminated from two sides (source

and antenna 1) and the addition of phases of the incident fields produce more variation in the induced current on the antenna. However, in all cases the variation of the magnitude of the current on the invisible antenna is bounded to almost 0.27e-3. By increasing the distance between the antennas the magnitude of the current at the invisible antenna is

Table 3.1. RCS of the studied antenna at its realizable invisible state when it is placed on different substrates.

Material	**Vacuum**	**Rubber**	**FR4**	**G-10**	**Mica**	**Roger 03006**	**Roger RT6010**
$\boldsymbol{\varepsilon_r}$	1	3	4.3	4.8	6	6.15	10.2
RCS (Cm^2)	0.1	32.71	69.39	85.52	146.41	149.4	390.46

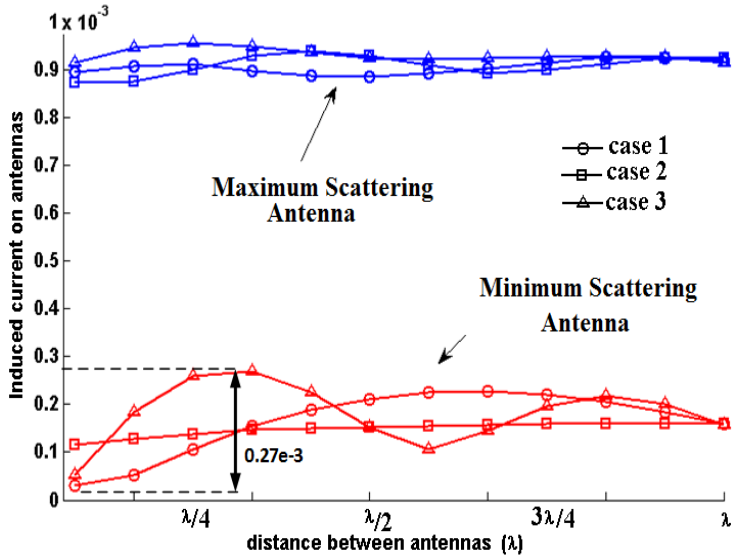

Figure 3.1. The variation of the magnitude of currents at the center of two side by side maximum and minimum scattering antennas.

converged to a fixed value which is its current at its alone state [15]. On the other hand, the magnitude of the current at antenna 1 (maximum scattering antenna) is almost constant in all cases. We conclude that although the invisible antenna is placed in the vicinity of an antenna which has the maximum RCS still the variation of magnitude of current on it is bounded. Furthermore, this variation does not disturb the distribution of the current on the neighbor antenna (antenna 1). Thus, the low scattering antenna is almost *invisible* in the field.

3.3 POLARIZATION & INCIDENT ANGLE MISMATCH

If the polarization of an antenna and the incident wave angle is not in agreement there will be polarization loss. Polarization loss factor (PLF) is defined as $PLF = |\rho_w . \rho_a|^2 = |Cos\ \emptyset|^2$ in that ρ_w and ρ_a are respectively unit vector of the incident wave and the antenna. Also, $\emptyset$ is the angle of between these two vectors as shown in Figure 3.2. In general, $0 < |PLF| < 1$. By decreasing PLF the received energy at the antenna is also reduced [16]. Thus, the best absorption efficiency happens at $\emptyset = 0$ where polarizations of the incident wave and the antenna are in agreements. Table 3.2 tabulates the RCS from the realizable invisible antenna at different incident angles. We understand that by increasing $\emptyset$ the RCS from the antenna is also reduced. In another words, the maximum RCS from an invisible antenna occurs at $\emptyset = 0$ and by increasing $\emptyset$ the antenna becomes more invisible. Overall, the RCS of the reliable invisible antenna is bounded in $5.2e-5\ Cm^2 < RCS < 0.82Cm^2$.

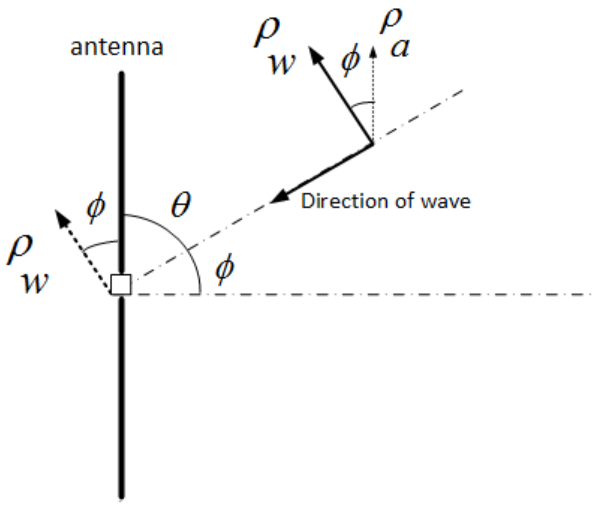

Figure 3.2. The angle between ρ_w and ρ_a (∅) has an impact on the RCS of the antenna.

Table 3.2. RCS of the studied antenna at its invisible state base on ∅.

∅ (**degree**)	0	14	44	64	75	83	89.99
RCS ($\boldsymbol{Cm^2}$)	0.1	0.07	0.046	0.023	1.91e-2	3.9e-3	5.2e-5

3.4 INVISIBILITY OVER FREQUENCY

Another factor which can affect the invisibility state of an antenna is the operation frequency. Since the invisibility state of the antenna is maintained by appropriate selection of the loads for the antenna by moving to other frequencies the loads will take different impedances. This change in the impedances may not result in the minimum integral of the current on the antenna structure anymore. Figure 3.3 shows the simulation and measurement results for the variation of RCS of two maximum and minimum scattering states of the studied antenna over a range of frequencies [15]. The RCS from maximum scattering antenna is decreased by moving over frequency. The minimum scattering

property of the studied antenna, however, is maintained over a large band of frequencies. After 1.2 GHz, however, the RCS from minimum scattering state increases and the antenna is no longer minimum scattering. In UHF RFID systems, the operation range of frequencies is bounded $860 - 960\ MHz$. For the studied antenna, there is no big variation in the RCS of the realizable invisible antenna over this range of frequencies.

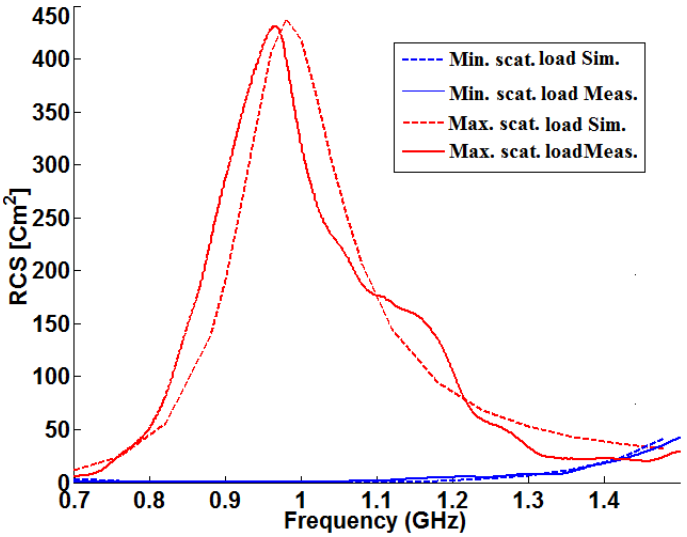

Figure 3.3. RCS of the minimum and maximum scattering antenna over a range of frequencies [15].

4. MEASUREMENTS

In this section, we explain our measurement setup and we present our measurement results. Furthermore, we discuss the issue with the absorption cross section of invisible antennas and how this issue affects the bulk reading in RFID networks using the proposed method in this paper for interference suppression.

4.1 MEASUREMENT SETUP

The *target antenna* is prepared for measurements as shown in Figure 4.1. A pin diode is used at the input port of the target antenna to modulate the incident wave on the antenna by two scattering states at the antenna: short (high scattering) and open (low scattering). The RCS of the antenna at short and open circuit states are respectively 8 Cm^2 and $135Cm^2$. When the diode is in forward and reverse biases the scattering state of the antenna is changed between short and open states respectively. The modulation of the scattered signal is necessary to extract the backscattering signal from the clutter, caused by scattering from the environment, at the reader antenna. To bias the diode the antenna is connected to rectangular pulse generator Agilent 81150A through thin wires. The pulse generator is set at $f = 10Hz$ and $\pm 0.7v$. To isolate the induced ac current on the antenna from the input port of the pulse generator, big inductors (L=100μH) are soldered between the pin diode and the bias wires. The bias wires are routed orthogonal to the polarization of the antenna and the reader to minimize the interference. A horn antenna is used as a reader antenna as shown in Figure 4.2. The input port of the horn antenna is connected to VNA Agilent E5061B where we measure S_{11}. The VNA is set at *f*= 1GHz, sweep time=10 *s*, averaging 36, IF BW=1kHz, EXT trigger, number of points=500. The measured S_{11} has

a direct relation to the scattered field from the target antenna. According to (1), the scattered field from the antenna depends on the integral of the current on the antenna. Thus, the variation of S_{11} will have direct relation to the variation of the current on the antenna. Furthermore, from (5.1) and (5.3) we conclude that the RCS from the target antenna and its current (I) are related by $\sqrt{\sigma} \propto I$. Measuring backscattering using 1-port VNA measurement is very sensitive to the variation of the environment and movements of the objects in the field of experiment setup. Figure 4.3 (a) shows a case where a disturbance has occurred in the measurement setup. In this case, it is possible to detect the presence of a modulated signal from the target antenna. However, the received signal cannot be used to measure the magnitude of the signal. In these cases, the measurement is repeated. Figure 4.3 (b) shows a correct measurement of S_{11} which can be used for characterizing the magnitude of the backscattered signal.

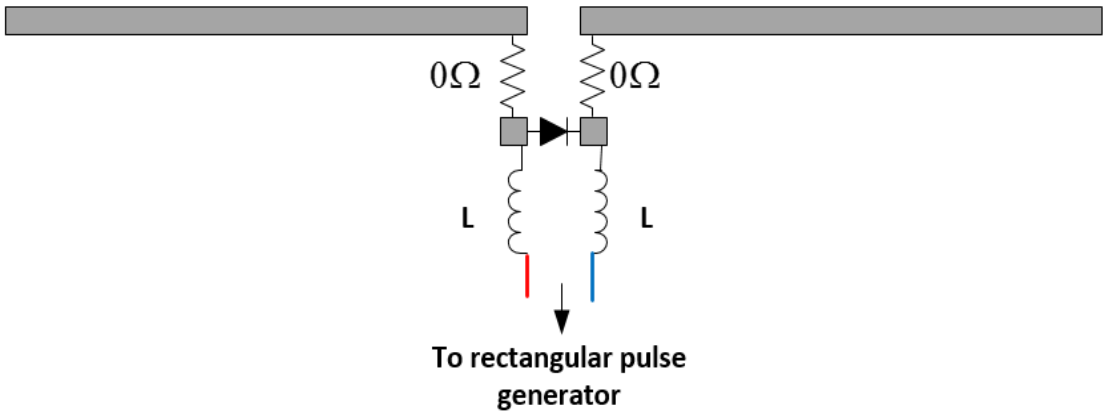

Figure 4.1. Two 1×1 mm pads are added to the antenna structure for soldering impedances. [15].

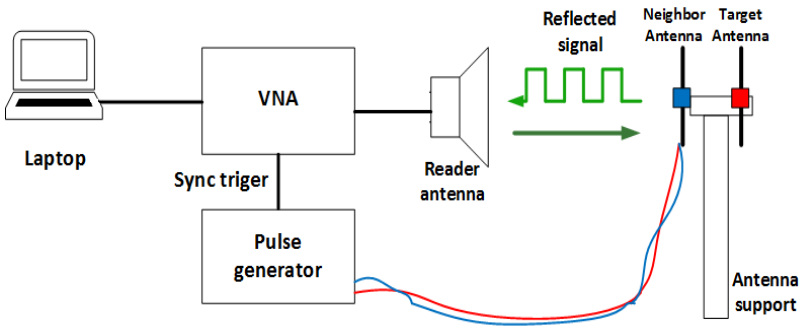

Figure 4.2. Measurement setup [15].

The received signal from target antenna at VNA is demodulated using

$$p_d = \frac{1}{N_p}\sum_{n=1}^{N} S_{11}(n).\Lambda(n) \quad (6)$$

where $\Lambda(n)$ is a sign function which is triggered to $+1/-1$ when the signal in high/low scattering states. For this setup, we use $N = 500$ and $N_p = 10$. Finally, *low scattering neighbor antennas* are prepared by soldering $R = 0\,\Omega$ and $L = 100\,nH$ to the antenna structures.

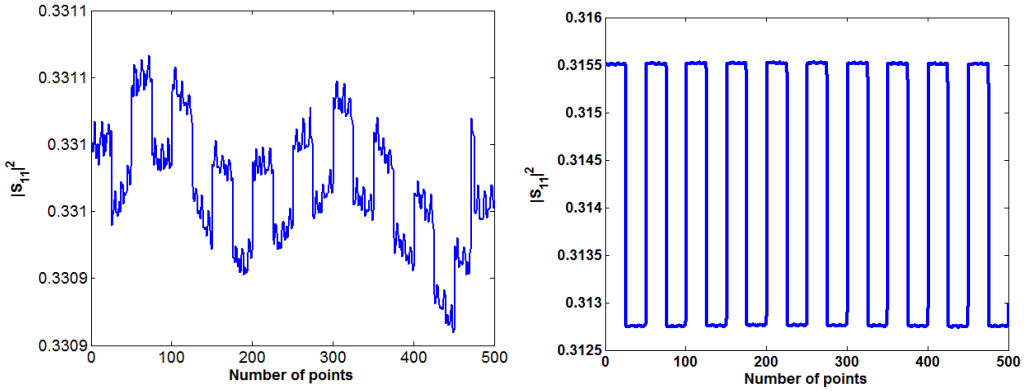

(a) Flawed measurement. (b) Correct measurement.

Figure 4.3. The measured S_{11} at VNA.

4.2 MEASUREMENT RESULTS

Three measurement scenarios are considered where one low scattering neighbor antenna is placed beside, behind and in front of the target antenna. These cases are respectively called side, back and front neighbor scenarios. The distance between antennas is increased and the backscattered signal from the target is measured. The same scenarios are simulated in CST Studio to find the variation of the induced current at the target antenna. Figure 4.4 shows the normalized simulated current and measured p_d for three side, back and front neighbor scenarios. The measured p_d and the simulated current at the alone state are also shown respectively by green and yellow markers. It is understood that in all cases the variation of the current at the target antenna when a low scattering antenna is placed in its vicinity is very negligible and is very close to its alone state. These results show that low scattering neighbor antenna has minimum effect on the target antenna. In another words, the neighbor antenna is *invisible* in the field. The slight difference between measurement and simulation results can be attributed to the parasitic resistance and inductance due to soldering and also measurement errors.

In the next step, we evaluate the effect of three factors on detecting the signal from the target antenna: increasing the number of neighbor antennas, random placement of neighbors, and random alignments of neighbor antennas (random $\emptyset$). Two type of neighbors are considered for our study: low scattering antennas and high scattering antennas (short circuit antennas). The RCS from the low and high (short circuit) scattering antennas are $0.1Cm^2$ and $135Cm^2$. The measurement setup in Figure 4.5 (a) is considered. Both E-plane and H-plane for the incident and backscattered fields are shown in Figure 4.5

(a). Each block is $10cm \times 10cm$. Throughout our study the target antenna is fixed in the field so that the incident angle of the field from the reader antenna is $\emptyset = 0$.

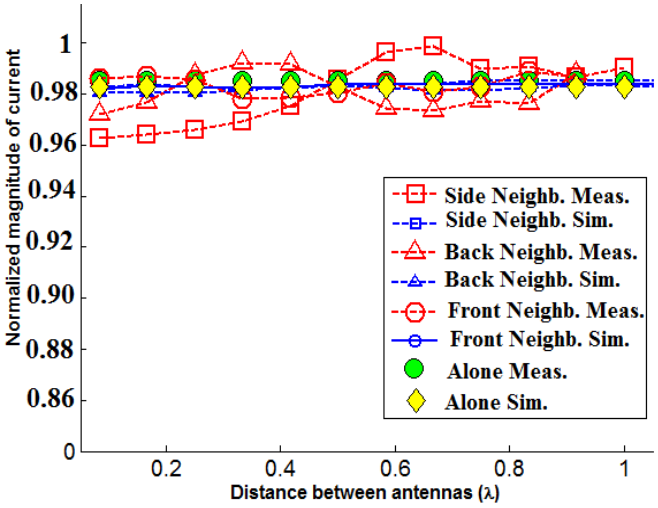

Figure. 4.4. Variation of the normalized p_d and simulated current at the target antenna.

Five case studies are considered. In each case study, first the number of neighbor antennas (i) is set to 1. A random configuration of neighbor antenna is chosen. At this random configuration the effect of using two types of neighbors antennas (high and low scatterings) on the variation of received signal from target antenna (p_d) is measured. The process of random selection of configurations of the neighbor antenna and measuring the signal from the target is repeated for N times for collecting statistics. This process is repeated by increasing the number of neighbor antennas from i =1 to i =9.

In the first case study, the effect of random placement of neighbor antennas within one block distance to the target antenna with $\emptyset = 0$ is studied. In the second case, the effect of random placement of neighbor antennas within two block distance to the target antenna with $\emptyset = 0$ is studied. Figure 4.5 (b) depicts a configuration for case study 2. In the third

case study, the effect of random placement and random polarization (random alignment in H-plane) of neighbor antennas within 1 block distance to the target antenna is studied. Figure 4.5 (c) depicts this scenario. In the fourth case study, the effect of random placement and random polarization (random alignment in H-plane) of neighbor antennas within 2 blocks distance to the target antenna is studied. Figure 4.5(c) depicts this scenario. Lastly, in case study 5 the effect of random placement and random incident angle mismatch (random alignment in E-plane) of neighbor antennas within 2 blocks distance to the target antenna is studied. Figure 4.5 (d) depicts this case study. The measurement for using both types of neighbor antennas in random configurations for case study 1,2,3,4 and 5 is respectively repeated for $N = 5,10,5,10$ and 10.

Figure 4.6 (a), (b), (c), (d) and (e) show the real and imaginary values of the demodulated signal (p_d) from the target antenna for case studies 1, 2, 3, 4 and 5 respectively. The measurement results of N measurements for i neighbor antennas ($i = 1:9$) are shown in these figures. The signal from target antenna at its alone state is also shown by a green marker. The demodulated signal from target antenna when its neighbors are all invisible antennas are shown by blue markers. The demodulated signal from target antenna when its neighbors are all short circuit antennas are shown by red markers. For all case studies, we understand that the demodulated signal from the target antenna surrounded by low scattering neighbors is very close to the signal of the target antenna at its alone state. The reason for this is that low scattering antennas have minimal mutual coupling effect on the target antenna. Thus, the current distribution at the target is less affected. And consequently, its RCS is mostly stabilized.

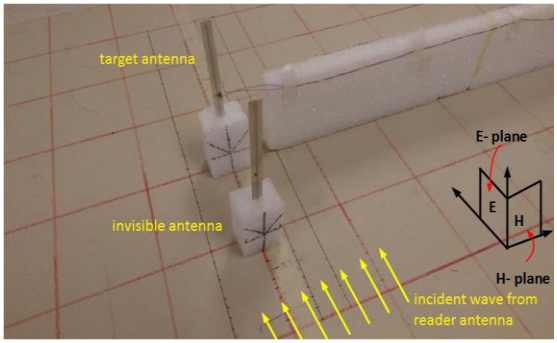

(a) Measurement setup.

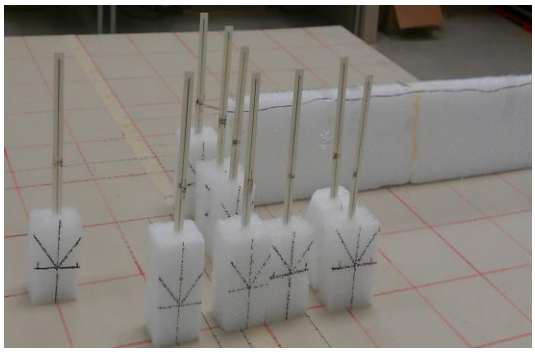

(b) Neighbors are aligned with the target antenna ($\emptyset = 0$)

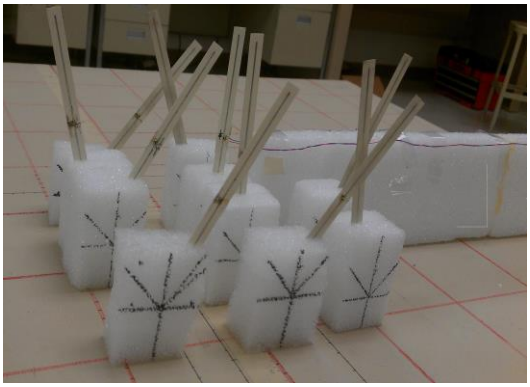

(c) Random polarization mismatch

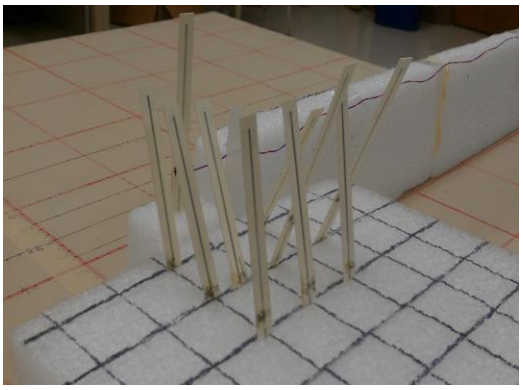

(d) Random incident angle mismatch

Figure 4.5. Random configurations of neighbor antennas.

On the other hand, when the target antenna is surrounded by high scattering antennas (short antennas) its demodulated signal is immensely degraded from the alone state of the antenna. In most cases for all case studies, the demodulated signal is very weak and is very close to zero. The reason for this is that the random placements and alignments of short neighbors produce random degradation of current distribution at the target antenna. Thus, in each measurement a new current distribution is form on the target antenna. Thus, a new value for the antenna RCS is obtained. The random interference from short circuit neighbors at the target antenna can produce constructive interference as well. If a

constructive interference from neighbor antennas is formed the resultant RCS from the target antenna is increased. Figure 4.6 (a), (b), (c) and (d) show several cases where the demodulated signal from the target antenna is stronger than its alone state. However, this is not always the case. In general, according to the results the probability of degradation of current at the target antenna and receiving very weak signal is considerably higher than having a stronger RCS from the target antenna.

In our study we understood that when short circuit neighbors are placed in front of the target antenna the probability of blocking the signal from the target is considerably higher. Instead, if short neighbors are placed behind the target antenna there is a better chance to detect the signal from the target antenna. Also, in cases where the short neighbor are placed very close to the target antenna the signal from the target antenna is lost. On the other hand, when short antennas are placed in farther distance to the target antenna their mutual coupling effect on the target is minimized. Thus, in this case the signal from the tag can be detected. Another important factor in detecting the signal from the target antenna is the alignment of neighbor antennas compared to the target.

When short neighbors have the same alignments the interference at the target is the highest. On the other hand, when short neighbors take different alignments their PLF decreases. Thus, they produce less interference to the target. In this case, the probability of detecting the signal from the target antenna is higher. The standard deviation (STD) of the demodulated signal of the target antenna from its alone state's signal is calculated for all cases. Figure 4.7 (a) shows the STD for all case studies using short antennas (high scattering) and low scattering antennas. From the results, we understand that the calculated STD for short circuit antennas is considerably higher comparing to the low scattering

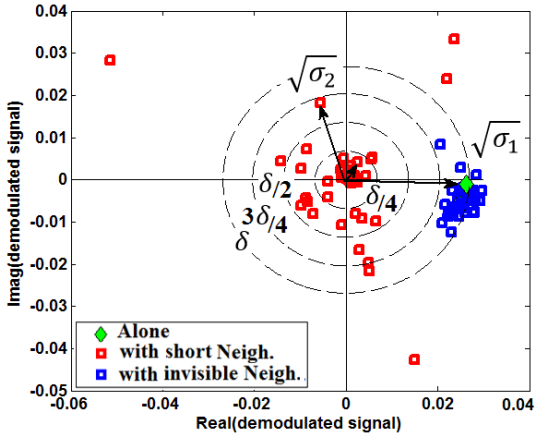

(a) Case 1

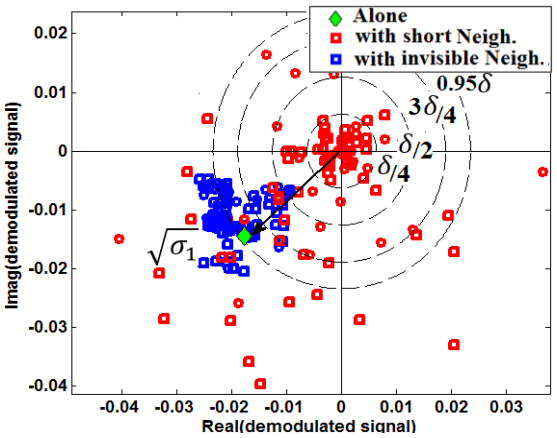

(b) Case 2

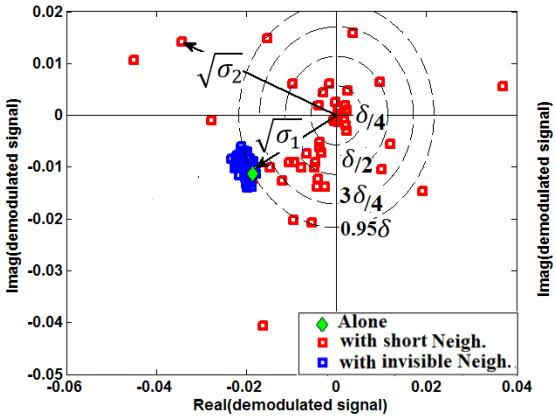

(c) Case 3

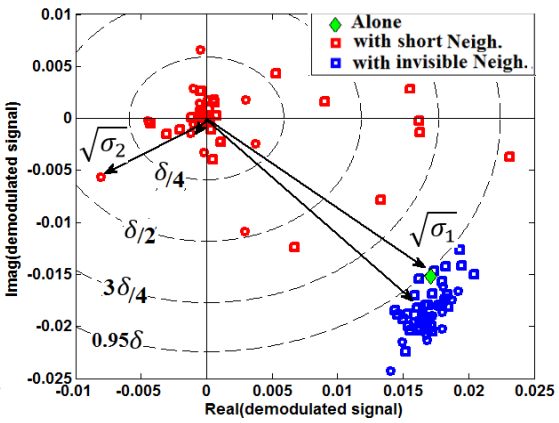

(d) Case 4

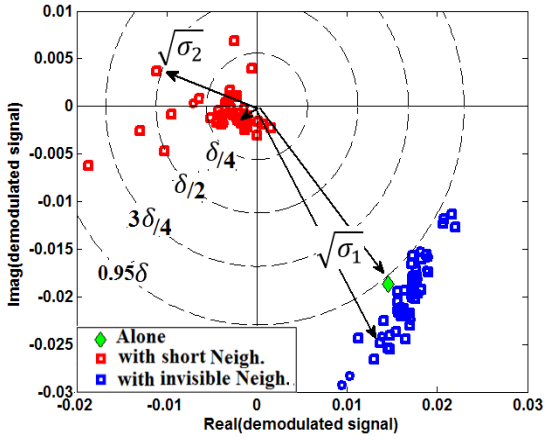

(e) Case 5

Figure 4.6. Demodulated signal from the target antenna.

antennas. Also, for both short and low scattering antennas by increasing the number of neighbors the STD increases. A study on read rate is also performed in this study. In order to detect the signal from a target antenna at a reader the received backscattered signal from target must be above a threshold. The lower the threshold at the reader antenna the more complex and expensive it is so that it can extract the signal of the target from the clutter of background noise. In our study, the magnitude of the demodulated signal from the target antenna at its alone state is called δ and is used to set thresholds for our read rate study. Four thresholds are considered to examine the read rate in our measurements $\left\{\frac{\delta}{4}, \frac{2\delta}{4}, \frac{3\delta}{4}, 0.95\delta\right\}$. These four threshold are shown in Figure 5.10 as circles with their centers at the origin and their radiuses set at $\left\{\frac{\delta}{4}, \frac{2\delta}{4}, \frac{3\delta}{4}, 0.95\delta\right\}$. According to figure 4.6, considerable number of demodulated signal measurements for cases of short circuit neighbors is inside the circle with radius $\frac{\delta}{4}$ and very close to zero. Thus, in all of these cases, when the threshold is set at $\frac{\delta}{4}$ the reader is not able to detect the signal from the target. When low scattering neighbors are used in the vicinity of the target antenna, however, the magnitude of the demodulated signal is higher than $\frac{3\delta}{4}$ for case studies 1 and 3, 0.95δ for case studies 4 and 5, and approximately $\frac{2\delta}{4}$ for all measurements in case study 2. Figure 4.7 (b) shows the read rate based on four specified thresholds for all 5 case studies. When the threshold is set at low values, i.e. $\frac{\delta}{4}$ and $\frac{\delta}{2}$, the read rates for using low scattering antennas is 100%. However, by using short circuit antennas in these situations the read rate is lower than 65%. As expected, by increasing the threshold the read rate also decreases for using both neighbor types. For case studies 1 and 2, the read rate reaches to ~ 50% for low scattering neighbor

antennas. In these two case studies the interference is the worst since the neighbors keep the same alignments as the target antenna. For case studies 3, 4 and 5 in low scattering neighbors, however, the read rate is above 80% even when threshold is set to 0.95δ. For all case studies when short neighbors are used and the threshold is set at 0.95δ the read rate reaches to approximately less than 20%. Specifically, for case study 5 the read rate reaches to zero.

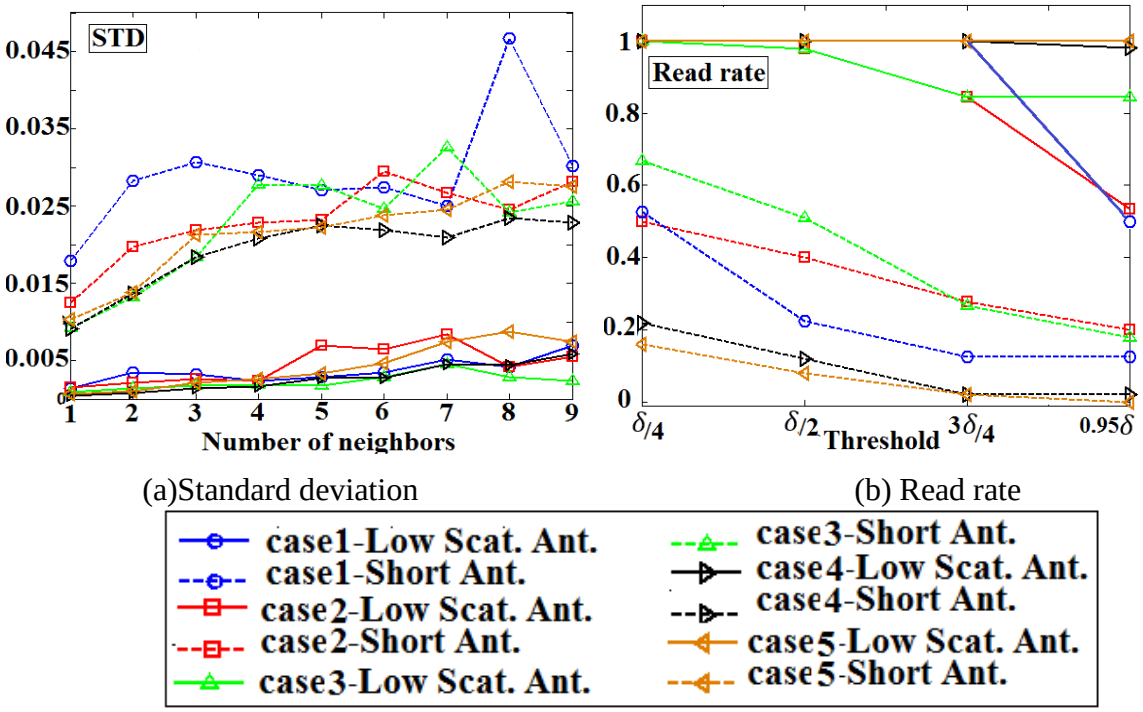

(a)Standard deviation (b) Read rate

Figure 4.7. (a) Standard deviation of demodulated signal from the alone state at target antenna (b) read rates.

The result of this study show that by using low scattering antennas in the vicinity of a target antenna the signal at the target stabilizes. In this situation, the neighbors have the less mutual coupling effects on the target antenna. Thus, the current distribution on the target is less degraded and the target can have a strong backscattering in response to the interrogation signal from the reader antenna. In this study, realizable low scattering

antennas in the lab at $RCS{\sim}50dbsm$ are used. By using ideal invisible antennas the result of this study can be improved. According to [15], the main lobes of an ideal invisible antenna are suppressed to below $-70dbsm$ and its RCS at any angle is below$-58dbsm$. Since ideal invisible antennas have the lowest interactions with their neighbors they are literally *invisible* in the field and they disturb a target antenna the lowest.

4.3 ABSORPTION CROSS SECTION

In this section, we study the absorption cross section of the studied antenna. As discussed in section 3, the absorption cross section at a tag must be above the threshold σ_a^{th} so that the tag can turn on its internal circuitry and also replies back to the reader. However, if a tag is left at its invisible state the absorbed cross section (~$0.033Cm^2$) is very low and cannot effectively stablish a backscattering link with the reader. This interesting observation reveals the fact that if an antenna is put at its invisible state it can never "*hear*" if it has been interrogated.

The absorption cross section of the studied antenna is simulated over the Γ plane of the antenna using (5). The step size $\Delta\Gamma = "0.1"$ is considered. On each point on Γ plane the corresponding load impedances are found using (5). This impedance is then used to simulate the absorption cross section of the antenna. The incident wave has the same polarization as the antenna. Figure 4.8 shows the absorption cross section over the Γ plane of the antenna. It is understood that at $\Gamma = 0$ where the antenna is matched ($Z_L = Z_a^*$) the absorption cross section is maximum. This is a well-known result and it was expected. On the other hand, by moving away from the matched state the absorption cross section of the antenna decreases. At circle $|\Gamma| = 1$ on which the farthest states to the matched state are

achieved absorption cross section reaches to a minimum. The realizable invisibility point of the studied antenna was achieved at $\Gamma = -0.9598 - 0.2807i$. This means that when the antenna is minimum scattering it is also *minimum absorbing*. Table 5.3 tabulates the absorption cross sections for a few scattering states. According to table 4.1 the absorption cross section at the matched and realizable minimum scattering states are 120 $Cm^2$and $0.033Cm^2$ respectively.

4.4 BULK READING

Bulk reading is desirable in many RFID applications. In this scenario, several tags need to be read in a short period of time. Current deployments of RFID systems do not provide sufficient reliability and accuracy. The reason for this is the interference among closely spaced RFID tags in application with bulk reading. The mutual coupling among closely spaced tags detune them from their designed input impedance and result in low power harvesting. Consequently, read rate in these networks reduces.

As a result of this study, we propose a new scattering states for RFID tags. The proposed new scattering state is the low scattering state of the RFID tags. This new scattering state is used at the tags to minimize their interference to their neighbors in bulk reading RFID applications. In our proposed model, a tag is left at its matched state. By receiving the signal from the RFID reader the tag switches its scattering states between matched and invisible states to minimize its interference in the network. Using the proposed model it is possible to suppress the high interference in RFID networks and increase the read rate.

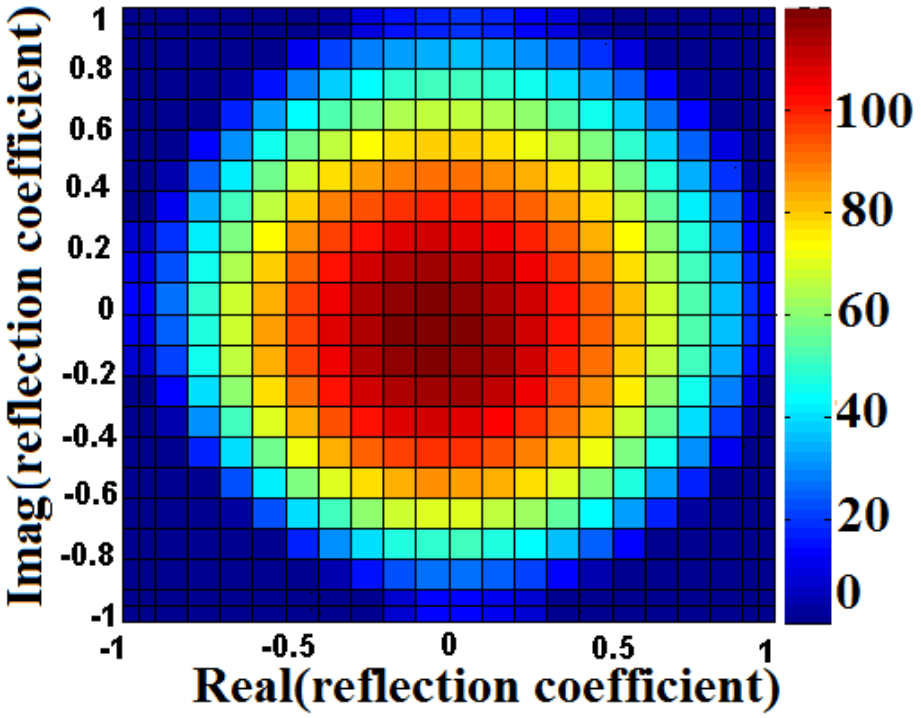

Figure 4.8. Absorption cross section (Cm^2) of the studied antenna over Γ plane.

Table 4.1. Absorption cross section of the studied antenna at $f = 1GHz$ at different scattering states.

Load	**Matched**	**Maximum scattering**	**Ideal invisible**	**Reliable invisible**	**Short circuit**
ACS ($\boldsymbol{Cm^2}$)	120	22	0.0066	0.033	0.38

5. CONCLUSIONS

In this paper, we propose a new scattering state for RFID tags to suppress interference in RFID networks. In this new scattering state tags will turn to low scattering states to reduce their interference to an ongoing backscattering link between the RFID reader and a target antenna. We showed by measurements that by using our proposed solution in a network of 10 tags the interference to the target is suppressed. In this situation, the RCS from the target antenna is stabilized and read rate increases. Our case studies shows 93.76% read rate when our solution is used. Whereas by using high scattering states at the neighbors the read rate drops to 14.16%.

REFERENCES

[1] Nikitin, P.V. ; Rao, K.V.S. , "Theory and measurement of backscattering from RFID tags.", Antennas and Propagation Magazine,IEEE Volume: 48 , Issue: 6 , 2006 , Page(s): 212 – 218.

[2] Lijuan Zhang, Wei Xiang, Xiaohu Tang, "An Adaptive Anti-Collision Protocol for Large-Scale RFID Tag Identification," IEEE Wireless Comm. Lett., vol. 3, no. 6, pp 601 – 604, Sep. 2014.

[3] A. Bletsas, S. Siachalou, J.N. Sahalos, "Anti-Collision Backscatter Sensor Networks," IEEE Trans. on Wireless Comm., vol. 8, no. 10, pp. 5018 – 5029, Oct. 2009.

[4] Qi Zhang, M.J. Crisp, R.V Penty, I.H. White, "Reduction of Proximity Effects on UHF Passive RFID Systems by Using Tags With Polarization Diversity," IEEE Transac. Antenn. Propag., vol. 63, no. 5, pp. 2264 - 2271, Feb. 2015.

[5] C. H. Loo, A. Z. Elsherbeni, F. Yang, D. Kajfez, "Experimental and Simulation Investigation of RFID Blind Spots," Journal of Electromagnetic Waves and Applications, vol 23, no. 5-6, Apr 2009.

[6] Asl, S.E, Ghasr, M.T, Zawodniok, M, Robinson, K.E., "Preliminary study of mutual coupling effect on a passive RFID antenna array," in proceeding Instrumentation and Measurement Technology Conference (I2MTC), 2013 IEEE International , May 2013.

[7] Feng Lu, XiaoSheng Chen, Terry T. Ye, "Performance analysis of stacked RFID tags," in IEEE Int. RFID Conf., April 2009, pp. 330 - 337.

[8] Sawaya, T. ; Taromaru, M. ; Ohira, T. ; Komiyama, B. "Experimental Proof of Electrically Invisible State of Inductively Loaded Dipole and Proposal of Electrically Invisible Meander-Lines", Antennas and Propagation, IEEE Transactions on Nov. 2006, Volume: 54 , Issue: 11 , Page(s): 3374 – 3382.

[9] Kahn, W. , Kurss, H. , "Minimum-scattering antennas" , Antennas and Propagation, IEEE Transactions on, Volume: 13 , Issue: 5 , Page(s): 671 – 675, Sep 1965.

[10] Semnani,B. Borji, A. "Lower Bound on Scattered Power from Antennas", Antennas and Wireless Propagation Letters, IEEE , 2012, Volume: 11, Page(s): 373 – 376.

[11] Chen, K. Ann Arbor, Liepa, V. "The minimization of the back scattering of a cylinder by central loading", Antennas and Propagation, IEEE Transactions on, Volume: 12 , Issue: 5 , Page(s): 576 – 582, Sep 1964.

[12] B.D. Popović, Theory of cylindrical antennas with lumped impedance loadings, Radio and Electronic Engineer (Volume:43 , Issue: 4), April 1973 , Page(s): 243 – 248.

[13] Yueh-Ying Hu, "Back-scattering cross section of a center-loaded cylindrical antenna." Antennas and Propagation, IRE Transactions on (Volume:6 , Issue: 1) January 1958 Page(s):140 – 148.

[14] R. Harrington, J. Mautz, "Straight wires with arbitrary excitation and loading," Transac. on Anten. and Propag., vol. 15, no. 4, pp. 502 – 515, Jul 1967.

[15] Shadi Ebrahimi-Asl, M.T Ghasr, M. Zawodniok, "Application of Low Scattering Antennas to RFID Networks," to be appear in proceeding of RFID Conference 2016.

[16] Constantin A. Balanis, Antenna Theory, Wiely, 2005.

[17] J.B. Andersen and A. Frandsen, "Absorption efficiency of receiving antennas," IEEE Trans. Antennas Propag., vol. 53, no. 9, pp. 2843 – 289, Sep. 2005.

[18] R. B. Green, "The general theory of antenna scattering," Report No. 1223-17, ElectronScience Laboratory, Columbus, OH, Nov, 1963.

[19] Chih-Chuan Yen, A.E. Gutierrez, D. Veeramani, D. van der Weide, "Radar Cross Section Analysis of Backscattering RFID Tags," Antennas and Wireless Propagation Letters, vol. 6 , pp. 279 – 281, 2007.

[20] Shadi Ebrahimi-Asl, M.T Ghasr, M. Zawodniok, "Implementation of Invisible Antenna with Application of RFID Systems," provisional patent application 62/248,870, October 2015.

[21] Daniel Mark Dobkin, "RFID Systems Including Tags Having Low RF Scattering Mode," U.S. Patent 2007/0115098 A1, May. 24, 2007.

V. PRELIMINARY STUDY ON MUTUAL COUPLING

ABSTRACT

The communication quality between an RFID tag and a reader in a RFID network is affected by several factors including the distance between a reader and a tag, orientation of the antennas, and scattering from neighbor tags. Some studies have analyzed those factors and their impact on a read-rate of RFID systems. However, they neglected the effect of a mutual coupling among neighbor tags. In this paper, we formulate the driving currents of a RFID antenna array considering the mutual impedance among tags. Afterwards, we both measure and simulate the mutual impedance for the used RFID tag that is Alien 9640 Squiggle Inlay and we compare the result with half wave dipoles which we construct. Simulation results show that current distribution on tags increases when compared with the case that mutual coupling is not considered among tags.

1. INTRODUCTION

In practical deployments of passive RFID networks, several tags are placed in close proximity making a passive (or parasitic) antenna array [1]. In such a scenario, mutual coupling between tags' antennas becomes significant factor in system performance in that the current distribution on an antenna changes based on the current distribution on another antenna in its near field zone. Therefore, tags will experience variable impedance characteristics, which alter the impedance matching between the RFID antenna and its IC. Consequently, the power transfer to the IC will not be optimal and the RF signal will be distorted thus reducing performance in terms of read rate and read range. In [2], it has been shown that the tags' read rate is affected by the presence of other tags in their close vicinity. However, these works did not completely explain the observed phenomena.

For backscattering RFID systems, there is a limited work that considers the mutual coupling effect into tag reading rate and backscattering [3], [4]. In [3], a theoretical model with simulations for analyzing mutual coupling among stacked RFID tags is presented. However, that work provided no experimental validation and verification, which is presented here. Also, in [4] the effect of separation distance, orientation arrangement and polarization on mutual coupling and read rate of tags were given.

Analytically evaluation of mutual coupling is a difficult task but can be done for simple elements [5]-[7]. Consequently, numerical methods, for instance the moment method and induced EMF method, are employed to study the mutual coupling effect for more complex antennas and antenna systems [8]-[9]. Also, circuit models for analyzing coupling effect were suggested and investigated in the literature [10], [12]. Also, the effect of mutual coupling in antenna array has long been thoroughly investigated in literature

[11]-[13]. However, such studies have yet to be carried out for RFID tags which are not typical, controlled antenna arrays. Against traditional antenna arrays, passive RFID arrays have no feed sources and they should harvest energy from the incident signal “as-it-is” received from the reader to power up their internal IC and modulate the scattered signal. Therefore, a new terminology for evaluating passive RFID antenna array should be defined.

In this paper, using a circuit model for an array of RFID tags we drive a simple formula for driving currents of each element in the array. Then, we analyze mutual coupling impedances for Alien 9640 Squiggle Inlay RFID tag by both measurement and simulation using CST Microwave Studio. The results are compared with a half wave dipole both in measurements and simulations. Simulating an array of ten RFID tags in a linear array configuration, the driving currents at tags are studied using measured mutual impedances. Finally, we show that mutual coupling can be utilized to enhance the read rate of an RFID tag by increasing the induced current at distant tags.

The rest of this paper is organized as follows. In Section 6.3 we develop our circuit model for an RFID antenna array. In Section 6.4, we present our work on the comparison between mutual impedance for RFID and half wave dipoles. In Section 6.5, simulation results for pattern of RFID antenna array and the effect of coupling on current distribution on tags are presented. Conclusions and future work are presented in Section 6.6.

2. AN ARRAY OF COUPLED RFID TAGS

Mutual coupling, being a near field phenomenon, results in changed input impedance of an RFID antenna which consequently results in a non-optimum power transfer to the chip. Thus, in applications where several RFIDs should work beside each other, mutual coupling should be taken into account to have an accurate design and performance study. To simplify the analysis of mutual coupling, Z-parameters are used in the literature [14]: $\bar{Z} = [Z_{ij}]$ *i, j=1,2* in which Z_{11} and Z_{22} are the input impedances of antenna 1 and 2 respectively and Z_{12} and Z_{21} are defined as the induced impedances in the circuit of antenna 1 from antenna 2 and of antenna 2 from antenna 1 respectively.

Let's consider *1, 2,..., N* RFID tags on y axis as depicted in Figure 2.1. A reader is considered at the coordinate's center to illuminate tags. The impinging electric field from the reader at a tag produces an incident power

$$\mathrm{P_{rad}} = \frac{1}{2}\,.\,|\mathrm{E} \times \mathrm{H}| = \frac{1}{2}.\frac{[\mathrm{E}]^2}{\eta} \tag{1}$$

The absorbed power by the tag would be

$$\mathrm{P_{tag}} = \mathrm{P_{rad}}.\,\mathrm{e_t} = \mathrm{P_{rad}}.\,(1 - |\Gamma|^2) = \mathrm{P_{rad}}.\left(1 - \left(\frac{\mathrm{Z_{ch}} - \mathrm{Z_a}}{\mathrm{Z_{ch}} + \mathrm{Z_a}}\right)^2\right) \tag{2}$$

where $\mathrm{e_t}$ is the efficiency of the tag and Γ is the reflection coefficient and Z_{ch} and Z_a are impedance of chip and antenna respectively. The induced voltage at the antenna would be calculated as $\mathrm{P}_{tag} = \frac{{V_{tag}}^2}{R_a}$ where R_a is the radiation resistance of the antenna. The induced current in the circuit of a tag would then be calculated as

$$I_{tag} = \frac{V_{tag}}{Z_a + Z_L} \tag{3}$$

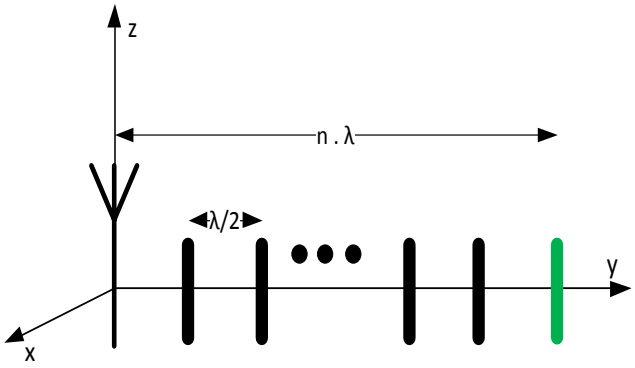

Figure 2.1. An array of passive RFID tags.

As soon as an induced current is produced in a tag's circuit, the mutual coupling phenomenon between adjacent antennas is formed which can be defined as additional power voltage in a tag's circuit as shown in Figure 2.2 (a). The additional voltage sources will alter the current distribution in the circuit of a tag. The new current distribution at the *i*th tag can be shown as

$$\mathrm{I'_{tag_i}} = \frac{\mathrm{V_i} + \sum_{j=1}^{M} \mathrm{V_{ij}}}{\mathrm{Z_a} + \mathrm{Z_{ch}}} \tag{4}$$

where *M* is the effective number of tags for which mutual coupling effect exists, V_{ij} is the mutual coupling voltage generated at the *i*th tag because of the current of the *jth* tag. The coupled voltage V_{ij} can be written as $V_{ij} = Z_{ij.}\mathrm{I}_j$ where Z_{ij} is the mutual impedance between *i*th and *j*th tag and I_j is the current in the *j*th tag. Using (3) in (4) we have

$$\mathrm{I'_{tag_i}} = \mathrm{I_{tag}} + \frac{1}{\mathrm{Z_a} + \mathrm{Z_{ch}}} . \sum_{j=1}^{M} \mathrm{Z_{ij.}} \mathrm{I_j} \tag{5}$$

Now, since the mutual coupling effect is considered as a near field phenomenon distant tags will have minimal contribution in the additional induced voltage sources in any tag. Assuming *effective mutual coupling distance* $d_{MC} = P.\lambda/2$ to be the distance where mutual coupling effect between two tags exist

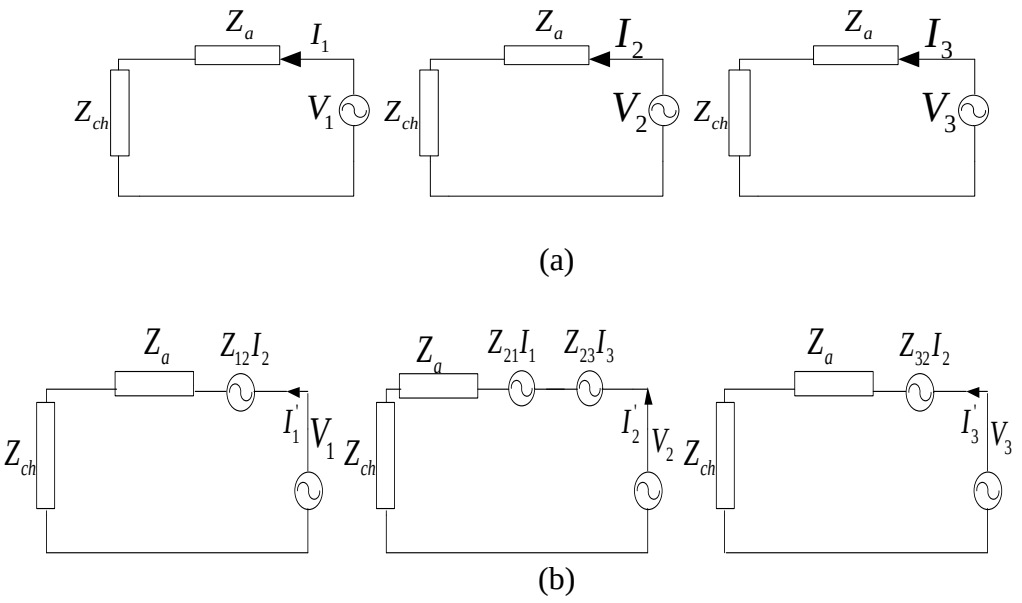

Figure 2.2. (a) Tags when currents are induced at their circuit. (b) Circuit model of mutual coupling effect in RFID antenna array for N=3, P=1.

$$\begin{pmatrix} I'_{tag_1} \\ I'_{tag_2} \\ \vdots \\ I'_{tag_{N-1}} \\ I'_{tag_N} \end{pmatrix} = \begin{pmatrix} I_{tag_1} \\ I_{tag_2} \\ \vdots \\ I_{tag_{N-1}} \\ I_{tag_N} \end{pmatrix} + \frac{1}{Z_a + Z_{ch}}.$$

$$\begin{pmatrix} 0 & Z_{11} & Z_{12} & \cdots & Z_{1P} & \cdots & 0 & 0 & 0 \\ Z_{21} & 0 & Z_{21} & Z_{22} & \cdots & Z_{2P} & \cdots & 0 & 0 \\ Z_{32} & Z_{31} & 0 & Z_{31} & Z_{32} & \cdots & Z_{3P} & \cdots & 0 \\ \vdots & \vdots & \vdots & \vdots & \vdots & \vdots & \vdots & \vdots & \vdots \\ 0 & 0 & \cdots & Z_{N-1.P} & \cdots & Z_{N-1.2} & Z_{N-1.1} & 0 & Z_{N-1.1} \\ 0 & 0 & 0 & 0 & Z_{NP} & \cdots & Z_{N2} & Z_{N1} & 0 \end{pmatrix} \begin{pmatrix} I_{tag_1} \\ I_{tag_2} \\ \vdots \\ I_{tag_{N-1}} \\ I_{tag_N} \end{pmatrix} \quad (6)$$

where Z_{ij} is the mutual impedance between tag i and j and the jth tag is $d = j.\lambda/2$ away from the ith. Now, the driving currents of tags $\overline{I'_{tag}}$ cause the chips turn on. But, to estimate I'_{tag} we need to know the values of mutual impedances.

3. EXPERIMENTAL VALIDATION OF MUTUAL COUPLING

In this section, the mutual coupling is both simulated and experimentally validated for two side-by-side Alien 9640 Squiggle Inlay RFID tags. It is shown in the results, that the mentioned RFID tag has a similar pattern to a half wave dipole. Thus, to have a benchmark, we construct two half wave dipoles and we also verify the well-known mutual impedance between half wave dipoles [14] by simulation and measurement.

3.1 MEASURING MUTUAL COUPLING

Two half wave dipole antennas was constructed for a *f=1GHz* as shown in Figure 3.1 (b). The dipole length is 15 cm and is fed by a short (~1" long) coaxial cable. To prepare the RFID tags for experiment, they were mounted onto a piece of cardboard slightly bigger than the antenna size for structural support as shown in Figure 3.1. The microchip was then removed from these antennas to allow contact points. These contact points were connected to an SMA connector through two thin copper strips.

Figure 3.1 (a) shows the experimental setup for measuring the mutual coupling between two antennas. The antennas were placed in a small anechoic chamber and connected to an Agilent 8753E vector network analyzer (VNA). The VNA was calibrated such that the measurements are referenced to the input of the antennas. The VNA measures the S-parameters (i.e, transmission and reflection coefficients) of the set up. The S-parameters are then transformed to Z parameters using

$$[\mathrm{Z}] = ([\mathrm{U}] - [\mathrm{S}])^{-1}.([\mathrm{U}] + [\mathrm{S}]) \qquad (7)$$

where U is unit matrix. These measurements were conducted three times with varying distance between the antennas for up to 45 cm separation and the average value is considered for analysis.

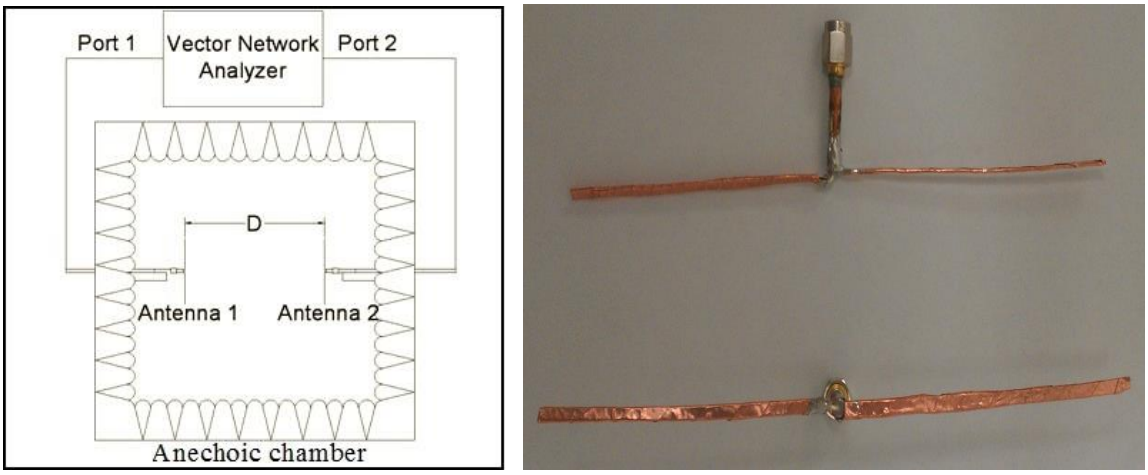

Figure 3.1. (a) Experiment setup; (b) Constructed dipole.

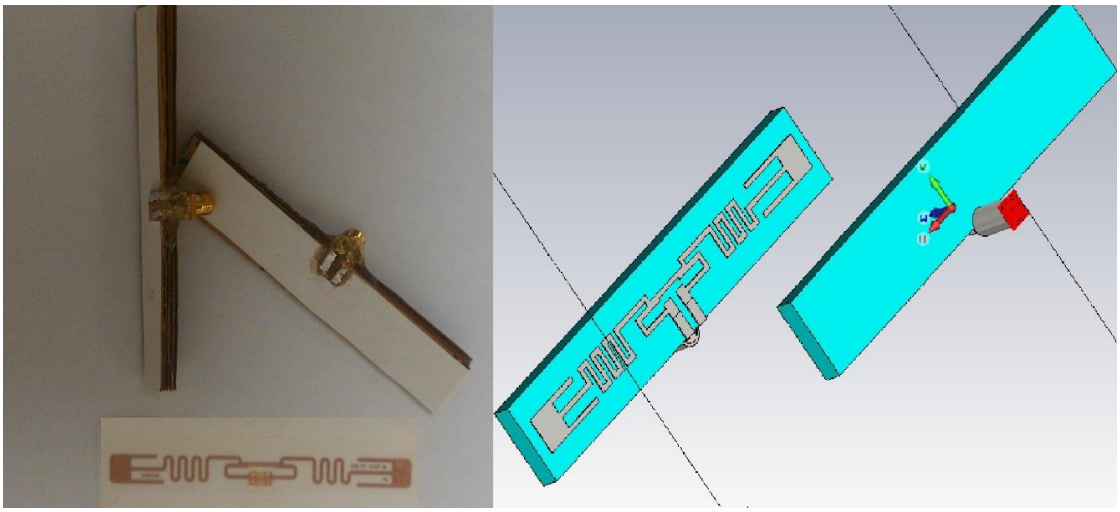

Figure 3.2. Prepared and simulated Alien 9640 Squiggle Inlay RFID tag.

The same set up of the experiment was simulated in CST Microwave Studio (numerical electromagnetic simulation tool) for both dipoles and the Alien tag. The simulation produced S-parameters and then these S-parameters were converted to Z-parameters as before. The S and Z Matrices were recorded and compared to the measured results.

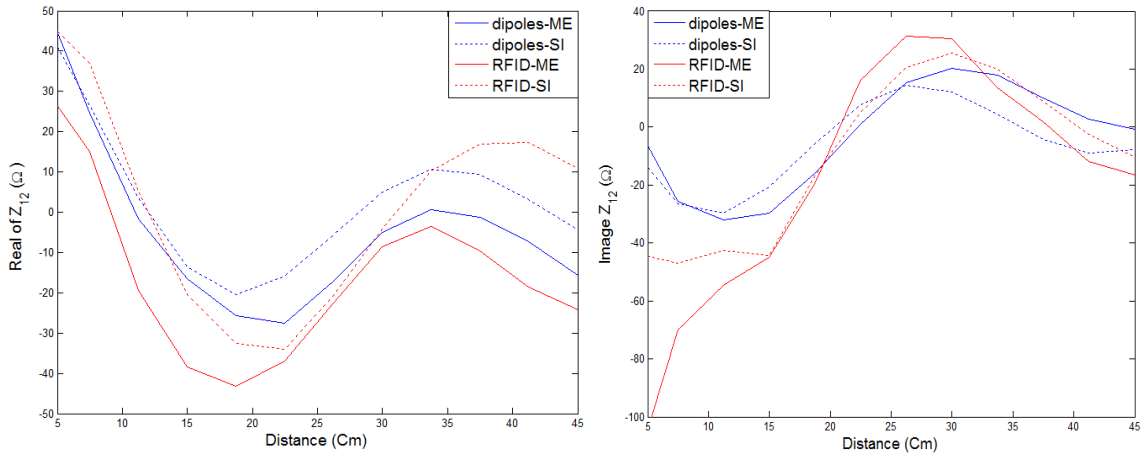

(a) (b)

Figure 3.3. A comparison between mutual impedance between two side by side antennas of RFIDs and half- wave dipoles. (a) Real part, (b) Imaginary part.

3.2 MEASUREMENT AND SIMULATION

Figure 3.3 (a) and (b) shows the real and imaginary parts of the mutual impedance for both RFID and dipole antennas. Since Z_{12} and Z_{21} show the interaction between two antennas their values are the same. As for dipoles, impedance values and trends of both measured and simulated graphs matched up well with each other and with the calculated mutual impedance for side-by-side configuration found in [14]. The differences in magnitude between graphs in here and [14] could be attributed to the dipole antenna thickness and the gap of the dipole feed point is not similar to the thin cylinder dipole in

[14]. The difference between measured and simulated versions also is attributed to measurement errors, construction of the RFID feed connector, and the poor quality of the very small anechoic chamber used in this experiment. Also, the values of impedance and trend of both measurement and simulation for the dipoles and RFID are similar. Furthermore, though in comparison to dipoles the magnitudes of mutual impedance are different, it is interesting to see that the trend of mutual coupling impedances for the RFID tag is similar to a half wave dipole both for real and imaginary parts.

4. CURRENT DISTRIBUTION FOR AN ARRAY OF RFID TAGS

A linear array with half-wave spacing of N=10 RFID tags with P=3 is considered for simulation. Figure 4.1 shows the normalized value of currents $\overline{I_{tag}}$ for tags based on their distances to the center. Though in the case where mutual coupling has not been considered a gradual decrease in the magnitude of current (Itag) is seen, where mutual coupling comes to consideration it is understood that the value of currents (I′tag) are not monotonically decreased. This shows that mutual coupling in RFID tags can help increase the read rate of tags since they increase the current induced on the tags comparing to the case of no mutual coupling.

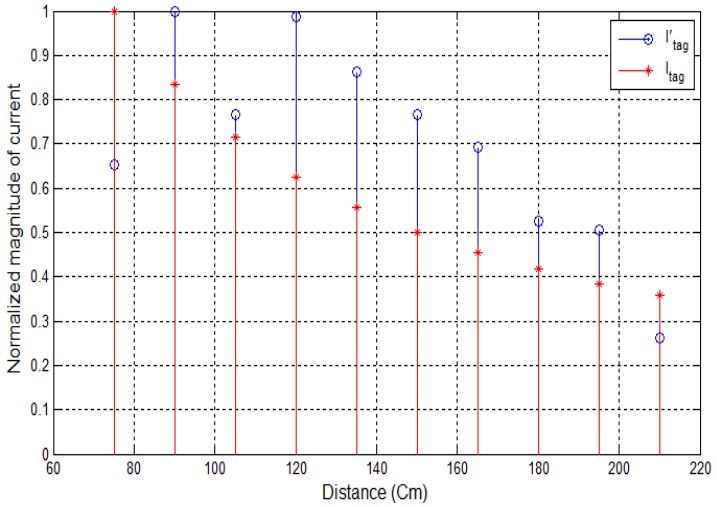

Figure 4.1. Normalized value of currents with and without mutual coupling.

5. CONCLUSIONS AND FUTURE WORK

In this paper, first, the driving currents for a passive RFID array are formulated. The mutual impedance between two side-by-side Alien 9640 Squiggle tags and half wave dipoles was measured experimentally and compared against results simulated in the CST Microwave Studio. The comparison shows that the particular RFID tag behaves similarly to a half wave dipole. The measured values for mutual impedances were used to simulate current distribution on an RFID array. Simulation results show that current level on the tags generally increases when compared with the case that mutual coupling is not considered among tags. In this work we assumed an RFID as a secondary power source which absorbs, generates and reflects power. The future work will include analysis of mutual coupling among RFID tags by considering RFID as a scatterer with dynamic impedance to control the amount of power received at any tag.

REFERENCES

[1] Ting-Jui Huang; Pei-Hsuan Pan; Heng-Tung Hsu "Adaptive Beam Steering Smart Antenna System for Ultra-High-Frequency Radio Frequency Identification Applications", Computer, Consumer and Control (IS3C), 2012 , Page(s): 713 – 716.

[2] Soylemezoglu, A.; Zawodniok, M.J.; Jagannathan,S., "RFID-Based Smart Freezer", Industrial Electronics IEEE Transactions on Volume: 56 , Issue: 7 , 2009 , Page(s): 2347 – 2356.

[3] XiaoSheng Chen ; Ye, T.T. "Performance analysis of stacked RFID tags", RFID, 2009 IEEE International Conference, Page(s): 330 - 337 ,2009.

[4] Hsueh-Jyh Li ;Hsin-Hsu Lin ; Hsin-Hung Wu , "Effect of antenna mutual coupling on the UHF passive RFID tag detection", Antennas and Propagation Society International Symposium, Page(s):1-4,2008.

[5] H.E. King, "Mutual Impedance of Unequal Length Antennas in Echelon", IEEE Trans. Antennas Propagat., Vol. AP-5, pp 306-313, July 1957.

[6] H.C. Baker, "Digital computation of the Mutual Impedance Between Thin Dipoles," IEEE Trans. Antennas Propagat., Vol 10, pp 172-178, 1962l.

[7] A.E. Gera, "Simple Expressions for Mutual Impedances," IEEE Proceedings, Vol. 135, Pt. H, pp 395-399, December 1988.

[8] G.J. Burke and A.J. Poggio, "Numerical Electromagnetics Code (NEC)-Method of Moments," Techincal Document 11, Naval Ocean Systems Center, San Diego, Calif., January 1981.

[9] A.J. Julian, J.M. Logan, and J.W. Rockway, "MININEC: A Mini-Numerical Electromagnetics Code," Techincal Document 516, Naval Ocean Systems Center, San Diego, Calif., September 6, 1982.

[10] Kun-Chou Lee , Tah-Hsiung Chu , "A circuit model for mutual coupling Analysis of a finite antenna array", IEEE Transactions on Electromagnetic Compatibility, Volume: 38 , Issue: 3 , Page(s): 483 – 489,1996.

[11] Svantesson, T, "The effects of mutual coupling using a linear array of thin dipoles of finite length", Statistical Signal and Array Processing, 1998. Proceedings., Ninth IEEE SP Workshop on, Page(s): 232 – 235.

[12] M. Thevenot, C. Menudier, A. El Sayed Ahmad, G. Zakka El Nashef, F.

[13] Fezai, Y. Abdallah, E. Arnaud, F. Torres, and T. Monediere, "Synthesis of Antenna Arrays and Parasitic Antenna Arrays with Mutual Couplings", International Journal of Antennas and Propagation, Volume 2012.

[14] Oraizi, H. , Fallahpour, M. , "Array pattern synthesis with mutual coupling consideration, Telecommunications, 2008. IST 2008. International Symposium , Page(s): 77 – 82.

[15] Constantin A. Balanis, antenna theory, Wiely, 2005.

VI. COOPERATIVE INTERFERENCE CONTROL IN NEIGHBORING PASSIVE ANTENNAS WITH APPLICATION TO RFID NETWORKS

ABSTRACT

Passive backscattering links suffer from mutual coupling among closely spaced neighbor antennas. This results in un-matched circuitry at input ports of antennas causing poor power harvesting, weak backscattering and overall low read rates. In this paper, cooperative control of interference through impedance switching at neighboring scattering antennas is proposed. Simulation and measurement results demonstrate that by using load switching at a neighbor RFID tag it is possible to control their mutual coupling effect to a target tag in order to enhance its communication performance. Also, we show that by using the proposed load switching at the neighbor antenna it is possible to improve the backscattering signal from the target from up to 3.4 dB over its backscattering signal when it is alone in the field. To this end, the position of the neighbor antenna with respect to the target and the incident wave have a great impact on this achievable gain.

1. INTRODUCTION

Radio frequency identification (RFID) is becoming more popular in short range data communication area due to its promising features: lower energy consumption, simple deployment and low maintenance. Data communication by RFID systems is performed by encoding the electromagnetic scattering wave from a target antenna. A target antenna is illuminated by a source signal from an RFID reader. The incident electric field induces a current distribution on the target antenna which results in backscattering. By using a switch and two load impedances at the target antenna, it is possible to encode the stored data (modulate the scattering) on top of source signal and reflect it back to the reader [1]. However, these systems suffer from a main drawback. Due to *mutual coupling phenomenon,* as soon as an additional (or more) antenna(s) is introduced in the field, the communication link with the target antenna experiences interference and poor backscattering [1]-[5]. This issue produces blind spots in these networks where the RFID reader cannot communicate with tags [3].

Network representation of mutual coupling for transmitting and receiving antennas has long been studied in the literature [6]. References [4] and [5], use this model to study the mutual coupling interactions in the *virtual antenna array* formed by RFID antennas. In the traditional model for mutual coupling, the voltages are open circuit voltages. Thus, the mutual coupling impedance Z_{12} (Z_{21}) is calculated when antenna 1 (antenna 2) is set at a non-functional state and its source is off, i.e. open circuit state: $I_1 = 0$ ($I_2 = 0$). Using this evaluation for receiving and scattering antennas produces some ambiguities. First, it is also well established that the current distribution is a strong function of the antenna loads [7]-[12]. Furthermore, it is well understood that by making antennas open circuit their

scattering will not go to zero and they are still functional. Due to these reasons, in [13], Hui introduced a new model for evaluating mutual coupling in *receiving antennas*

$$\begin{bmatrix} V_1 \\ V_2 \end{bmatrix} = \begin{bmatrix} V_1^{alone} \\ V_2^{alone} \end{bmatrix} + \begin{bmatrix} 0 & Z_{12} \\ Z_{21} & 0 \end{bmatrix} \begin{bmatrix} I_1 \\ I_2 \end{bmatrix} \quad (1)$$

where V_1^{alone}, V_2^{alone} are the induced voltage on the antennas when the neighbor antenna is placed at distance d=∞. And $V_1^{MC} = Z_{12}I_2$ and $V_2^{MC} = Z_{21}I_1$ are the additional induced voltage at each antenna due to the presence of a neighbor antenna in their vicinities. The mutual coupling impedance between two side by side monopoles with reference to standard impedances (short, open, 50Ω) is measured using 2-port VNA measurements in [13], [14] in that the load in neighbor monopole is changed and the variation of the voltage in the target antenna is monitored by measuring S_{21}.

Measuring Z_{12} and Z_{21} in (1) for scattering antennas is very challenging. To measure these values, the voltages and currents of both antennas at their ports must be measured. However, by introducing any measuring instrument at the input port of the scattering antenna the distribution of the current is altered resulting in flawed measurements. On the other hand, mutual coupling in scattering mode cannot be measured by using 2-port VNA measurements. First, in general, scattering antennas can have different load values and not only standard loads. Second, by connecting the antennas to the input port of the VNA the distribution of the current is altered. In this paper, we use 1-port measurement to study the variation of the current of the antennas in (1) in backscattering links.

Controlling the mutual coupling interactions among closely spaced antennas has long been studied in the literature in Yagi antennas and later on in *Electrically-Steerable Parasitic Array* [6], [15],[16]. In these works, the goal has been to design and direct the

pattern of the overall antenna structure toward a desired direction. However, in RFID networks, the goal is to extract individual signals from each tag in the network from the all the chaos of interference in the network [1]. To overcome the low read rate due to mutual coupling issue in RFID networks, spatial, frequency and polarization diversities have been proposed in the literature [4], [17]. Some resources develop collision detection and collision avoidance techniques to solve this problem [18], [19]. In the proposed solution in [20], all tags of the same type call out the same pre-agreed-message at the same time in response to the interrogation signal from the reader. In this method, tags will *cooperate* to synchronize their scattering instead of producing interference to each other. However, this method faces its own challenges and shortcomings. First, if tags are located in a blind spots (caused by interference due to mutual coupling) they cannot cooperate [3]. Second, synchronization of independent and randomly located tags is a big challenge in this method. Furthermore, this method is unable to filter out the backscattering signals of individual tags in the network to access to their data.

Two factors in controlling the mutual coupling must be considered: 1) the distance between antennas, 2) their load impedances. In [2], the effect of the load impedance of the target antenna on the level of destructive interference from neighboring tags at different distances is studied. In [1], we have shown that in a two tag system by putting one antenna at a low scattering state it is possible to suppress its interference at the other antenna regardless of its distance to it. One major challenge in controlling mutual coupling in RFID networks is that the distance among tags is not a known variable. Thus, the introduced method in [1] is a strong solution since it is not dependent on the distance among antennas.

Multi-port RFID tags have already been proposed in the literature for RFID sensing applications [21], [22]. In this paper, first we study the effect of mutual coupling between closely spaced scattering antennas. We propose an analysis method which is numerically based for evaluating the mutual coupling in scattering antennas. In the next step, we extend our study in [1] to a case where the neighbor antenna helps a target antenna to increase its backscattering signal over the case when it is alone in the field. We show that if tags "cooperate" they will not produce interference to each other and instead they can help each other to increase their backscattering signal strength. Our proposed solution contains a multi-port RFID which switches to different load impedances depending on its distance to the target to avoid destructive interference and instead produce constructive interference at the target antenna. We study the effect of both distance and load impedance of the neighbor antenna on the level of interference in the backscattering signal from the target antenna. We show if the neighbor is placed in front of the target it completely blocks the backscattering signal from the target. In this situation, by switching to an appropriate load at the neighbor which is within $\boldsymbol{0 < d < \lambda}$ distance to the target antenna the signal strength from the target can be improved from up to $\boldsymbol{3.28dB}$ over its signal when it is alone in the field ($\boldsymbol{\lambda}$ represents the operation wavelength). When the neighbor is placed either in the back or side of target antenna, depending on its distance to the target it can switch to different loads to increase the signal strength of the target. This increase in the signal strength from the target is up to 3.4dB and 3.24dB respectively for when the neighbor is placed within $\boldsymbol{0 < d < \lambda}$ at the side or back of the target antenna over its signal when it is alone in the field. We use a non-invasive method to measure the interference in closely spaced antennas. In this method, we use Modulated Scattering Technique to measure the

scattered filed from the target antenna at reader antenna by 1-port VNA measurements [1], [6]. The contribution of this paper is: (1) Proposing an analysis method for evaluating mutual coupling impedance in scattering antennas (2) introducing a multi-port RFID tag to avoid destructive interference and instead increase the backscattering signal strength in RFID networks. (3) Using Modulated scattering technique to measure and study interference in backscattering links.

2. PROBLEM FORMULATION AND ANALYSIS

The backscattered field from a linear antenna with length l on z axis can be characterized as [6]

$$E_s = j\eta \frac{ke^{-jkr}}{4\pi r} Sin\theta \left[\int_{-l/2}^{l/2} I(x', y', z') e^{jkz' Cos\theta}\, dz' \right] \quad (2)$$

where I represents the current distribution on the antenna. The general form of the induced current distribution is strongly dependent on the selected load for the antenna as well as the antenna structure [1], [6]-[12]. The scattered power from the antenna is characterized by its radar cross section (RCS)

$$\sigma = \lim_{r\to\infty} 4\pi r^2 \frac{|E_s|^2}{|E_i|^2} \quad (3)$$

in that E_s is characterized by (2) and E_i is the incident wave on the antenna. In this paper, the *alone state* for an antenna is attributed to the case where the antenna is alone in the field. A half-wave dipole antenna ($f = 1\ GHz$) is considered. The antenna is illuminated by a plane wave with the same polarization (linear) as the antenna. The RCS and the induced current on the antenna at its alone state are studied based on capacitive loads (0 to15 pF). Figure 2.1 (a) and (b) show the real and imaginary values of the induced current at the input port of the antenna and also its RCS based on the used loads. At small capacitive load impedances the load acts as an open circuit. This results in very small current at the antenna and RCS. For capacitive load equal to C~1.25 pF the current and RCS at the antenna reaches to a maximum. Beyond this capacitance value, the magnitude of current decreases until it converges to a constant value.

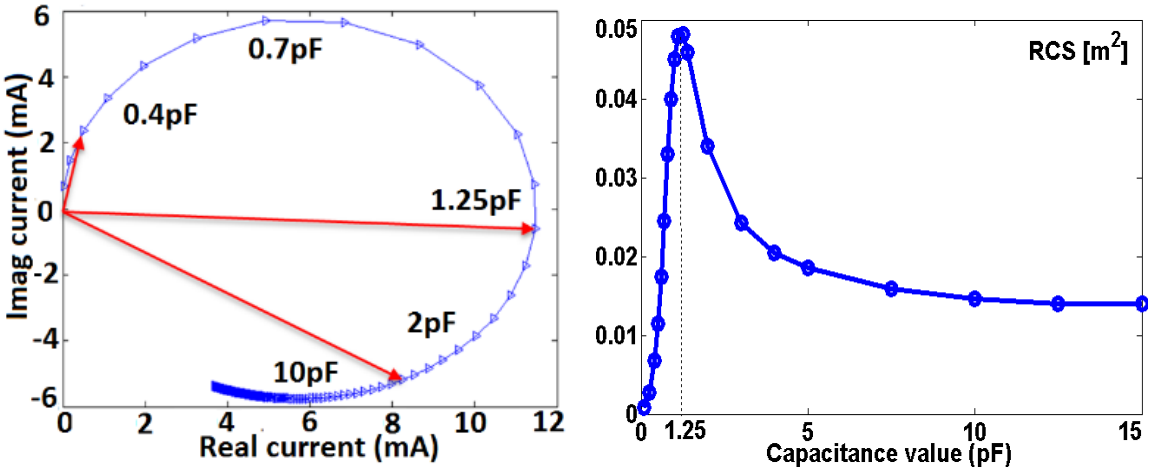

(a) (b)

Figure 2.1. (a) Alone state current based on capacitive loads (b) Antenna RCS based on capacitive loads.

By introducing a second antenna (neighbor antenna) in the field the current distribution on the antenna (now called target antenna) is altered due to the mutual coupling effect. This change in the current distribution will result in the degradation of the backscattered field from the antenna. An identical half-wave dipole (antenna 2) with a different load impedance is placed beside antenna 1 as shown in Figure 2.2. In steady state, the induced currents on the antennas are equal to: $I_1 = I_1^{alone} + I_1^{MC}$ and $I_2 = I_2^{alone} + I_2^{MC}$, where I_1^{alone} and I_2^{alone} are respectively the induced currents at antennas 1 and 2 at their alone states. Subsequently, I_1^{MC} and I_2^{MC} are the steady state induced mutual coupling currents at antenna 1 and 2 when the other antenna is placed in the field. Similarly, the steady state voltages at antenna 1 and 2 are V_1 and V_2 respectively.

The direction of incident wave has a great impact on the induced voltages (and currents) at both antennas. To study this, load impedances 50Ω and $1pF$ are considered for antenna 1 and 2. These loads are an example of low scattering (50Ω with $RCS \sim 0.008\, m^2$)

and high scattering ($1pF$ with $RCS{\sim}0.048\ m^2$) states for the studied antenna. Three scenarios are considered where the incident wave impinges (*i*) on both antennas simultaneously, (*ii*) First impinges on antenna 2 and then after that on antenna 1 as shown in Figure 2.2. (*iii*) First impinges on antenna 1 and then after that on antenna 2.

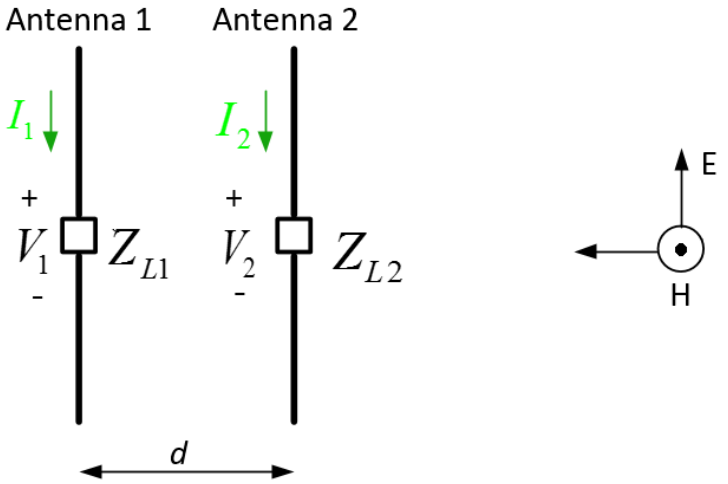

Figure 2.2. Scattering scenario in a two antenna system.

Figure 2.3 (a) shows the real and imaginary values of the induced voltages in both antennas for three scenarios when the distance (d) between them is increased to 4λ. The variation of the voltages in each antenna is shown by a marker and a color. The marker types show either antenna 1 (50Ω) or antenna 2 ($1pF$) (respectively circles and squares for antenna 1 and 2). The red, blue and green colors show respectively the studied scenario (*i*), (*ii*) and (*iii*). In all cases, the voltages at the antennas are diverged from their alone states because of the mutual coupling effect from the neighbor. In scenario (*i*), by increasing the distance the voltages of both antennas are converged to their alone states in spiral forms. In case (*ii*) and (*iii*), the antenna in front, i.e. antenna 2 and antenna 1 respectively, are

illuminated from two sides: the source wave and the antenna in the back. By increasing d the two incident waves come in phase and thus the total induced voltage at the antenna go through 360° phase. Figure 2.3 (b), shows the magnitude of the voltage at front antennas based on the distance between antennas. It is understood that for both antennas the magnitude of the voltage is converging to its alone state. At $d = \infty$, the voltages on the antenna will converge to their alone state values. On the other hand, for back antennas in case (*ii*) and (*iii*), i.e. antenna 1 and 2 respectively, by increasing d the voltages quickly converge to their alone states.

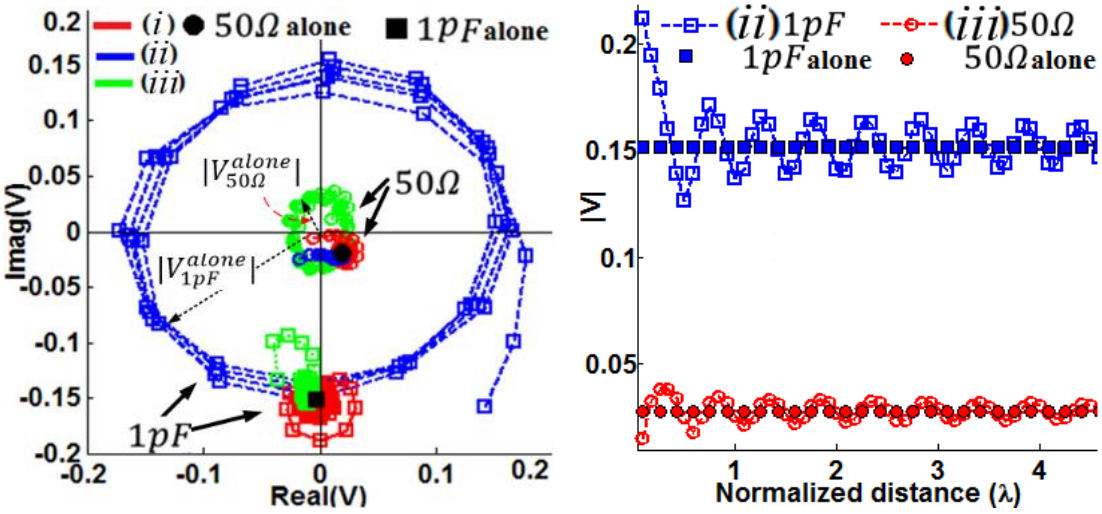

(a) Real and imaginary of V (b) magnitude of V

Figure 2.3. Variation of the voltages at two side by side antennas.

The studied scenarios can be explained by using mutual coupling model in (1) since: 1) the voltages are diverged from their alone state due to the presence of a neighbor, 2) the voltages are converged to the alone state of the antenna at $d = \infty$, 3) the voltage at the antenna is a function of the load – and consequently the current – at the neighbor. The

dependency between the antenna voltage and the current of its neighbor is described by mutual coupling impedance, i.e. $Z_{12}$and Z_{21} in (1).

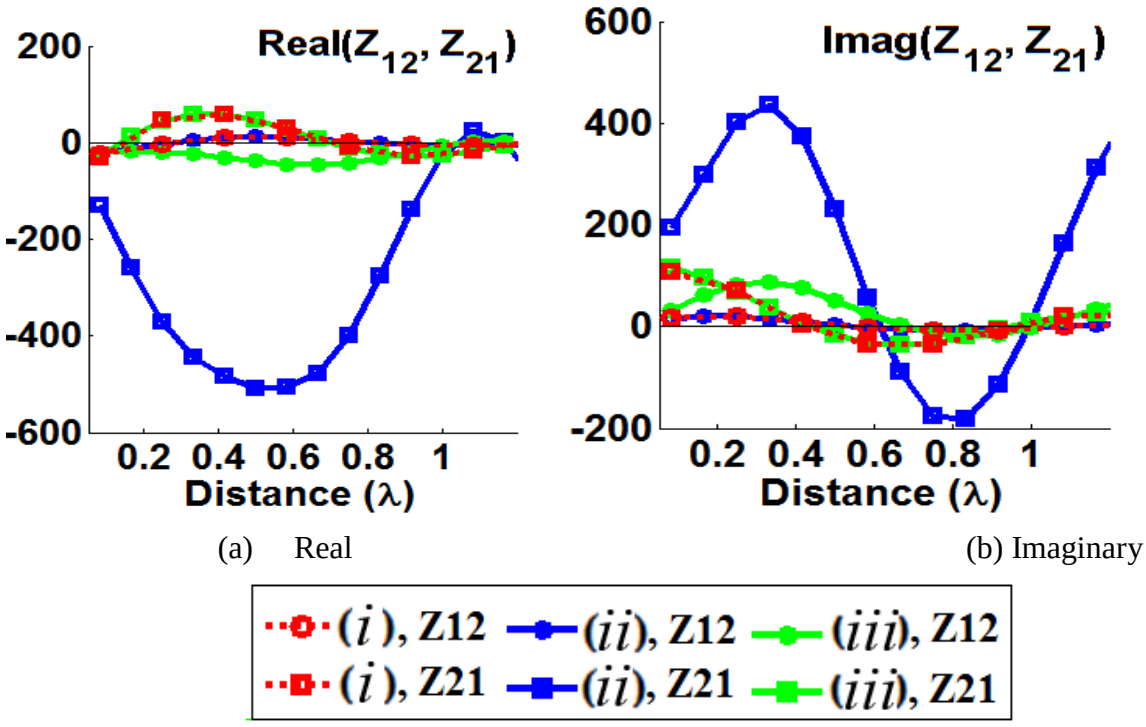

(a) Real (b) Imaginary

Figure 2.4. Simulated Real and Imaginary (Z_{12}) and (Z_{21}) for non-identical loads.

Figure 2.4 (a) and (b) show the real and imaginary values of the mutual coupling impedances for case (*i*), (*ii*) and (*iii*). These case studies are respectively are shown by red, blue and green graphs. The resultant mutual coupling from antenna 2 to antenna 1 (Z_{12}) and from antenna 1 on antenna 2 (Z_{21}) are characterized by square and circle markers respectively. In (1), the mutual coupling impedances depends on: 1) how quickly the voltage at the antenna is converged to its alone state, 2) how strong the current on the neighbor antenna is formed. In the case studies, antenna 1 is low scattering and its voltage converges to its alone state fast. On the other hand, antenna 2 is high scattering and its

voltage takes longer to converge. Thus, in each case study the mutual coupling impedance for two antennas with different loads result in $Z_{12} \neq Z_{21}$. In cases where the induced voltages on antenna is quickly converged to its alone state's value both real and imaginary values of the mutual coupling impedance is very small and close to zero (i.e. Z_{12} in case study (*i*) and (*ii*)). For front antennas (i.e. antenna 2 in case (*ii*) and antenna 1 in case (*iii*)), the induced voltage is immensely diverged from its alone state and it is slowly converged to the alone states. In these cases, both real and imaginary values of impedance takes very big values (i.e. Z_{21} in case study (*ii*) and Z_{12} in (*iii*)). For these case, the mutual coupling converges to zero when $(V - V_{alone}) \rightarrow 0$. Interestingly, the mutual coupling impedances for both antennas in the back antennas, i.e. Z_{12} in case (*ii*) and Z_{21} in case (*iii*), are equal to those values for case study (*i*) where the antennas are placed beside each other.

According to [23]: "*A reciprocity theorem states that a response of a system to a source is unchanged when source and measurer are interchanged"*. This scenario is realizable in traditional definition of mutual coupling in that V_1 and V_2 in turn act as a source in the system. Accordingly, this leads to $Z_{12} = Z_{21}$ showing the fact that the mutual coupling interactions for a transmitter and a receiver antenna is equal [6], [23]. However, for evaluating the mutual coupling in scattering antennas we always have a three (or more) antenna system where one antenna is the source of the system. When the source is on two scattering antennas have mutual interaction and when it is off the mutual coupling among them is zero. On the other hand, in this scenario changing the source and measurer is not meaningful since the main source is the incident wave. In general, we conclude that the mutual coupling and the interference between multiple scattering antennas depends on the antenna loads and antenna placements with respect to the incident wave.

3. LOAD SWITCHING

In this Section, we perform measurements to study the effect of a neighbor antenna in the backscattering link of a target antenna. We perform simulations to confirm our results. Printed half wave dipole at *f*=1GHz is considered on a Roger RO4350 substrate. The antenna and the structural support thickness are $0.05\ mm$ and $0.5\ mm$ respectively. Two-conductor pads $1\ mm \times 1\ mm$ are added to the antenna structure for soldering impedances to the antenna structure as shown in Figure 3.1. To modulate the scattered signal from the target antenna a pin diode is used at the input port of the target antenna. The impedance of the diode at forward bias is $1\Omega + 0.7nH$. To bias the pin diode the target antenna is connected to signal generator Agilent 81150A through thin wires. The signal generator is set at *f*=$10Hz$ and $\pm 0.7v$. To isolate the induced *ac* current from the wires which are connected to the signal generator inductors *L*=$100\mu H$ are used between the pin diode and wires. To minimize interference from wires they are made orthogonal to the polarization of the reader antenna and antennas. The target is illuminated by a horn antenna. The horn antenna is connected to the Agilent E5061B vector network analyzer (VNA) where we measure S_{11}.

In this paper, 1-port VNA measurement is used to measure backscattering signal from the target antenna. By measuring S_{11} at the VNA the scattered field from the target is measured with respect to an internal incident wave at the input port of reader antenna. According to (2), the scattered field from the target is directly related to the induced current distribution on the antenna. Thus, the measured S_{11} have a direct relation with the variation of the current at the target antenna. Furthermore, according to (3) the RCS also depends on the current distribution on the antenna by $\sqrt{\sigma} \propto I$. The demodulation of the backscattered

signal from the target antenna is performed by using $p_d = \frac{1}{N_p}\sum_{n=1}^{N} s_{11}(n).\Lambda(n)$ where $s_{11}(n)$ is the received backscattered signal at the VNA. And $\Lambda(n)$ is a sign function which is triggered to $+1/-1$ when the diode is ON/OFF. In this setup, $N_p = 10$ and $N = 500$. Since $s_{11} \propto I$ we have $p_d \propto I$ and $p_d \propto \sqrt{\sigma}$.

We consider two groups of loads at the neighbor antenna as shown in Table 3.1 and 3.2. In the first group, i.e. $\{Z_{L1}, Z_{L3}, Z_{L5}, Z_{L7}\}$, the current at the alone state of the antenna has 90°<ΔΦ<180° phase shift comparing to the alone state at the target antenna. In the second group, i.e. $\{Z_{L2}, Z_{L4}, Z_{L6}, Z_{L8}\}$, the current at the antenna has 0°<Φ<90° phase shift comparing to the alone state of the target antenna. The load impedances are soldered to neighbor antennas. The neighbor antennas were put individually beside the target antenna for measurements. Three scenarios are considered for measurements in that the neighbor antenna is placed in the back, side and front of the target antenna. These scenarios are called back, side and front neighbor scenarios. The distance between antennas (d) is increased and the scattered signal from the target is recorded.

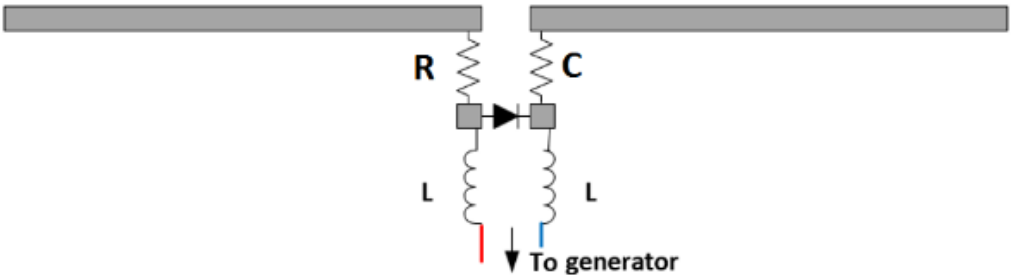

Figure 3.1. Prepared printed half wave dipole at *f*=1GHz for measurements.

Figure 3.3, 3.4 show the normalized $|p_d|$ and also simulated current at the target antenna respectively for side and back neighbor scenarios based on the distance between

antennas. We only present a few cases of impedance switching in the neighbor antenna in each figure. The measured and simulated values of the alone state current are shown with green and yellow markers respectively.

Table 3.1. Group 1.

Group 1		
Load	**RCS (Cm^2)**	**~ ΔΦ**
Z_{L1}= 20Ω +0.7pF	346	105°
Z_{L3}= 50Ω +0.6pF	250	115°
Z_{L7}=118+0.5pF	155	135°
Z_{L5}= 118Ω +0.2pF	80	150°

Table 3.2. Group 2.

Group 2		
Load	**RCS (Cm^2)**	**~ ΔΦ**
Z_{L2}= 4.5Ω +1pF	441	85°
Z_{L4}= 50Ω +2pF	183	65°
Z_{L6}= 118Ω +12nH	35	35°
Z_{L8}=10Ω +22nH	25	10°

In general, measurement and simulation results keep the same trend and are in agreement with each other. The difference between the simulated and measurement results can be attributed to the parasitic effect of the soldered impedances and also error in placing neighbor antennas at the same exact locations during the measurements. For all cases, the induced current at the target antenna converges to the alone state when the neighbor antenna is placed at farthest distances to the target antenna.

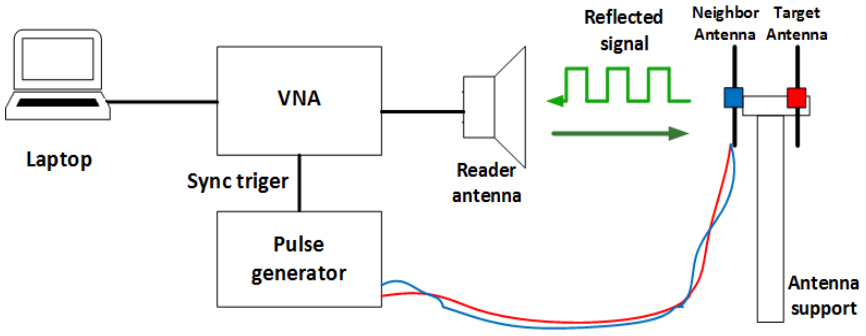

(a) Measurement setup.

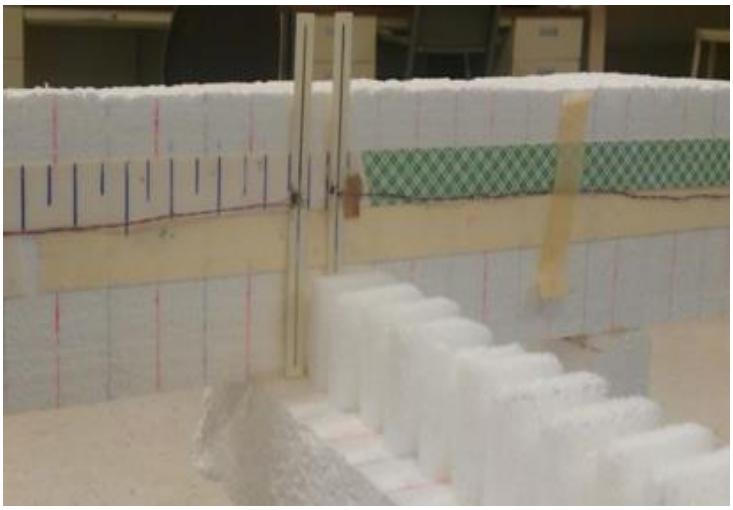

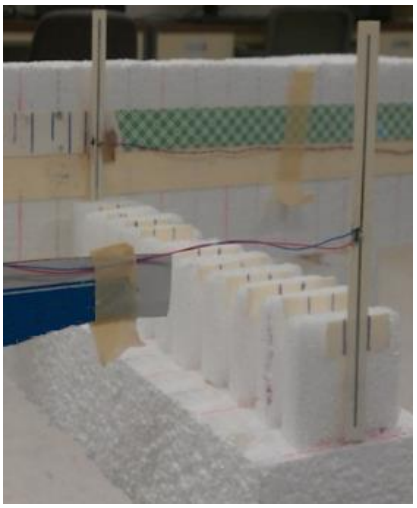

(b) side neighbor scenario (c) front/back neighbor scenario.

Figure 3.2. (a) Measurement setup (b) Side neighbor (c) Back/front neighbor.

This convergence behavior of the current is periodic for side and back neighbor scenarios. The period of the repeating pattern of magnitude of current at the target for side neighbor and back neighbor scenarios are ~ λ and ~ 0.5λ respectively. The reason for this can be attributed to the fact that the scattered signal from the neighbor travels twice the distance between the antennas in back neighbor comparing to side neighbor scenario in order to reach to the target antenna.

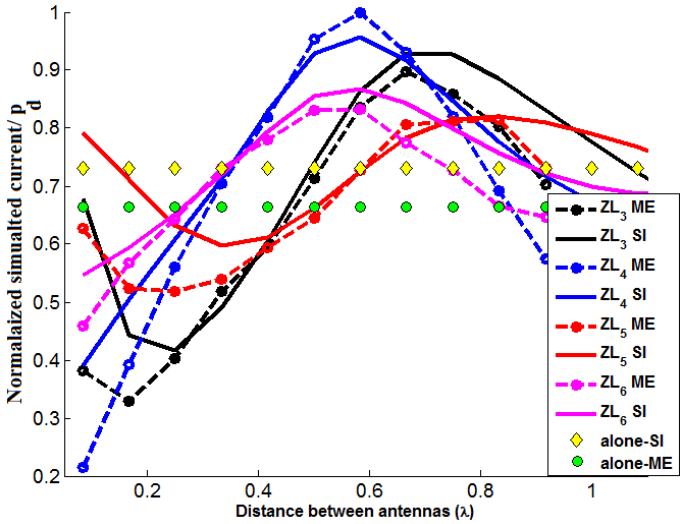

Figure 3.3. Variation of the magnitude of current and p_d at the target antenna based on distance between antennas in side neighbor scenario.

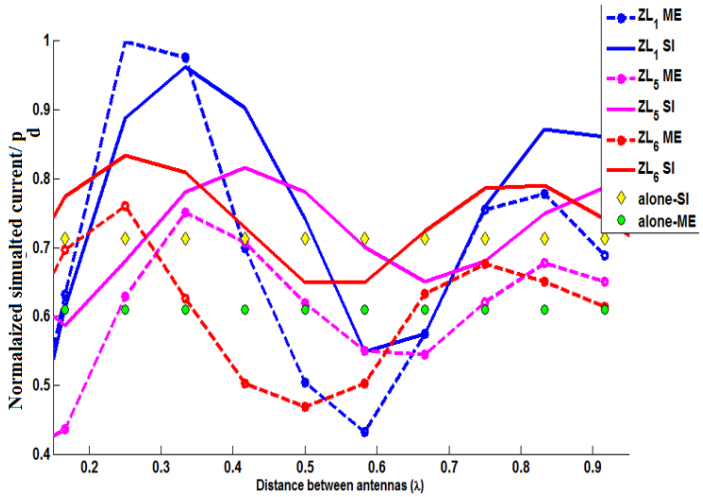

Figure 3.4. Variation of the magnitude of current and p_d at the target antenna based on distance between antennas in back neighbor scenario.

In side and back neighbor scenarios loads from both groups can produce constructive or destructive interference depending on their distances to the target antenna. To produce constructive interference at the target antenna in side and back neighbor scenarios, the neighbor must switch to different loads depending on its distance to the

target. Using different loads at the neighbor antenna, induces different phases at the induced mutual coupling currents at the target antenna. When the phase of the induced mutual coupling current from the scattered field from the neighbor antenna is in alignment with the alone state current of the target antenna a constructive interference will be produced. Using different loads in the neighbor will also change its RCS. Using high scattering states at the neighbor antenna we expect better improvement in the current at the target when the phases of both alone state current and mutual coupling current align (and a constructive interference is produced).

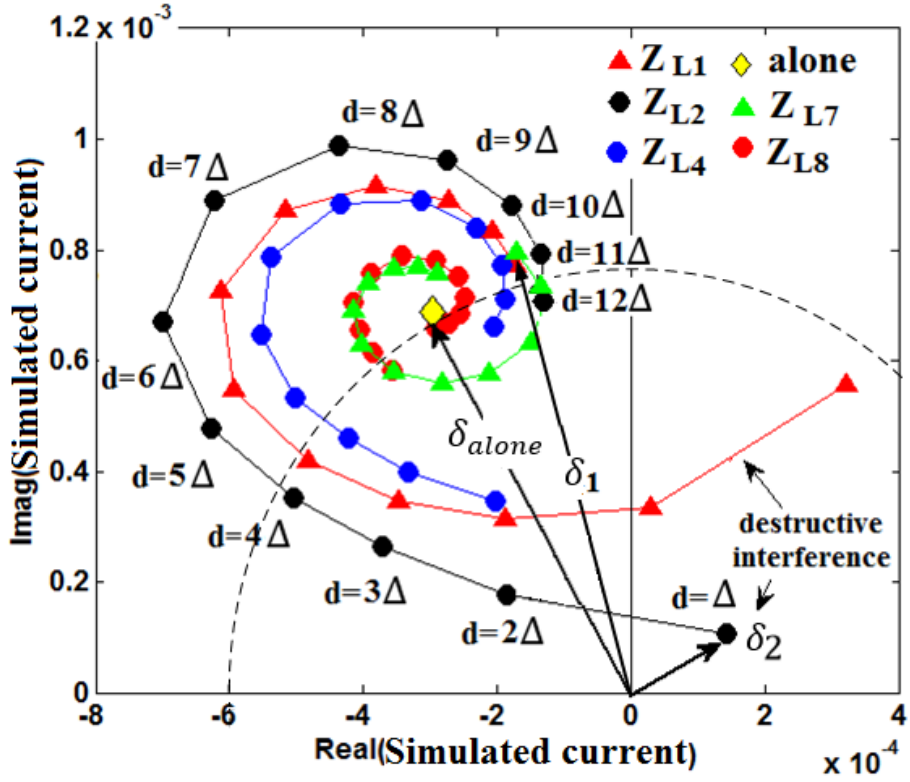

Figure 3.5. Variation of the current at the target for different load switching in the neighbor within $\lambda/_{12}<d<\lambda$. The distance between antennas for using Z_{L2} at neighbor is characterized on the figure ($\Delta=\lambda/_{12}$).

Figure 3.5 shows the real and imaginary values of the simulated induced current at the target antenna when its side neighbor antenna is loaded with five different loads. The magnitude of the current at the alone state in the target antenna is characterized by δ_{alone}. The distance between antennas is increased uniformly within $\lambda/_{12} < d < \lambda$ with step side $\Delta = \lambda/_{12}$. For all cases, by increasing the distance between antennas the induced current at the target is converged to its alone state in a spiral form. Each marker on the five traces in Figure 3.5 characterizes a *state* which represent two factors: (1) the load impedance at the neighbor, (2) the distance between antennas.

A circle with its center at the origin and radius δ_{alone} characterizes the constructive and destructive region for induced current at the target antenna. At all markers (states) which are located inside this specified circle, the magnitude of the target antenna is reduced comparing to its alone state. Thus, at these states (distances and loads) the effect of the neighbor antenna is destructive. On the other hand, at states which are outside the specified circle the magnitude of the induced current at the target antenna is increased. Thus, at these states (distances and loads) the effect of neighbor is constructive. Destructive or constructive interference at the current of the target antenna is directly related to a decrease or increase in the RCS of the target antenna. An example of a destructive state is using Z_{L1} or Z_{L2} at $d < 2\Delta$. However, if at these distances the neighbor switches to Z_{L7} the effect of the neighbor can be constructive and the RCS from the target increases. The magnitude of induced current at the target is characterized by δ_1 in this case on Figure 3.5. To maintain the constructive effect at the target at distances $2\Delta < d < 5\Delta$ and $5\Delta < d < 6\Delta$ the neighbor should switch to Z_{L8} and Z_{L4} respectively. As understood from Table 3.3 by employing Z_{L8} in neighbor antenna the resultant RCS from neighbor antenna is very low (10 Cm^2). Thus,

since the backscattering from the neighbor in this load is low it is not possible to increase RCS from the target antenna very much above its alone state. However, by using this impedance at the neighbor it is possible to stabilize the current at the target antenna and avoid destructive interference. On the other hand, by using Z_{L2} at the neighbor antenna it becomes maximum scattering ($441Cm^2$). As understood from figure 3.5, at $6\Delta < d < 9\Delta$ the phase shift between the induced mutual coupling current and the alone state current at the target antenna align (constructive interference) and as a result the magnitude of the induced current in the target improves. After this at $9\Delta < d < 12\lambda$ the neighbor antenna should switch to Z_{L1} so that the current at the target antenna reaches to a maximum. As an example, at $d = 10\Delta$, by using all five loads at the neighbor antenna a constructive interference at the target antenna occurs. However, using Z_{L1} produces the highest constructive interference which increases the current at the target the most. Table 3.3 tabulates the results for producing constructive interference at the target by load switching at the neighbor antenna. The maximum achieved gain over the alone state current is defined as $Gain = 20\log\left(\frac{\delta}{\delta_{alone}}\right)$ and is tabulated in Table 7.3. It is understood that by impedance switching at the neighbor antenna at different distances to the target antenna it is possible to achieve a gain up to $0.72dB < Gain < 3.4dB$ over the alone state at the target antenna in side neighbor scenario. This study is repeated for back neighbor scenario. For back neighbor scenario, the period of interference pattern is $\vartheta \sim 0.5\lambda$. Interestingly, almost the same order of load switching is obtained at the neighbor for this case when the neighbor is placed at farther to the target antenna. The results are tabulated in Table 7.3. The archived gain over the alone state at the target antenna is up to $1dB < Gain < 3.24dB$ by using different loads at different distances between antennas.

Table 3.3. Load switching in neighbor antenna.

Side neighbor	**Max(Gain) over alone state**	**Back neighbor**	**Max(Gain) over alone state**	**Load**
$d < 2\Delta$	0.72 dB	${}^{6}/_{7}\,\vartheta < d < \vartheta$	1.77 dB	Z_{L7}
$2\Delta < d < 5\Delta$	1.20	$d < {}^{2}/_{7}\,\vartheta$	1.00 dB	Z_{L8}
$5\Delta < d < 6\Delta$	2.33 dB	-	-	Z_{L4}
$6\Delta < d < 9\Delta$	3.4 dB	${}^{2}/_{7}\,\vartheta < d < {}^{4}/_{7}\,\vartheta$	3.24 dB	Z_{L2}
$9\Delta < d < 12\Delta$	2.6 dB	${}^{4}/_{7}\,\vartheta < d < {}^{6}/_{7}\,\vartheta$	2.61 dB	Z_{L1}

In our study, we understood the different pattern of the degradation of current at the target antenna in front neighbor scenario comparing to side and back neighbor scenarios. Figure 3.6 shows the normalized $|p_d|$ and also the normalized simulated current at the target antenna in front neighbor scenario based on the distance between antennas. According to the results, in front neighbor scenario using all loads in group 1 in the neighbor antenna produces constructive interference to the target. On the other hand, using all loads which are in group 2 in neighbor antenna produces destructive interference to the target. Figure 3.7 also shows the real and imaginary values of the simulated induced current at the target when load switching is used in the front neighbor. In all cases, by increasing the distance the induced current in converged to the alone state. Using Z_{L1} and Z_{L4} (respectively from group 1 and 2) have respectively the most constructive and destructive effects on the target. By using Z_{L7} and Z_{L8} (respectively from group 1 and 2) we still see

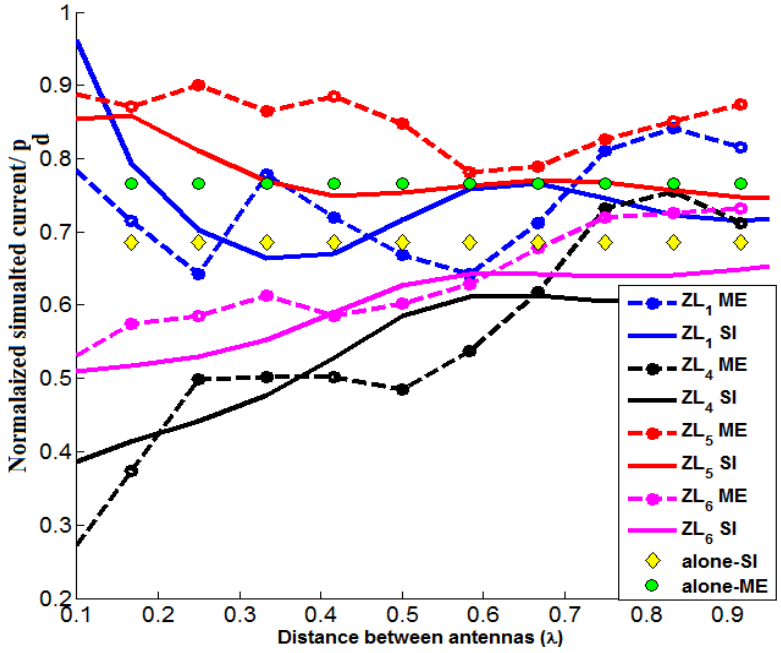

Figure 3.6. Variation of the magnitude of current and p_d at the target antenna based on distance between antennas in front neighbor scenario.

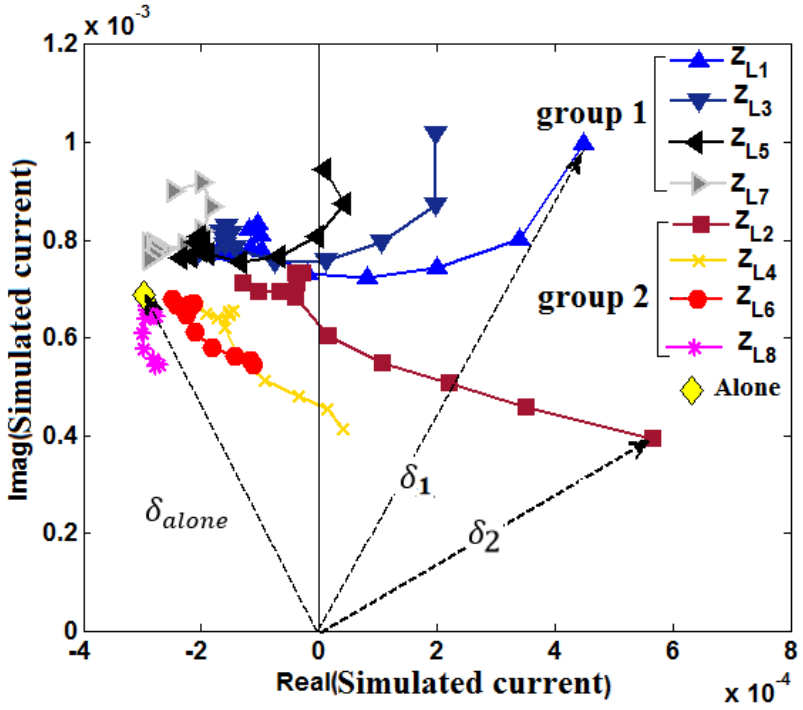

Figure 3.7. In front neighbor scenario loads in group 1 and 2 produce respectively constructive and destructive interference to the target antenna.

the constructive and destructive effects from the neighbor. However, comparing to Z_{L1} and Z_{L4} the resultant magnitude of the current due to both degradation and improvement in the current at the target antenna is very close to the alone state in target antenna. The highest achieved gain of constructive interference within $0 < d < \lambda$ using loads in group 1 is $0.58dB < Gain < 3.28dB$.

Improving current and fading away the current at a target antenna are both desirable in different applications. While improving current at a target antenna can help increasing the read rate and also read range in RFID systems, fading away the current from a target antenna can also help hiding a target antenna from undesired access and investigations. Overall, we understand that the backscattering from a target antenna is strongly dependent on the loading of its neighbor antenna as well as the placements of the neighbor with respect to the incident source signal. According to the achieved results when a neighbor antenna is within an effective radius to a target antenna it has considerable effect on the variation of the current at a target antenna. Outside this effective area the effect of the neighbor antenna on the target antenna is minimized and can be neglected.

Figure 3.8 depicts a map for the variation of the magnitude of the current at the target antenna when an identical neighbor with identical load $(1\Omega + 0.7nH)$ is placed beside it in the field. The target antenna is placed at $(0,0)$. The plane wave illuminates the antennas from $(-y)$. The magnitude of current at alone state at the target is ~ "6.7e-4". Interestingly, at $\left(\pm\frac{\lambda}{2}, \frac{\lambda}{8}\right)$ using an identical neighbor can increase the signal at the target antenna. However, exactly in front of the target antenna ($y < 0$) the identical neighbor will block the signal from the target as understood from Figure 3.8. By increasing the distance between the antennas over to λ in front neighbor still the effect of neighbor is destructive.

In this case, by switching to tabulated loads in group 3.1 in Table 3.2 it is possible to overcome to destructive interference effect at the neighbor and improve the backscattering signal. Load switching in back and side neighbor scenarios can also be used in blind or low scattering spots to improve the backscattering at the target.

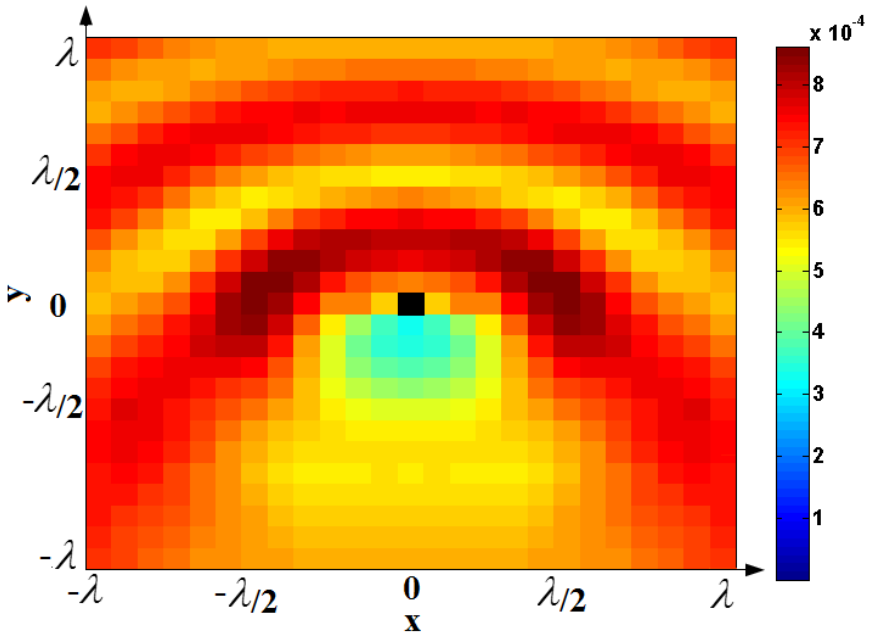

Figure 3.8. The variation of the current at the target antenna when an identical neighbor is placed beside it in the field. The target antenna is placed in the center of the field.

The result of this study can be used in passive RFID networks for improving the signal strength from a target RFID antenna. The proposed model consist of an RFID antenna which is equipped with several loads that can be used depending on different scenarios in order to help a target antenna in the vicinity to improve its backscattering signal. In this scenario, not only the neighbor antennas do not produce blind spots but also they help a target RFID antenna to improve its signal strength. This technique can help increasing the read rate at the RFID networks.

4. CONCLUSIONS

In this paper, controlling the mutual coupling interactions in two side by side scattering RFID antennas is studied and discussed by using the definition in (1). It is shown by measurements and simulations that by load switching in a neighbor antenna the interference in closely spaced RFID antennas can be controlled to 1) avoid destructive interference at a target antenna 2) produce constructive interference at the target antenna to increase its backscattering signal strength. It is shown that by cooperative communication in RFID networks it is possible to overcome to blind spots and instead improve the backscattering from a target antenna. A multi-port passive RFID antenna is proposed which consists of several load impedances. This model can be used in neighboring antennas to switch to different loads depending on theirs placements with respect to the incident wave and the target antenna to help a target increases its signal strength.

REFERENCES

[1] Shadi Ebrahimi-Asl, M.T Ghasr and M. Zawodniok, "Application of Low Scattering Antennas to RFID Networks," to be appear in Proceeding of IEEE RFID conference, Orlando, USA, 2016.

[2] Y. Tanaka, Y. Umeda, O. Takyu, M. Nakayama, K. Kodama, "Change of read range for UHF passive RFID tags in close proximity," in Proc. RFID Conference, 2009, Orlando., USA, pp. 338 – 345.

[3] C. H. Loo, A. Z. Elsherbeni, F. Yang, D. Kajfez, "Experimental and Simulation Investigation of RFID Blind Spots," Journal of Electromagnetic Waves and Applications, vol 23, no. 5-6, Apr 2009.

[4] Feng Lu, XiaoSheng Chen, Terry T. Ye, "Performance analysis of stacked RFID tags," in IEEE Int. RFID Conf., April 2009, pp. 330 - 337.

[5] S. Ebrahimi-Asl, M.T Ghasr, M. Zawodniok, K.E. Robinson, "Preliminary study of mutual coupling effect on a passive RFID antenna array," in Proc. I2MTC Conference, Minneapolis, 2013, pp. 138 – 141.

[6] C.A. Balanis, Antenna Theory. New Jersey: John Wiley & Sons, 2005.

[7] P. Pursula, D. Sandstrom, K. Jaakkola, "Backscattering-Based Measurement of Reactive Antenna Input Impedance," IEEE Transactions on Antennas and Propagation , vol. 56, no. 2, pp. 469 – 474, Feb. 2008.

[8] B.D. Popović, Theory of cylindrical antennas with lumped impedance loadings, pp. 243-248, April 1973.

[9] Tang, T., Gunn, M.W. "Current distribution on a receiving dipole antenna," IEEE Transactions on Antennas and Propagation, vol. 29, no. 5, pp. 817 – 822, Sep 1981.

[10] Yueh-Ying Hu, "Back-scattering cross section of a center-loaded cylindrical antenna," IRE Transactions on Antennas and Propagation, vol. 6, no. 1, pp. 140 – 148, January 1958.

[11] Popovic, B.D., Dragovic, M.B., "Capacitively loaded thin cylindrical antenna." Proceedings of the Institution of Electrical Engineers, vol. 121, no. 2, pp. 101 – 108, February 1974.

[12] R. Harrington, J. Mautz, "Straight wires with arbitrary excitation and loading," IEEE Transac. on Anten. and Propag., vol. 15, no. 4, pp. 502 – 515, Jul 1967.

[13] H.T.Hui, “A new definition of mutual impedance for application in dipole receiving antenna arrays,” IEEE Antennas Wireless Propag. Lett, vol.3, no. 1, Dec. 2004.

[14] Hsueh-Jyh Li, Hsin-Hsu Lin, Hsin-Hung Wu “Effect of antenna mutual coupling on the UHF passive RFID tag detection”, in Proc. IEEE Ant. And Propag. Int. Symp., Jun. 2008, pp. 1-4.

[15] Adv. Chen Sun, Kyoto, Japan , A. Hirata, T. Ohira, N.C. Karmakar, “Fast beamforming of electronically steerable parasitic array radiator antennas: theory and experiment,” in IEEE Transac. Antennas Propag., vol. 52, no. 7, pp. 1819 – 1832, Jul. 2004.

[16] L. Petit, L. Dussopt, J. Laheurte, “MEMS-switched parasitic-antenna array for radiation pattern diversity,” in IEEE Transac. Antennas Propag., vol. 54, no. 9, pp. 2624 – 2631, Sep. 2006.

[17] Qi Zhang, M.J. Crisp, R.V Penty, I.H. White, “Reduction of Proximity Effects on UHF Passive RFID Systems by Using Tags With Polarization Diversity,” IEEE Transac. Antenn. Propag., vol. 63, no. 5, pp. 2264 - 2271, Feb. 2015.

[18] Lijuan Zhang, Wei Xiang, Xiaohu Tang, “An Adaptive Anti-Collision Protocol for Large-Scale RFID Tag Identification,” IEEE Wireless Comm. Lett., vol. 3, no. 6, pp 601 – 604, Sep. 2014.

[19] A. Bletsas, S. Siachalou, J.N. Sahalos, “Anti-Collision Backscatter Sensor Networks,” IEEE Trans. on Wireless Comm., vol. 8, no. 10, pp. 5018 – 5029, Oct. 2009.

[20] D. M. Dobkin, T. Freed, C. Gerdom, C. Flores, E. Futak, C. Suttner, "Cooperative tag communications,”IEEE International Conference RFID Technology and Applications (RFID-TA), pp. 27 - 32, 2015.

[21] S. Capdevila, L. Jofre, J. C. Bolomey, J. Romeu, “RFID Multiprobe Impedance-Based Sensors,” IEEE Transactions on Instrumentation and Measurement, vol. 59, no. 12, pp. 3093 – 3101, Aug 2010.

[22] G. Marrocco, L. Mattioni, C. Calabrese, “Multiport Sensor RFIDs for Wireless Passive Sensing of Objects—Basic Theory and Early Results,” IEEE Transac. on Anten. and Propag., vol. 56, no. 8, pp. 2691 – 2702, Aug 2008.

[23] R.F. Harington, Time-Harmonic Electromagnetic Fields. New York: McGraw-Hill, 1961.

[24] S.R. Best and B.C. Kaanta, "A Tutorial on the Receiving and Scattering Properties of Antennas," IEEE Antennas Propag. Mag., vol. 51, no. 5, pp. 26 – 37, Oct. 2009.

[25] Daniel J. P. , "Mutual coupling between antennas for emission or reception--Application to passive and active dipoles," IEEE Transac. on Antenn. and Propag., vol. 22, no. 2, pp. 347 – 349, Mar 1974.

[26] Hoi-Shun Lui, H. T. Hui, Mook Seng Leong, "A Note on the Mutual-Coupling Problems in Transmitting and Receiving Antenna Arrays," IEEE Antennas and Propagation Magazine, vol. 51, no. 5, pp. 171 – 176, Oct. 2009.

SECTION

4. CONCLUSIONS

This dissertation addresses two major challenges in passive RFID networks by studying the root causes and provides solutions for them. A measurement methodology is developed for estimating the structural scattering coefficient of a linear antenna. *Linear-Minimum Variance Unbiased Estimator* is used to develop an estimation methodology for the scattering model of a linear antenna in *Green model*. The absolute value of the error (ϵ) of the estimated value and the simulated *true value* of this parameter (A_s) can get as low as $|\epsilon| < 0.053$ when the PDF of white Gaussian noise is ensured in the measurement setup. Next, the well-known *Green model* for evaluating the radar cross section (RCS) of an antenna over its Γ plane for two types of antennas is studied: half wave-dipole and T-match bowtie antenna. The variation of RCS of a linear half-wave dipole over its Γ plane is as described by this model. However, it is discovered that Green model cannot completely explain the behavior of a T-match bowtie antenna over its Γ plane. Both by measurements and simulations it is shown that a T-match bowtie antenna has two maximum scattering areas over its Γ plane. This led the research to create a manipulation on the studied T-match bowtie antenna to use dual loading on its structure. The first stimulus on the studied T-match bowtie antenna is produce by creating a $1mm$ gap at the center of the antenna and the second stimulus is produced at the original input port of the antenna. By using a combination of loads at both stimuluses of the new antenna a variety of scattering states with different magnitudes over 360° can be created. This feature of the new antenna design is used to : *i*) increase the vector differential RCS *ii*) produce a quasi-32-QAM. In the next

step, the mutual coupling interactions of two and more RFID antennas is studied. A new state in RFID tags is investigated to suppress interference in a dense deployment of RFID tags. In this new state, RFID tags switch to a low scattering state to avoid a chaos of interference in the network. By measurements and simulations it is shown that using this method when a target antenna is located among nine neighbor antennas in its close vicinity, the magnitude of its scattered signal (δ) is stabilized at the level in that the target and the RFID reader are alone in the field. This means that by using the proposed method the neighbors are actually *invisible* in the field and do not produce any interference to the target. Using δ, a read rate study is performed for the network consisting of one target antenna and 9 neighbor antennas in close proximity of each other. When the threshold of read rate at the RFID reader is set at "0.75 δ" the average read rate of the target antenna is 93.76% when low scattering neighbors are used. In case high scattering neighbors (short circuit neighbors) are used the average read rate is 14.16%. In the last step, a numerically based method for evaluation of mutual coupling in scattering antennas is developed. For scattering antennas the current at an antenna is a function of the load impedance at its neighbors. A multi-port RFID antenna which can switch to different load impedances to help a target antenna in its vicinity – who is queried from the RFID reader– to increase its backscattering signal over its signal where it is alone in the field. This increase in the signal strength at the target can be up to $3.4dB$ over the case when the target is alone in the field.

5. FUTURE WORK

The result of this study in this dissertation showed that the current state of literature lacks a full understanding of the behavior of RCS of different RFID antennas over their Γ planes to design their maximum differential RCS in their backscattering links. Thus, a study on this topic seems to be necessary toward extending the coverage range of passive RFID networks. Base on the behavior of RCS in T-match bowtie antenna, a dual loaded RFID antenna is invented which can produce various scattering states with different magnitudes over 360° phase span in the in-phase and quadrature plane. In this dissertation, only a few combinations of loads at the two stimuluses of the designed dual loaded antenna are evaluated. The possibility of more scattering states by using other combination of loads will be investigated in future works. Furthermore, this invention is employed in other types of RFID antennas to investigate the possibility of increasing the vector differential RCS and also higher order modulations in passive RFID systems.

The result of this work show that there is a need for more comprehensive study on the mutual coupling interactions among scattering antennas. This study can be used in Electronically Steerable Antenna Arrays to design more educated and efficient pattern synthesis from the antenna array structure.

REFERENCES

[1] R. B. Green, "The general theory of antenna scattering," Report No. 1223-17, ElectronScience Laboratory, Columbus, OH, Nov, 1963.

[2] Chih-Chuan Yen, A.E. Gutierrez, D. Veeramani, D. van der Weide, "Radar Cross Section Analysis of Backscattering RFID Tags," Antennas and Wireless Propagation Letters, vol. 6 , pp. 279 – 281, 2007.

[3] C. A. Blanis, Antenna Theory: Analysis and Design, 3rd ed. Hoboken, NJ:Wiely, 2005.

[4] P.V Nikitin, K.V.S. Rao, "Theory and measurement of backscattering from RFID tags," IEEE Ant. Propag. Mag., vol 48 , no.6, pp. 212 – 218, Dec. 2006.

[5] P. V. Nikitin, K. V. S. Rao, and R. Martinez, "Differential RCS of RFID tag," Electronics Letters, vol. 43, no. 8, pp. 431-432, 2007.

[6] A. Bletsas , A.G. Dimitriou, J.N. Sahalos, "Improving Backscatter Radio Tag Efficiency," IEEE Transactions on Microwave Theory and Techniques , June 2010 Volume: 58 , Issue: 6 , pp. 1502 – 1509.

[7] Huan-Yang Chen, Bhadkamkar, A.S., Tzu-Han Chou, Van Der Weide, "Vector Backscattered Signals Improve Piggyback Modulation for Sensing With Passive UHF RFID Tags," Microwave Theory and Techniques, IEEE Transactions, vol. 59, no. 12, pp. 3538-3545, November 2011 .

[8] T. Sawaya, M. Taromaru, T.Ohira, B. Komiyama, "Experimental Proof of Electrically Invisible State of Inductively Loaded Dipole and Proposal of Electrically Invisible Meander-Lines," IEEE Transac. Antenn. Propag., vol. 54, no. 11, pp. 3374 – 3382, Nov. 2006.

[9] Kastner, R. , Avraham, T., Sternfeld, L., Socher, E., "Structural scattering and the virtual aperture of a half-wavelength dipole antenna," APSURSI, 2012 IEEE, pp. 1 – 2, July 2012.

[10] N. Nakamoto, T. Takahashi, T. Nomura, M. Otsuka, "A method to measure the antenna mode and structural mode for antenna RCS reduction using circulator and phase shifter," ISAP, pp. 21 – 22, Kaohsiung, Dec. 2014 .

[11] A. G. Dimitriou , J. Kimionis, A. Bletsas, J. N. Sahalos , "A fading-resistant method for RFID-antenna structural mode measurement," International RFID-TA, pp. 443 – 448, Nice, Nov. 2012.

[12] Dimitriou, A.G., Bletsas, A., Sahalos, J.N. “Practical considerations of ASK modulated passive tags,” Antennas and Propagation (EUCAP), 2012 6th European Conference on, March 2012, Page(s):3476 – 3480.

[13] A. Bletsas , A.G. Dimitriou, J.N. Sahalos, “Backscattering improvement of UHF RFID tag efficiency,” Antenna Technology iWAT, pp. 1 – 4, 2010.

[14] S.J. Thomas, E. Wheeler, J. Teizer, M.S. Reynolds, “Quadrature Amplitude Modulated Backscatter in Passive and Semipassive UHF RFID Systems ,” IEEE Transactions on Microwave Theory and Techniques, vol. 60, no. 4, pp. 1175 – 1182, February 2012.

[15] J. Besnoff, M. Abbasi, D. S. Ricketts, “High Data-Rate Communication in Near-Field RFID and Wireless Power Using Higher Order Modulation,” IEEE Transactions on Microwave Theory and Techniques, vol. 64, no. 2, pp. 401 – 413, February 2016.

[16] S. J. Thomas, M. S. Reynolds, "A 96 Mbit/sec, 15.5 pJ/bit 16-QAM modulator for UHF backscatter communication,” RFID (RFID), 2012 IEEE International Conference on, pp. 185: 190, April 2012, Orlando FL.

[17] C. Mandel, M. Schüßler, M. Nickel, B. Kubina, R. Jakoby, M. Pöpperl, M. Vossiek, “Higher order pulse modulators for time domain chipless RFID tags with increased information density,” European Microwave Conference, Sept. 2015, Paris.

[18] Shadi Ebrahimi-Asl, M.T Ghasr, M. Zawodniok, “ Method and Device for Improving Performance of RFID Systems,” US Provisional Patent Application 62/236,490, October 2015.

[19] C. H. Loo, A. Z. Elsherbeni, F. Yang, D. Kajfez, “Experimental and Simulation Investigation of RFID Blind Spots,” Journal of Electromagnetic Waves and Applications, vol 23, no. 5-6, Apr 2009.

[20] Lijuan Zhang, Wei Xiang, Xiaohu Tang, “An Adaptive Anti-Collision Protocol for Large-Scale RFID Tag Identification,” IEEE Wireless Comm. Lett., vol. 3, no. 6, pp 601 – 604, Sep. 2014.

[21] A. Bletsas, S. Siachalou, J.N. Sahalos, “Anti-Collision Backscatter Sensor Networks,” IEEE Trans. on Wireless Comm., vol. 8, no. 10, pp. 5018 – 5029, Oct. 2009.

[22] Feng Lu, XiaoSheng Chen, Terry T. Ye, “Performance analysis of stacked RFID tags,” in IEEE Int. RFID Conf., April 2009, pp. 330 - 337.

[23] S. Ebrahimi-Asl, M.T Ghasr, M. Zawodniok, K.E. Robinson, “Preliminary study of mutual coupling effect on a passive RFID antenna array,” in Proc. I2MTC Conference, Minneapolis, 2013, pp. 138 – 141.

[24] Qi Zhang, M.J. Crisp, R.V Penty, I.H. White, “Reduction of Proximity Effects on UHF Passive RFID Systems by Using Tags With Polarization Diversity,” IEEE Transac. Antenn. Propag., vol. 63, no. 5, pp. 2264 - 2271, Feb. 2015.

[25] D. M. Dobkin, T. Freed, C. Gerdom, C. Flores, E. Futak, C. Suttner, "Cooperative tag communications,”IEEE International Conference RFID Technology and Applications (RFID-TA), pp. 27 - 32, 2015.

[26] Shadi Ebrahimi-Asl, M.T Ghasr, M. Zawodniok, “Implementation of Invisible Antenna with Application of RFID Systems,” provisional patent application 62/248,870, October 2015.

[27] Daniel Mark Dobkin, “RFID Systems Including Tags Having Low RF Scattering Mode,” U.S. Patent 2007/0115098 A1, May. 24, 2007.

[28] Shadi Ebrahimi-Asl, M.T Ghasr, M. Zawodniok, “ Method and Device for Improving Performance of RFID Systems,” US Provisional Patent Application 62/236,490, October 2015.

VITA

Shadi Ebrahimi-Asl was born in Tehran, Iran. She earned her bachelor's degree at Electronics Engineering from Guilan University in Rasht, Iran. She finished her master's degree in Electrical Engineering at Iran University of Science and Technology. During her education she completed a thesis entitled "Dynamic Channel Allocation in Distributed Cognitive Networks using DS-Spread spectrum".

In June 2011, she started her Doctorate of Philosophy in Electrical Engineering at Missouri University of Science and Technology. She worked as a research assistant with Dr. Maceij Zawodniok. Her work was based on experimental performance evaluation for passive RFID systems. In October 2015, her PhD research resulted in two provisional patent applications. She received her PhD degree in July 2016.